Design of Continuous Bridges Using Precast, Prestressed Concrete Girders Without End Blocks

WA-RD 155.1

Final Report
October 1987

Washington State Department of Transportation
Planning, Research and Public Transportation Division

in cooperation with the
United States Department of Transportation
Federal Highway Administration

WASHINGTON STATE DEPARTMENT OF TRANSPORTATION

Duane Berentson, Secretary
A.D. Andreas, Deputy Secretary
James P. Toohey, Assistant Secretary for Planning, Research and Public Transportation

Washington State Transportation Commission Research Committee
William O. Kamps, Chair
Bernice Stern, Commissioner
Leo B. Sweeney, Commissioner

WSDOT Research Executive Committee
A.D. Andreas, Chair, Deputy Secretary for Transportation
E.W. Ferguson, District 4 Administrator
H. W. Parker, Assistant Secretary for Marine Transportation
Robert C. Schuster, Assistant Secretary for Highways
James P. Toohey, Assistant Secretary for Planning Research & Public Transportation

WSDOT Research Technical Committees
Highway Operations and Development
Don Senn, Chair, District 2 Administrator
John Aspaas, District 4 Project Engineer
William P. Carr, Associate Research Director
John Conrad, District 1 District Operations Engineer
Rich Darnell, District 3 Maintenance & Operations Engineer
C. Stewart Gloyd, Bridge/Structures Engineer
Wayne Gruen, State Traffic Engineer
Dennis Jackson, Roadway Construction Engineer
Stan Moon, Location/Design Engineer
Dick Shroll, District 6 Maintenance Superintendent
Ken Thomas, Operations Engr., Bellingham Public Works Dept.
George Tsiatis, Structural Engineer, Washington State University

Materials and Product Evaluation
Del Vandehey, Chair, State Construction Engineer
Keith W. Anderson, Federal Program Manager
Jim Buss, District 5 Construction Engineer
Newton Jackson, Pavement/Soils Engineer
Steve Kramer, Assistant Professor, Civil Engineering, U of W
Bob Krier, Bridge Operations Engineer
Bob Spratt, District 2 Maintenance Engineer
John Strada, Materials Engineer

Planning and Multimodal
Don Tranum, Chair, District 6 Administrator
Ron Anderson, Manager, District 6 Management Services
Ken Casavant, Professor, Washington State University
King Cushman, Director, Pierce County Transit Development
Kris Gupta , Manager, Transportation Data Office
Charles Howard, Transportation Planning Office
Jerry Lenzi, Manager, Multi Modal Branch
Jim Slakey, Manager, Public Transportation
Ray Deardorf, Service Planning Manager, Ferry System

WSDOT Research Implementation Committee
Stan Moon, Chair, Location/Design Engineer
Jack E. Hanson, Location Engineer
Dennis Ingham, State Maintenance Engineer
Dennis Jackson, Roadway Construction Engineer
Kern Jacobson, Engineering Superintendent, WSF
Bob Krier, Bridge Operations Engineer
Ed Schlect, Construction Engineer, Paving
Gerald Smith, District 1, Assistant I-90 Construction Engineer
Bob Spratt, District 2 Maintenance Engineer
John Strada, Materials Engineer

WSDOT Research Office
John Doyle, Director
William P. Carr, Associate Director
Keith W. Anderson, Federal Program Manager
Julie Leverson, Database Coordinator
Carl Toney, Research Administrator

WSDOT Research Liaisons
District 1 - John Conrad, Public Transportation & Planning Engr.
District 2 - Dave House, Project Development Engineer
District 3 - Bob George, Assistant Location Engineer
District 4 - Richard N. Coffman, Maintenance Engineer
District 5 - Robert MacNeil, Design Engineer
District 6 - Richard Larson, Design and Planning Engineer
WSDOT Library - Barbara Russo, Librarian

Transportation Research Council
Transportation Commission
Leo B. Sweeney, Chair
William J. Kamps, Vice Chair
Vaughn Hubbard
Bernice Stern
Richard Odabashian
Albert D. Rosellini
Jim Henning

Federal Highway Administration
Paul C. Gregson, Division Administrator

Private Sector
Milton "Bud" Egbers, President, Skagit Valley Trucking
Richard Ford, Managing Partner, Preston, Thorgrimson, Ellis, Holman
Tom Gaetz, Project Manager, David Mowat & Company, Bellevue
Lawrence Houk, Vice President, Lockheed Shipbuilding
Charles H. Knight, President, Concrete Technology
H. Carl Munson, VP for Strategic Planning, Boeing Co., Seattle
Michael Murphy, President, Central Pre-Mix Concrete
Richard Norman, President, Associated Sand & Gravel, Everett
John Ostrowski, Public Works Director, Vancouver, WA
Richard S. Page, President, Washington Roundtable
Sudarshan Sathe, Dir., Technical Services, Polycarb Inc., Cleveland, OH
Gerald E. Weed, Public Works Director, Snohomish County

Universities
Gene L. Woodruff, Vice Provost for Research, UW
Robert V. Smith, Associate Provost for Research, WSU
Neil Hawkins, Associate Dean for Research, College of Engineering, UW
Reid Miller, Dean, College of Engineering, WSU
Colin Brown, Professor and Chair, Civil Engineering, UW
Surinder K. Bhagat, Professor and Chair, Civil Engineering, WSU

Washington State Department of Transportation
Duane Berentson, Secretary
A.D. Andreas, Deputy Secretary
C.W. Beeman, District 5 Administrator
R.E. Bockstruck, District 1 Administrator
J.L. Clemen, Assistant Secretary for Finance & Budget Management
Don Senn, District 2 Administrator
R.L. Daniels, Administrator, Public Affairs Office
E.W. Ferguson, District 4 Administrator
W. H. Hamilton, Assistant Secretary for Aeronautics
W.I. Hordan, State Aid Engineer
H. W. Parker, Assistant Secretary , Marine Transportation
R.C. Schuster, Assistant Secretary for Highways
A.T. Smelser, District 3 Administrator
J.P. Toohey, Assistant Secretary for Plng, Res., and Pub. Trans.
M.D. Tranum, District 6 Administrator
D.J. Vandehey, State Construction Engineer

Representative George Walk, Chair - Legislative Transportation Committee

Federal Highway Administration
M. Eldon Green, Region 10 Administrator
Otis C. Haselton, Region Office Research and T2 Engineer
Ernest J. Valach, Director, Regional Planning and Program Development

Paul C. Gregson, Division Administrator
Barry Brecto, Division Office Programming and T2 Engineer
Charles W. Chappell, Division Transportation Planner
Mike Duman, Assistant Transportation Planner

Washington State Transportation Center (TRAC)
G. Scott Rutherford, Director
Richard Fragaszy, Deputy Director, WSU
Joe P. Mahoney, Deputy Director, UW
Khossrow Babaei, Senior Research Engineer
Don Ernst, Technology Transfer
Mark Hallenbeck, Senior Research Engineer
Alison Kaye, Word Processing Technician
Ed McCormack, Research Engineer
Amy O'Brien, Editor
Bev Odegaard, Program Assistant
Ron Porter, Word Processing Technician
Cy Ulberg, Senior Research Engineer
Duane Wright, Research Aide

DESIGN OF CONTINUOUS BRIDGES USING PRECAST, PRESTRESSED CONCRETE GIRDERS WITHOUT END BLOCKS

by

Rafik Y. Itani, Ph.D.,
Professor of Civil and Environmental Engineering
(509) 335-3233

Girish S. Hiremath,
Graduate Research Assistant

Washington State Transportation Center
Structural Engineering Section
Department of Civil & Environmental Engineering
Washington State University
Pullman, WA 99164-2910

and

Umesh Vasisth
Supervising Bridge Engineer

Washington State Department of Transportation

Washington State Transportation Center
Washington State Department of Transportation
Olympia, WA 98504-5201

Final Report
Research Project Y-3400
Task 14

Prepared for
Washington State Transportation Commission
Department of Transportation
and in cooperation with
U.S. Department of Transportation
Federal Highway Administration

October, 1987

ABSTRACT

This study investigated the feasibility of eliminating end blocks from pretensioned continuous bridge girders. The removal of end blocks is estimated to reduce girder cost by 5 percent to 10 percent. The girders studied were the pretensioned, series 14 type used by the Washington State Department of Transportation. These girders are characterized by 5 in. thick webs and are prestressed with both harped and straight 1/2 in. diameter grade 270 strands. Previous research had recommended the elimination of end blocks for simple span bridges. This study dealt with continuous bridges.

The research was conducted in two phases. The first phase was a field test, while the second phase consisted of a destructive laboratory test. A series 14 girder with end blocks and two series 60 girders without end blocks were monitored from the time they were manufactured to the time loads were tested on a bridge. The girders were instrumented with strain gages on the shear reinforcement and concrete surface of their end regions near the continuous support. Strains were measured during detensioning and various stages of loading.

A laboratory test on two 20-ft. long series 14 girders was performed. The girders were without end blocks and continuous throughout the deck. Their joint details were similar to those normally used in the field. At the continuous ends, strains induced in the stirrups and concrete surface were monitored. Strain readings were taken during the detensioning process, as well as during various stages of loading. The load was applied at a distance of 13 ft. 10 in. from the continuous end. The limiting load at which the flexural steel yielded was 408 kips. The maximum applied load was 480 kips. The

pattern of cracks achieved was consistent with the theory of flexure-shear and web shear cracking. Even though the nominal strength of the concrete in the diaphragm was less than that in the girder, the cracks were restricted to the girders. The maximum 28-day compressive strength of the concrete in the diaphragm was 4000 psi, as compared to the 9880 psi of the girders.

The first visible cracks occurred at a load of 210 kips. These were flexural cracks and were located in the slab and the top flange. The limiting load at which the deck reinforcement yielded was 408 kips. The corresponding maximum strain in the concrete was 0.000698. At an applied load of 270 kips, which equaled the factored design shear, the deflection of the free end was 1.2 in. At this stage, flexural and flexural-shear cracks occurred. The shear reinforcement yielded an applied load of 480 kips. The combination of the applied load with the maximum unfactored dead load shear equaled 500 kips, which was 54 percent higher than the recommended ultimate design shear of 325 kips. The maximum deflection at this load was 3.3 in., of which 2.4 in. were recovered after the applied load was removed.

The modified girders performed effectively under applied loads. Therefore, end blocks may be removed from continuous series 14 girders with normal diaphragms. The study recommends that one series 14 continuous girder without end blocks be designed and monitored through the various stages of construction and service in another bridge.

ACKNOWLEDGMENT

This study was carried out by the Department of Civil and Environmental Engineering at Washington State University. The researchers wish to express their gratitude for the cooperation extended by the Washington State Department of Transportation. Special appreciation is extended to Stew Gloyd and Edward Henley of the Department of Transportation for their valuable technical assistance. Acknowledgment is also due to Rick Anderson of Concrete Technology Corporation of Tacoma for his suggestions in conducting a destructive test.

Special gratitude is due to the Washington State Transportation Center (TRAC) for its support of this research. Thanks are extended to Bill Carr and Scott Rutherford for their interest in this project. Appreciation is also due to FHWA for its support of the research program under which this project has been conducted.

The cooperation of Morse Brothers of Portland, Oregon and D. B. Murphy Construction of Federal Way, Washington during the field test is appreciated. Appreciation is also due to Mr. Chuck Prussack and Central Premix Concrete Co. of Spokane for their assistance and contribution to the laboratory test.

Special thanks is extended to the faculty and staff of Department of Civil and Environmental Engineering. The efforts of H. C. Sorensen and R. Pellerin in conducting the full scale test are greatly appreciated.

The efforts of technicians Tony Nilson, Norman Martel and Tommy Hellesto and his staff are appreciated. Finally, a special thanks to

Kevin Cullinan, a former graduate student at WSU, for his efforts and help during the field test.

TABLE OF CONTENTS

LIST OF TABLES

LIST OF ILLUSTRATIONS

CHAPTER 1

INTRODUCTION

Prestressed concrete, because of its structural efficiency and because it is more cost--effective than reinforced concrete, is widely used in long span constructions. The basic principle of prestressing was known several centuries ago. It involves the intentional creation of permanent stresses in a structure or assembly for the purpose of improving its behavior and strength under various service conditions. Modern day structures that use high strength materials have created an increasing demand for prestressed concrete. Although prestressed concrete has a wide range of applications, the most significant of these is in bridge construction. For bridges with unusual layouts and long spans, the posttensioning method of prestressing is commonly used. Otherwise, precast and pretensioned, prestressed concrete girders are used for spans between 40 ft. and 140 ft. This research deals mainly with a particular type of precast and pretensioned, prestressed concrete girder.

Standard AASHTO and PCI girder types I through VI were developed in the early 1960s. Since the mid-1950s, the state of Washington, like the states of Illinois, Colorado and Texas, has adopted its own standards for these girders. These I-shaped girders have proved to be extremely efficient due to their 5-in. thick web and small flange fillets. These girders carry thick sections at the ends. This provision is thought to be necessary for the distribution of prestressing force. Such a portion of any prestressed concrete structure that is thickened or enlarged to be rectangular is known as the end block. In the case of posttensioned systems, the end blocks provide sufficient room for embedding the bulky

anchorage hardware. The transfer of force in posttensioning systems is through bearing. On the other hand, in pretensioning systems, the prestress is transferred through the bond between the concrete and the prestressing stands over a short length known as the "lead-in-zone." Hence, mechanical anchorages are not required. As a result, pretensioned and precast bridge girders without end blocks have become the state of the art.

The possibility of eliminating end blocks from the WSDOT series of bridge girders has been under study for five years. Previous investigations have established that end blocks can be eliminated when the girders are simply supported.

This investigation focused on the elimination of end blocks when these girders have live-load continuity.

Continuity between precast girders can be achieved in many different ways. The most commonly used method is the placement of the deformed bar reinforcement in the situ-cast deck slab and diaphragm.

Fig. 1.1 shows the construction sequence that results in continuity under live load. Each precast, prestressed girder is cast and erected on temporary supports. The temporary supports carry the dead weight of the girders, the slab and the intermediate and end diaphragms. Twenty-four hours after casting, the intermediate and end diaphragm reinforcement in the slab and the diaphragms are arranged. A minimum of 30 days after the release of the prestress, the diaphragms at the continuous end are placed up to about half the depth. After the concrete in the diaphragms has attained a minimum compressive strength of 2000 psi the remaining portions of the diaphragms and the slab are placed. The temporary supports have been removed after all the

concrete, except that in the traffic barrier, has been in place and has developed the specified strength. Depending on the location and the orientation of the cross beam, the WSDOT standard practices include the following types of continuity joints:

1. intermediate hinge diaphragm (Fig. 1.2),
2. raised X-beam [41], and
3. drop X-beam with a 15-degree maximum skew end cast into the diaphragms about 1-1/2 in. deep [41].

The first two of these are square end butt joints. In Figure 1.2, the diaphragm is connected to the supporting beam through hinge bars, which extend up to half the depth of the diaphragm. Thus, the diaphragm is free to rotate about these bars, which serve as hinges. The bars, which extend from the end of each of the girders, are embedded in the diaphragm. The rotation of the diaphragm induces rotation of the composite section, which consists of the slab and the prestressed girder. Therefore, the moment caused by the externally applied loads is resisted by the girders on either side of the diaphragm, but no moment is transferred to the supporting beam. The diaphragm at the intermediate support is commonly referred to as the intermediate hinge diaphragm. This study examines the feasibility of establishing continuity through an intermediate hinge diaphragm connection for girders without end blocks.

End blocks have been successfully removed from AASHTO girder types I through VI, which have 8-in. webs, and from other girders with 6-in. webs. Their removal results in uniform web thickness throughout the span length. A typical WSDOT series girder has 5-in. webs with end zones enlarged from 12 in. to 16 in. Series 10 and 14 girders, which

are typically used for long span bridges, have 16-in. and 12-in. wide end blocks, respectively. The AASHTO specifications do not require end blocks to be provided where all tendons are pretensioned, seven wire strands. Since, WSDOT's I-section girders have a higher depth to web ratio than AASHTO's series, end blocks have been employed in the state of Washington.

At an intermediate support, the highly stressed end zones of the girders may be subjected to a moment that results in compression in the bottom fiber of the girders. The diaphragm, which provides the continuity, is in compression, while the slab provides resistance for the tensile zone. Previous research has shown that the continuous joint at the interface of the girder and the diaphragm fails, even though the concrete strength of the diaphragm is less than that of the girder. With the elimination of the end blocks from the girder, the shear at the interface becomes more critical than before. This concern about the reduction in the shear friction area due to elimination of the end blocks is addressed in this study.

This study explores the possibility of eliminating end blocks from continuous, series 14 WSDOT girders. An actual field test was the first stage of the work plan. The stress distribution in the end zones of a series 14 girder with end blocks and two series 60 girders without end blocks was monitored through various stages of construction and finally, under service load conditions. In the second stage of this research a laboratory test was conducted. This involved destructive testing of a series 14 girder without end blocks. The final phase of the work plan included conclusions and recommendations based on the findings of the destructive test.

the work plan included conclusions and recommendations based on the findings of the destructive test.

Chapter 2 focuses on earlier research and a literature review. The effects of creep and shrinkage on prestressed concrete structures are studied in Chapter 3.

Chapter 4 describes the field test in detail, and Chapter 5 presents the results.

The details of the destructive laboratory test are presented in Chapter 6. Chapter 7 presents interpretation of the corresponding data. The conclusions and recommendation are given in Chapter 8.

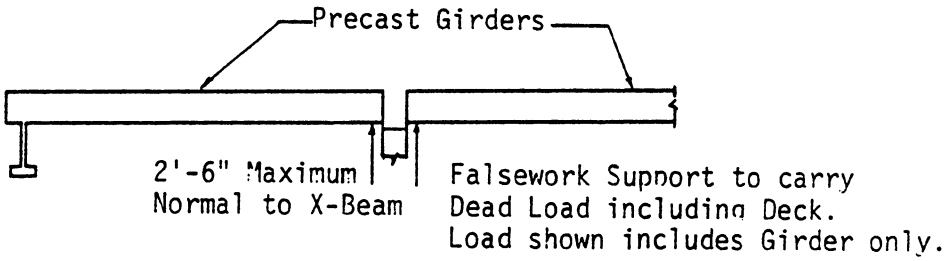

STAGE 1 - SET GIRDERS IN PLACE

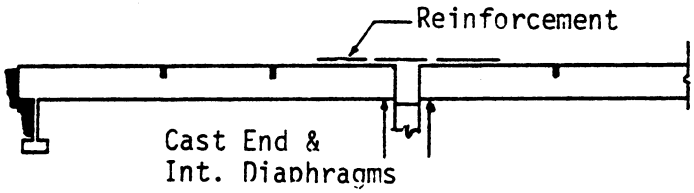

STAGE 2 - POUR DIAPHRAGMS & PLACE REINFORCEMENT

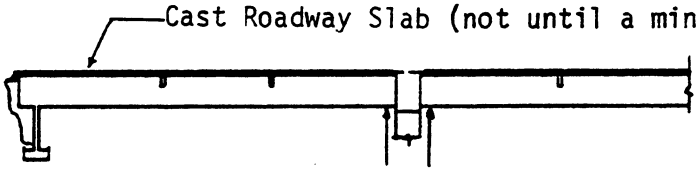

STAGE 3 - POUR ROADWAY SLAB

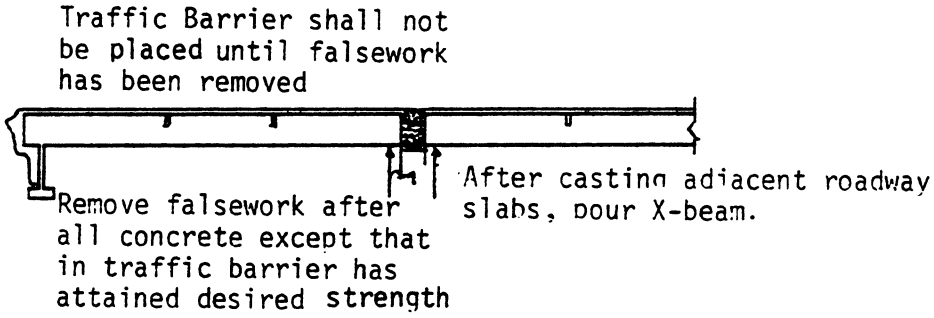

STAGE 4 - POUR X-BEAM & TRAFFIC BARRIER

Figure 1.1 Sequence of Construction

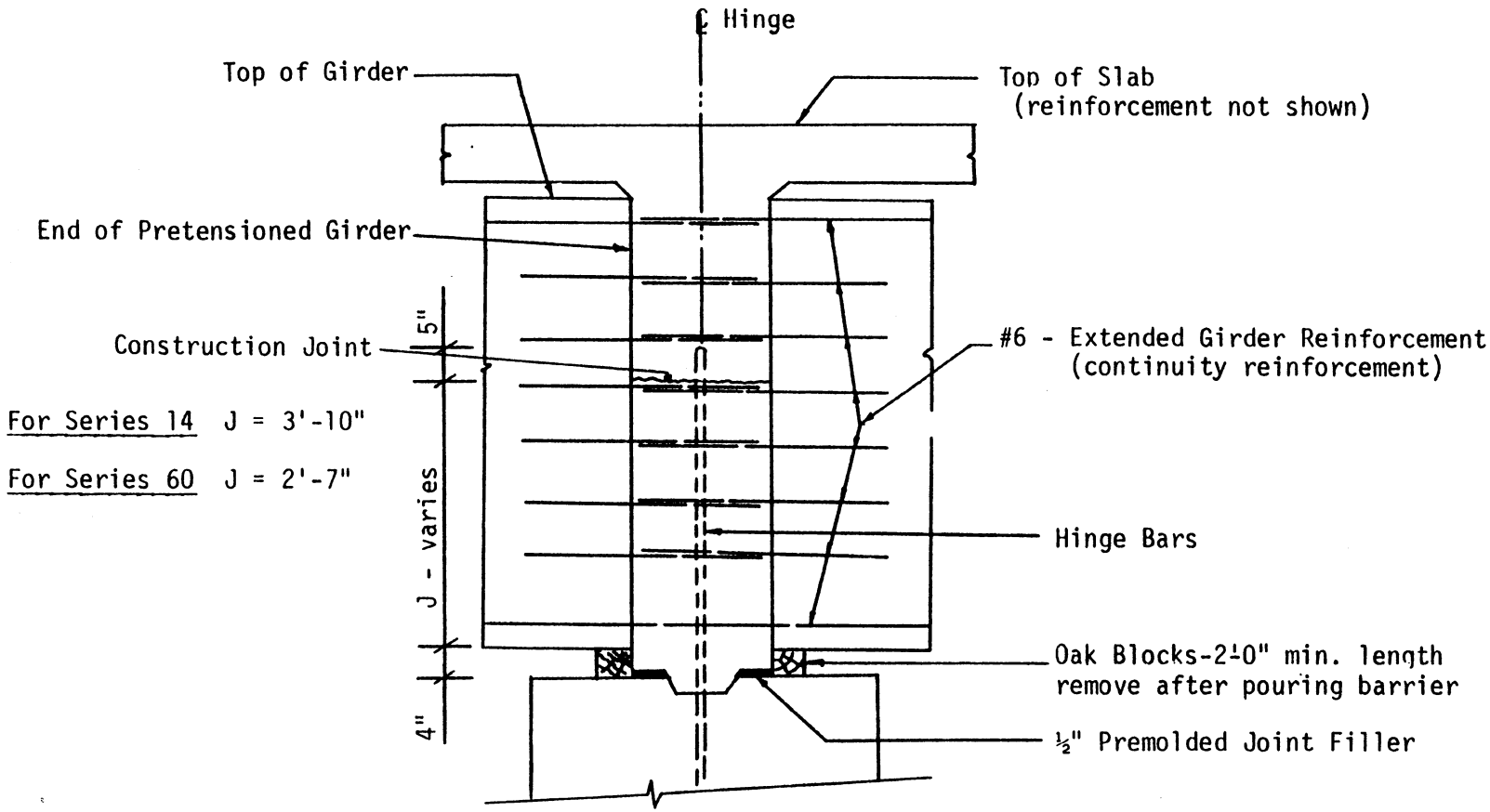

Figure 1.2 Typical Hinge Section

CHAPTER 2

LITERATURE REVIEW

The advantages in providing structural continuity over an intermediate support in bridges built with prestressed, precast girders are obvious. Some of these are as follows.

1. The reduction in bending moment and deflection due to structural continuity allows use of slender and, thus, lighter girder sections.
2. The elimination of joints in the deck provides a smooth riding surface for vehicles. It also prevents seepage of water and salts through the deck slab into the piers and girder ends. Thus, the cost of maintenance is reduced and durability is improved.
3. In the case of overloads, moment redistribution without serious distress is possible with continuity over the support.
4. In the case of prestressed concrete, the ultimate load carrying capacity of a structure can be significantly influenced by the proper selection of the cable profile.
5. Studies have shown that continuity in bridges helps in resisting the sesmic forces efficiently.

The different methods several countries presently use to establish continuity for prestressed girders have their own advantages as well as disadvantages [31]. Most often in this country, deformed bar reinforcement is placed longitudinally in the deck slab across the intermediate piers supporting the girders to create continuity from span to span for live loads. The effectiveness and reliability of such a connection has been well proven.

The concept of continuity in prestressed concrete structures came to light in the early 1950s. Parme and Paris [30] presented a design method for continuity in prestressed concrete structures that assumed that the curved cables exert a continuous upward force on the concrete along the entire length of the member. Raud [32] argued that such an assumption was not correct. He added that not only the normal pressure created by the cables but the eccentricity of the cables would affect the bending moments in continuous structures. Significant contributions were made to the subject after extensive testing was done in the late 1960s at PCA [31]. The following important conclusions were drawn in these studies.

1. Adequate continuity and negative support moment resistance is possible with the placement of deformed bar reinforcement in the deck slab across the piers supporting the girders.
2. Necessary plastic hinges can be developed to form a collapse mechanism and moment redistribution with this type of connection.
3. The effects of shrinkage and creep can be eliminated and controlled. These do not influence the ultimate load carrying capacity of a continuous girder.
4. The behavior of this type of bridge is essentially elastic when the bridge is subjected to design service loads and appreciable overloads.
5. The torsional stiffnesses of the girders have a considerable effect on the lateral load distribution of concentrated loads applied to the bridge deck structure.

6. The intermediate diaphragm has an appreciable effect on the lateral distribution of loads if it is fully continuous across the width of the bridge.
7. The prestress effect can be ignored when a low percentage of deck steel (up to 1) causes the tension zone to control the capacity of the section.

Several tests were carried out on this type of bridge, but their work scopes were limited.

1. The girders used in these tests had only straight strands. There were no girders with harped strands.
2. The AASHTO-PCI standard girders were considered.
3. The end regions of the girders were designed as reinforced sections to ensure that the ultimate stress in the top fiber at ultimate moments would be greater than the modulus of rupture, which was assumed to be equal to $7.5\sqrt{fc'}$.
4. One important point was the recommendation and development of positive moment connection. The AASHTO Specifications for Highway Bridges [1] recognize and recommend such a connection.

Freyermuth [15] concluded that full compression would not occur at beam ends due to the strand transfer length, and hence, negative live load and prestress would not cause high compression. The diaphragm at the support would strengthen the area by providing lateral restraint. As a result, the ultimate strength of the section at the pier would not be affected.

Along with continuity in bridges built with prestressed, precast girders, the elimination of end blocks is also an important consideration. Many researchers have recommended elimination of the end

blocks in pretensioned girders. The anchorage zone stresses in a prestressed concrete member has been a problem of major concern. The study by Guyon [17] and Magnel [25] was the pioneering work. But the first significant contribution towards elimination of end blocks in a pretensioned girder was by Marshall and Mattock [26]. They concluded that end blocks were not necessary for the satisfactory performance of the end zones of pretensioned, prestressed girders and that a small amount of vertical stirrup reinforcement would exert adequate control on the cracking in the end zones.

Investigations by Gergely, Sozen and Siess [16] demonstrated that transverse tensile stresses aimed away from the line of the load were greater for an end block with a rectangular section rather than with an I-section. This supports the contention that end blocks are unnecessary for satisfactory performance. The next significant experimental work concerning the stress distribution in pre-tensioned beams came from Arthur and Ganguli [5]. They observed that tensile strains were not at their highest when the prestressing force was concentrated in both flanges. Hawkins [19] also suggested that for I-beams, rectangular end blocks should be avoided.

The experimental work done by Marshall and Mattock [26] and Arthur and Ganguli [5] considered only simply supported girders. Of these two, Arthur and Ganguli considered I-sections with web thicknesses of 3, 2-1/2, and 2 in. However, the beam's depth was only 12 in. and the span was 9 ft. Thus the work did not reflect field conditions.

A comparison of the structural efficiency and cost effectiveness of selected prestressed, precast girders commonly produced in the United States indicated that the Bulb-T, Washington state series and the

Colorado state series are more efficient structurally and economically than the AASHTO standard sections (32). The webs of the Washington series, Colorado series and the Bulb-T series are only 5 in., which means they are thinner than AASHTO standards. Of all these 5-in. web girders, the Washington series girders have the highest depth to web ratio, and hence, are more critical. Therefore the Washington series has retained the end blocks as a measure of safety.

Sarles and Itani [38] applied the finite element method to study the anchorage zone in prestressed members. They particularly related their work to Washington state girder series 10 and 14. The study recommended elimination of end blocks from eccentrically loaded members. An experimental study by Itani and Galbreith [20] on Washington series 14 and 10 girders without end blocks determined that the elimination of end blocks from these girders is possible as long as the girders are simply supported.

The AASHTO specifications [1] do not require end blocks in pretensioned girders. Most of the research on end blocks accounts for concentrated prestressed force acting at the end of the beam. In the case of a continuous girder, there is an external moment in addition to a concentrated force at the end of the beam. In the particular case of pretensioned girders, the force is transferred to the concrete over a certain length of span. Such a consideration and the continuity connection involving thin web sections has not been dealt with directly.

The particular method of construction for continuous bridges built with pretensioned girders has to account for shear friction present at the interface of the prestressed girder and the intermediate diaphragm.

The removal of end blocks causes reduction in the area available for shear transfer.

Chapter 3

CREEP AND SHRINKAGE

This chapter deals with the effects of creep and shrinkage. The scope of the chapter is limited to a brief description of studies related to these phenomena. First, the effects and importance of creep and shrinkage on bridges built with pretensioned girders and cast-in-place roadway slabs are described. The research and study related to the process of creep and shrinkage are discussed in the next section. Then the experimental and theoretical study conducted to evaluate the effects of creep and shrinkage on concrete structures is discussed. Finally, Mattock's pioneering research related to the present study is briefly described.

Creep and Shrinkage Effects on the Continuous Joint

The effects of creep and shrinkage become significant in the case of prestressed concrete because of the prestressing of the concrete and steel. Loss of prestress results in excessive deflection and moment redistribution, which are important design considerations for a prestressed concrete bridge.

Of special interest to this study is the influence on continuous joints of the creep deformation of a prestressed, precast girder caused by applied force and by differential shrinkage between the precast girder and the cast-in-situ roadway slab. In this type of construction, the prestressed, precast girders, while they are simply supported, are free to rotate at the ends. Creep of the girder will result in an increase in elasticity. As a result of creep, the final rotation at end of the girders will be greater than the initial slope. The deck slab

and the end diaphragm together form a continuous joint over the support. When the deck slab is placed to form a continuous joint, the adjacent ends of the girders are restrained. As a result, a moment is established in the end of the girder that prevents free rotation of the ends of the girder.

The effect of the different shrinkage is the opposite of the effect of creep due to the action of prestress force on the girder. The girders are precast in a prestressing yard. There is a time lag between the manufacturing and erection of the girder and the casting of the roadway slab. Since shrinkage is dependent on the age of the concrete, the new concrete of the deck slab will shrink more than the oldest concrete of the girders. The bond between the slab and the girders will not allow the deck slab to shrink freely. As a result, tensile stresses will be induced in the deck and the top portion of the girders, while at the same time the bottom part will experience compressive stresses. The partial fixity at the end of the girder due to the continuous joint causes negative restraint moment at the end of the girder.

Although several researchers have emphasized the importance of considering creep and shrinkage in design, the mathematical analysis and design of structures remains a formidable task.

Evaluation of Creep and Shrinkage Coefficient

Creep is the time-dependent course of strain under sustained stress, while relaxation is the change in stress under sustained strain. The concept of creep is simple to understand and analyze when it is broken into its several components. Creep can be considered as the following:

$$\epsilon_c = \epsilon_d + \epsilon_i + \epsilon_{f_b} + \epsilon_{f_{dr}}$$

where, ϵ_c = creep strain

ϵ_d = strain due to delayed elastic deformation

ϵ_i = strain due to rapid initial strain

ϵ_{f_b} = strain due to basic flow

$\epsilon_{f_{dr}}$ = strain due to drying flow

The strain due to delayed elastic deformation ϵ_d, is also referred to as elastic post-action, or post-effect. The delayed elastic deformation depends on the porosity of the body. Thus, in the case of steel, such an effect does exist, but its influence is very low. On the other hand, since concrete is a porous material, it exhibits considerable delayed elastic deformation. The reversible strain that appears with some delay is due to the presence of viscous fluid in the voids. When the load is applied, the elastic deformation of solids is resisted by viscous fluid. As time passes, the viscous fluid gradually transfers the load to the solids.

The irreversible part of creep strain is known as flow. Even after only one day of sustained load, a significant amount of irreversible strain develops. This is termed "rapid initial strain" [35]. The rapid initial strain is particularly significant for low strength concrete as well as for younger concrete. Plastic flow is the other part of irreversible strain that occurs in concrete.

Early investigators believed that plastic flow was caused by slips produced in the crystal lattice along critical planes. However, such a hypothesis cannot be [35] applied to concrete for the following reasons:

1. Concrete shear strength is higher than its tensile strength. If the hypothesis were true, the result would be a separation of the material before creeping.
2. Concrete creeps even at very low sustained loads.
3. Creep strength and strains for loads ranging from 20 to 50 percent of the ultimate strength are linearly dependent.
4. Creep strains produce changes in bulk concrete.

Different hypotheses are proposed on the mechanics of concrete creep deformation. They all ascribe the cause of the phenomenon to water migration from cement stone. When this takes place without exchange between the concrete and the environment, it is called drying flow. This significant separation of plastic flow was proposed by Neville [35].

The following is a summary of the components of creep.

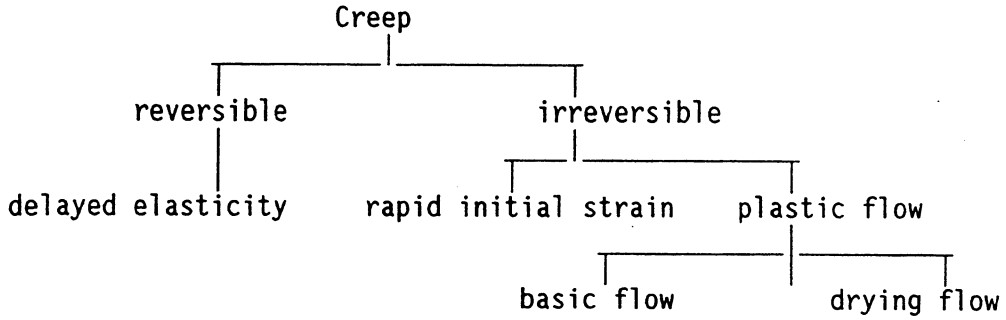

The creep and relaxation phenomenan can be explained with help of rheological models. Springs, dampers, and frictional components are the basic components of a rheological model. Different combinations of these components represent the elastic, plastic, and viscous properties of a body. Concrete exhibits elastic, viscous, and plastic properties. These are represented by complex rheological models.

Estimation of creep and shrinkage involves several variables. Researchers have suggested different methods to analyze creep effect.

In general these methods can be divided into the following categories [35].

Level 1 methods.--An approximate estimation of the final deformation can be obtained by using such methods. These methods consider a few parameters such as thickness of a member, relative humidity, and age of the concrete.

Level 2 methods.--All significant parameters are considered in estimating the magnitude of the deformations. These parameters have evolved on the basis of diagrams or equations.

Level 3 methods.--These procedures are used for precise estimation of creep effects. Normally these are employed for special problems in which creep and shrinkage effects are unusually important, such as construction of a bridge by the cantilever method.

The methods can also be classified based on the actual procedures involved in applying the methods. In some methods, the time-dependent deformations of concrete are a product of several co-efficients representing different principal parameters, such as the age of the concrete, relative humidity, and the thickness of a concrete member.

In some cases, creep effect is presented as the sum of the components of creep, which are delayed elasticity and flow or basic flow plus drying flow. Table 3.1 presents an overview of the few methods.

The ACI 209 [1] method is based on Product Format. The final creep coefficient is expressed as a product of several factors that are applied to the ultimate value of the creep and shrinkage coefficient. The ultimate creep coefficient is the ratio of the ultimate strain to the initial strain. These experimental values are determined as a

product of several correction factors and a constant. The corrections account for the following:

. the age of the concrete at load application

. relative humidity,

. average thickness of the concrete,

. the consistency of the concrete based on slump,

. the content of fine aggregate particles,

. the air content of the concrete,

. curing periods, and

. cement contents.

The ACI 209 model is simple and representative of many practical situations.

The CEB-FIP model code 1978 and the German Prestressed code DIN 4227-1979 are based on the Rusch-Jungwirth method. The method assumes that creep is made up of delayed elastic strain and flow.

The drying shrinkage term in Bazant's [2] method is dependent on ζ_{sh}, which is shrinkage-square half time and which accounts for size effects. The shrinkage-square half time characterizes the amount of time in which one-half of the final shrinkage-square value is attained. The concept of shrinkage-square half time is based on diffusion theory.

A brief review of realistic methods for computing creep and shrinkage was given by Rusch, Jungwirth and Hilsdorf [35]. Out of the different methods discussed the Dischinger's method was one of the first to calculate creep effect with the aid of a differential equation. This approach did not consider delayed elasticity. Such an effect was observed only 20 years later. But the original Dischinger equation can be modified to account for the delayed elasticity component of creep.

An important improvement upon the Dischinger method was provided by Nielson [29]. This method is based on linear visco-elastic behavior of concrete. Trost [1] suggested a time dependent relationship between stress and strain. This method is simple to apply, even for statically indeterminate structures. Jevtic [1] simplified the stress-strain relationship of creep using integral and differential equations. The coefficient in these methods can be determined by tables and curves provided by Rusch-Jungwirth. Some of these coefficients are increased by about 30 percent in CEB-FIP and DIN codes [35].

The ACI 209 method [2] is not suitable for the prediction of sudden change in stress and in the case of unloading. The Rusch-Jungwirth method provides a good estimate of creep under these circumstances. The assumption that the flow is represented by a single function is suited for some computational methods.

As pointed out by Bazant and Panula [2], the ACI 209 and CEB-FIP models make no distinction between drying creep and basic creep. The coefficient introducing humidity and size effects multiplies a term that is supposed to represent both the drying and basic creep. The CEB model separates strain in four parts. Although the humidity and size effects do not enter into reversible strain, they are considered in irreversible strain. The irreversible strain term represents basic strain as well as a term that is independent of humidity. The method suggested by Bazant and Panula [2] assumes creep is made of basic and drying components.

Muller and Hisdorf [42] compared methods for predicting the creep coefficient of structural concrete with experimental data. The following methods were compared with the statistical approach:

1 ACI committee 209 (ACI),

2. Bazant and Panula (Bap),

3. CEB/FIP model code 1978 (C78),

4. German Prestressed Concrete Code (DIN),

5. CEB/FIP recommendations 1970 (C70), and

6. British Concrete Society (BCS).

The comparison led to the following conclusions.

1. More complicated procedures were not necessary for more accurate results. Except for Bap, the difference in accuracy between the various method was minor.

2. The ACI method was weak for older concrete at loading and for basic creep. The Bap method was erroneous for very young concrete. The C78, C70 and DIN methods showed relatively poor results for drying creep, but C78 and C70, particularly, agreed well with creep data for basic creep. The average errors for the final values of the creep functions were similar.

3. ACI and C70 overestimated the effect of member size, while Bap, C78 and DIN estimated it lower than the experimental data.

4. The effect of relative humidity was over-estimated by all methods.

5. The prediction methods left room for improvement.

6. Such improvement might include better optimization of the methods, including the relations for predicting elastic strains.

7. Because of the large errors in the prediction of creep functions for creep sensitive structures, they suggested that an analysis be carried out both for lower and upper bound creep functions.

Nielsen [42] presented a composite theoretical method in which only three parameters control the creep function. These parameters are

Young's modulus, the delayed elasticity coefficient, and the flow modulus. These are all related in a simple way to concrete composition to account for the consolidation effect. According to him, this is a more logical approach than the approach of many codes. The illogical approach of codes lies in the fact that the creep functions are constructed by the multiplication of a quantity that is often evaluated accurately by another quantity that is determined by a crude estimate of a strength data.

Research on Structural Members

Tadros, Gahli and Dilger [39] used a step-by-step method to account for the effects of concrete creep and shrinkage and relaxation of prestressing steel in an analysis of composite frames. The method assumes linearity between creep and stresses and thus, the principle of superposition is considered to be valid. The stresses and deformation at the end of each time interval are calculated in terms of those obtained in the first interval and the stress increments that occurred in the preceding intervals. The analysis is thus simplified to an incremental linear analysis. The researchers concluded that simplicity and versatility are two major advantages of such an approach. The illustration by the authors, which included an analysis of a two-span prestressed bridge, pointed out the need for an accurate evaluation of stresses and deformations due to creep and shrinkage of concrete and relaxation of steel.

Roelfstra [34] developed a computer program to simulate the construction of a bridge by the cantilever method. These types of bridges show considerable deflection due to creep and shrinkage. This time dependent deformation was computed according to the CEB-FIP model

code for concrete structure. The program predicts deformations, allowing adjustment of shuttering height and correct alignment of the bridge.

Hass [18] pointed out the importance of properly modelling a construction sequence and the corresponding load history in computer software for the analysis of creep and shrinkage. His findings were based on a theoretical and experimental study of a prestressed concrete bridge.

Khalil, Dilger and Ghali [23] used a step-by-step method that would account for the construction sequence to analyze prestressed concrete frames. Creep and shrinkage of concrete and relaxation of steel were also considered. The computer analysis accounted for variation in the geometry, loads and support conditions. The study concluded that creep and shrinkage can be controlled by proper selection of construction sequence and schedule.

Dilger's [13] simplified approach was based on the Muller-Breslau principle for analyzing time-dependent forces developed in continuous concrete structures. In his approach, the relaxation coefficient is used to account for creep and shrinkage.

Neville , Dilger and Brooks [28] dealt extensively with the effects of creep and shrinkage on prestressed and continuous structures.

El-Shafey, Jordan and Loov [14] conducted field experiments to measure time-dependent deflections of prestressed concrete members. The field strains and the predictions by the CEB-FIP and ACI-209 procedures were compared. Although measured strains did not compare well with theoretical predictions, good agreements were found for deflection. The ACI-209 procedures overestimated the final deflection.

Jevtic [22] conducted several tests on prestressed concrete beams for determining deflection, relaxation and failure under long-term loadings. The predictions of deflection and relaxation by the CEB procedures were found to be sufficiently accurate for young concrete.

Branson, Meyers and Kripanarayan conducted [12] a thorough study of the time-dependent deformation of noncomposite and composite prestressed concrete structures. The study included a material study, laboratory tests on composite and noncomposite beams, and field measurements of the camber in prestressed girders. The study resulted in methods for predicting material behavior and structural response and design procedures for calculating strength and elasticity.

In reporting some observations on structures, Russell, Meyers and Day [35] commented on creep and shrinkage of concrete. The authors suggested guidelines for planning a field measurement program. One of the bridge structures they mentioned was included in study by Pauw. In 1971, Pauw conducted deflection measurements on a five-span box girder bridge. He found that there was no significant deflection after eight months and concluded that the ultimate sustained load deflection can be predicted with a reduced modulus value. Data collected from the monitoring of prestress and concrete bridges with solid sections, led to the conclusion that environmental conditions affect the creep and shrinkage of concrete.

Russell and Shiu [36] instrumented concrete structures to measure instantaneous shortening, creep and shrinkage. Of the bridges measured, one was a precast, longitudinally posttensioned, concrete box girder bridge. The 1170-ft. bridge consisted of five spans constructed by the cantilever method. Strains of up to 750 millionths were measured after

one and one-half years. They observed that changes in strain gradients occurred as the cantilever was segmentally erected and that large strain gradients resulted in large deflections at the end of the cantilevers.

Jávor [21] observed that concrete creep in a bridge erected by the cantilever method settled after four years. He conducted field experiments on various prestressed bridges through various construction stages. The creep coefficient for five-year old concrete in a highway bridge was 1.78, while in a railway bridge it was 2.06.

In composite bridges, casting the slab caused an elastic deflection and a corresponding dependent prestress gain, a time dependent deflection, and prestress gain due to differential shrinkage and creep. The ultimate loss of prestress at the midspan of the bridge girders caused by the composite slab was 11 percent.

Research on Pretensioned Girders with a Cast-in-Situ Slab

Mattock [27] conducted an experimental and analytical study to determine the influence on a continuous joint over a long time of the creep deformation of a prestressed, precast girder when the creep was caused by applied force and the differential shrinkage between the precast girder and the cast-in-situ roadway slab. His experimental findings led the two-step practical design procedure below.

1. The restraint moments caused by the prestressing force and dead load moments are calculated. This can be accomplished by using any statically indeterminate method based on the theory of elasticity. The prestressing force causes moment if it is eccentrically applied.

2. The restraint moments caused by creep of the precast girder after the erection of continuity are then obtained by multiplying the moments, calculated in step one, by $(1-e^{-\phi})$

where, e = the base of Naperian logarithm

ϕ = the ratio of creep strain to elastic strain

A similar approach is used to calculate restraint moments caused by shrinkage.

1. The differential shrinkage moment applied to the girder along its entire length is given by

$$Ms = \epsilon_s E_B A_B (e'_2 + t/2)$$

where, Ms = the differential shrinkage moment applied to the girder along its entire length

ϵ_s = differential shrinkage strain

E_B = elastic modulus for deck stab concrete

A_B = cross-sectional area of deck slab

e'_2 = the distance from the centroid of the composite section to the top of precast girder

t = the thickness of the deck

2. The restraint moments are obtained by multiplying Ms by $(1-e-\phi)/\phi$.

One of Mattock's most important suggestions was the necessity of creating a positive moment connection at the bottom portion of the continuous joint. In the absence of such a connection, the positive restraining moment results in cracking of the diaphragm. The importance of the positive connection is also recognized by AASHTO [1]. His study further concluded that the ultimate load carrying capacity of the girders is not affected by creep and shrinkage, but restraint moment and cracking do influence the behavior of the girders.

Freyermuth [15], in his discussion about the design of continuous highway bridges with precast, prestressed concrete girders, emphasized the importance of creep and shrinkage effects. This study was the product of the above mentioned research at PCA [27]. Freyermuth suggested that for design purposes, 20 years of creep could be considered the design creep and that within 28 days, 40 percent of the ultimate creep would take place. As a result, the positive moment connection recommended by Mattock [27] should be capable of handling 60 percent of the resultant creep and shrinkage effects. Note that although creep and shrinkage tend to counteract each other, they have a significant role in the design of continuous bridges built with prestressed, precast girders.

Table 3.1

Methods to Estimate Creep

Method	Year	Level	Principle
CEB 70	1970	2	product
Meyers et al.	1972	1-2	-------
Rusch-Jungwirth	1976	2	sum I*
BCS	1977	1-2	-------
Branson	1977	2	product
CEB 78	1978	2	sum I
ACI 209	1972	2	product
Din 4221	1979	2	sum I
Bazant-Panula	1979	3	sum II**
Bazant-Panula	1979	2-3	sum II

*Sum I = delayed elastic strain + flow

**Sum II = basic creep + drying creep

CHAPTER 4

THE FIELD TEST

For the field test, a bridge consisting of series 60 girders without end blocks and series 14 girders with end blocks was identified. At two locations where live load continuity between adjacent spans was established, the girders were instrumented. The main objective of the field test was to establish a basis for the destructive testing. The details and the procedure of the field test are described in the following sections.

Details of the Girders

A multi-span, prestressed concrete bridge, which would serve as a viaduct over a Burlington Northern railroad crossing (BNRRC), was chosen for the field test. This bridge is located on the SR501 in the city of Vancouver, Washington.

Figure 4.1 shows the layout of the bridge. Figures 4.2.a and 4.2.b show the framing plans of spans 1, 2 and 3 and spans 4 and 5. Girder 5D, which is one of the series 14 type girders with end blocks, forms a part of the continuous joint at Pier 5. At Pier 3, girders 2C and 3C, which are series 60 girders without end blocks, together with the deck slab, form a continuous joint. These girders were monitored for stresses in the end region adjacent to the continuous joint after the prestress transfer and during various stages of construction. These construction stages included erection of the girders at the site and casting of the deck slab and the diaphragms. The final stage of the field test was to monitor the strains while the bridge was subjected to service loads.

Girder 5D has 12-in. wide and 3-ft. 6-in. long end blocks on both ends. Each end block tapers down to merge with a 5-in. thick web over a transition length of 7 ft. 6 in. (Fig. 4.3). The total length of the girder is 131 ft. 9-3/8 in. It spans between bent 5 and bent 6. The girder is provided with sawteeth and extended bars at the end, which form a continuous joint at bent 5 (Fig. 4.4). The other end at bent 6 is simply supported. The girder has 46, 1/2-in., uncoated seven-wire prestressing strands, conforming to ASTM 1418/Grade 270. Sixteen of the strands are harped and are located in the web near the top flange. The remaining 30 straight strands are located in the bottom flange. In Figure 4.5, the section through the mid-span can be seen. The spacing of the stirrups in the end region is shown Figure 4.6.

Girders 2C and 3C (Fig. 4.7) are series 60 type, and span 49 ft. 5-3/4 in. and 49 ft. 11-1/4 in., respectively. These do not have end blocks and their webs are 5 in. thick throughout the length. Girder 2C spans between bent 2 and bent 3, while girder 3C spans between bent 3 and bent 4. Both ends of girder 2C and the end of girder 3C at bent 3 are provided with sawteeth and extended reinforcement. Girder 3C has a simply supported end at bent 4.

In Figures 4.8 and 4.9, the transverse view of the continuous end and the section at the mid-span are shown. Each girder is provided with 14 harped strands located in the web and four straight strands in the bottom flange. All strands are 1/2 in. in diameter, uncoated and made of seven-wires, meeting the specifications of ASTM 1418/Grade 270.

The continuity reinforcement and spacing of the stirrups in the end region are shown in Figure 4.10.

Instrumentation

The objective of instrumenting the end regions of the girders was to observe the stress pattern after the prestress transfer during various construction stages and under service load conditions.

Strains were measured on the surface of the concrete and on the shear reinforcement embedded in the concrete. Two types of strain gages were used for this purpose. On the surface of the concrete PL90-11 type wire gages were arranged to form a 45-degree rosette (Fig. 4.11). The shear-reinforcement was provided with QFLA-6-11 type foil gages (Fig. 4.11). The details of the strain gages and the procedures used for mounting and protecting these gages are given in Appendix A.

The rosettes on the surface of the concrete were located so that the principal stresses at various locations on the surface of the concrete in the end regions could be computed. No special consideration was given to the location of the centroid of the girders or the resultant prestressing force.

The stirrups were provided with strain gages at the centroid of the girder and at the centroid of the composite section. Some of these stirrups were provided with additional strain gages at the junction of the web and the bottom flange of the girder. The strain gages on the stirrups were provided with sufficiently long wires so that these could come out through the top flange of the girder after the concrete had set in the forms. The strain gage configuration on the surface of concrete and on the stirrups in girder 5D are shown in Figures 4.12.a and 4.12.b. The arrangement of the strain gages that was used to monitor girder 2C is shown in Figures 4.13.a and 4.13.b. Figure 4.14 shows the strain

gages on the surface of girder 3C. Gages were not provided on the stirrups of girder 3C.

Data Acquisition

The data related to strain gages, camber in the girders, and the strength of the concrete were collected at the following stages.

Manufacturing of the Girders

The girders were manufactured in Portland, Oregon, at the prestressing facilities of Morse Brothers Prestress, Inc. The production of girder 5D was undertaken on November 1, 1985. The 46-1/2 in. strands were tensioned so that the force in each strand was 28.9 kips. The stirrups with strain gages were placed at their designated locations. The remaining shear reinforcement, along with other reinforcement, was arranged and the form work was positioned in place (Figs. 4.15 and 4.16). This was followed by the steel reinforcement in the top flange. Concrete was placed and steam-cured at about 2 P.M. The next day at about 7 A.M., the form work was removed. The strain gages were then mounted on the surface of the concrete.

About 7 A.M. on November 4, the detensioning of the cables began. The pretensioned cables were cut with a torch so that the concrete would be subjected to precompression. The data from the strain gages were recorded immediately after the "prestress transfer" operation was over and while the girder was still in the prestressing bed. The girder was then moved to the storage area.

Similar procedures were followed for girders 3C and 2C. Weather conditions did not allow observations for microcracks. Some Figure 4.15

microcracks were observed after two to three weeks. As each girder was placed in storage, the camber in the girder was recorded.

Casting of the roadway slab

The girders were transported to the site on February 18, 1986, and erected in position. Figure 4.17 shows the portion of girders 2C and 3C at pier 3. The form work and reinforcement for the roadway slab and the diaphragm were built during the next week. In Figure 4.18, a portion of the reinforcement in the deck can be seen. However, the weather delayed the placement of the concrete until April 4, 1986. Concrete was pumped in the form work of the slab and the diaphragms and proper compaction was achieved with a heavy vibrator cum compactor (Fig. 4.19). All strains were measured using a 110 channel data logger. It was initialized before placement of concrete began. Strain gage readings were recorded after the deck was cast. Thus, the data recorded accounted for the weight of the wet concrete in the slab. They did not, however, account for the weight of the reinforcement.

Under Live Load Condition

The form work for the slab and the diaphragms was removed and traffic barriers were constructed. Before the bridge was opened for traffic on June 11, 1986, the live load test was conducted. The data logger was initialized before the test began.

A truck whose axle weight was known drove over the bridge with one side of the axle over the center line of the girders (Fig. 4.20). The truck was stopped at certain intervals and the engine was turned off.

The strain gage data were acquired at each interval. This was the last phase of the field test.

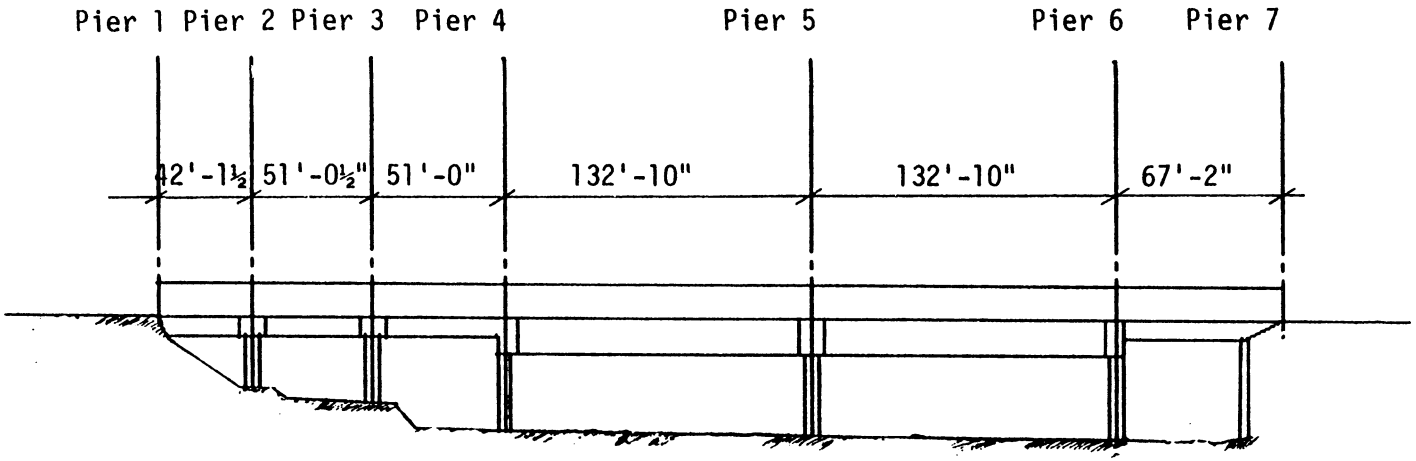

Figure 4.1 Field Test - Layout of BNRR Overcrossing - SR 501

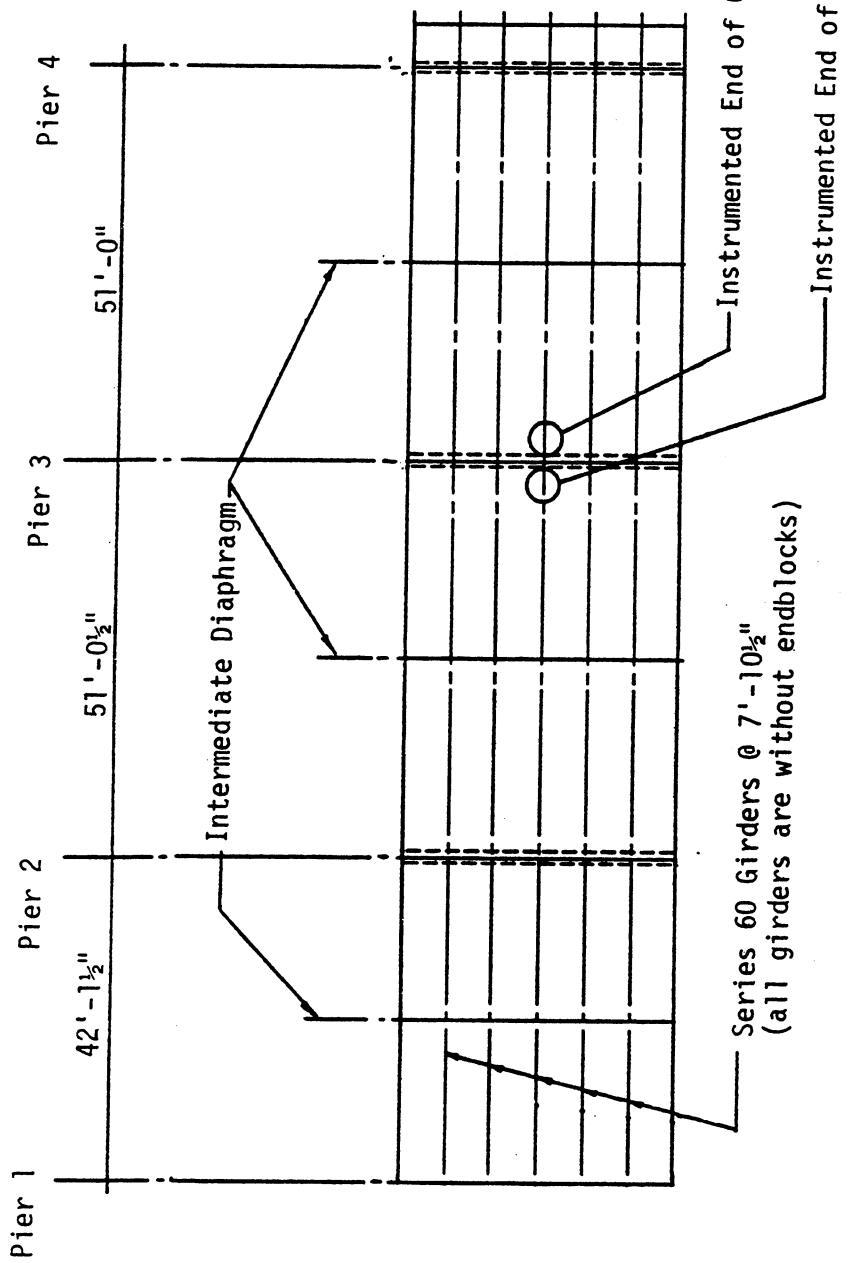

Figure 4.2.a Field Test - Framing Plan for Spans 1, 2, and 3

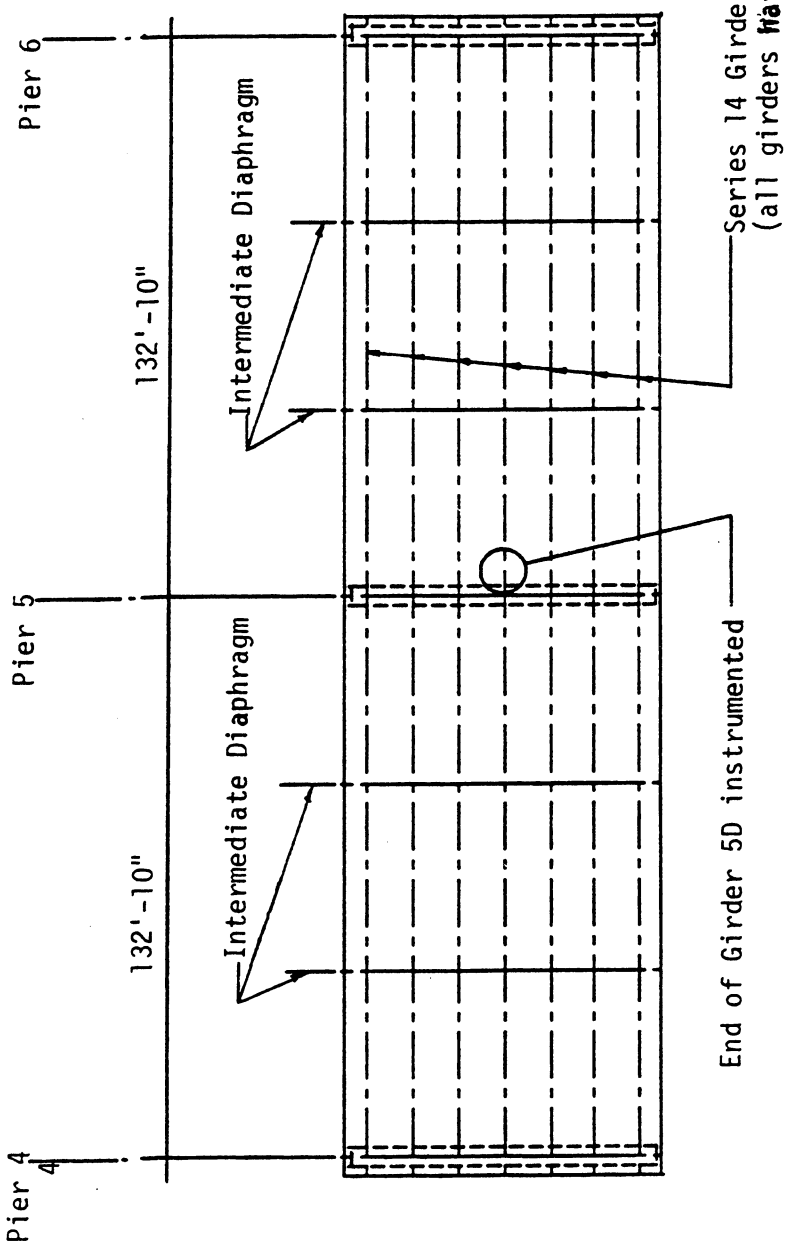

Figure 4.2.b Field Test - Framing Plan for Spans 4 and 5

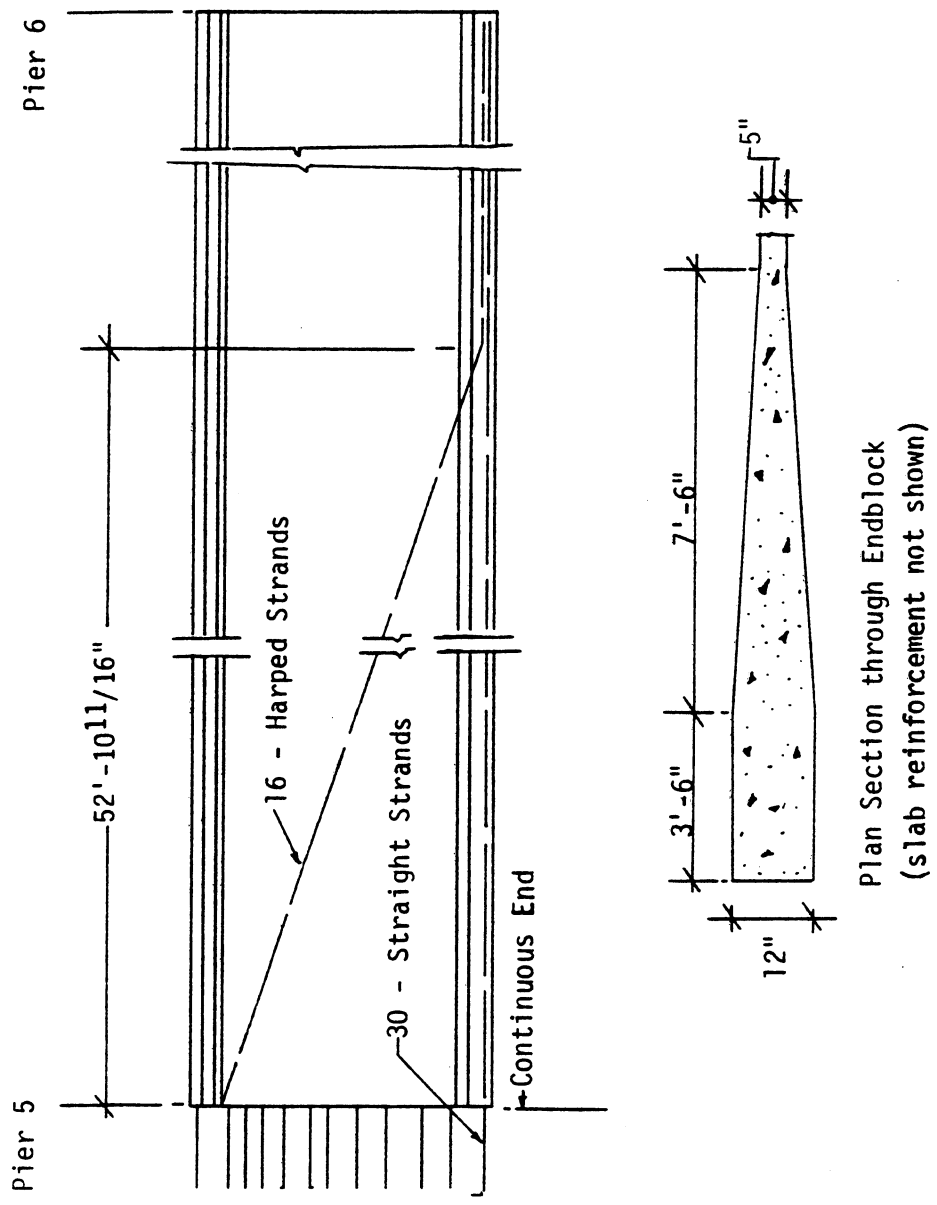

Figure 4.3 Field Test - Elevation of Girder 5D - Series 14 with Endblocks

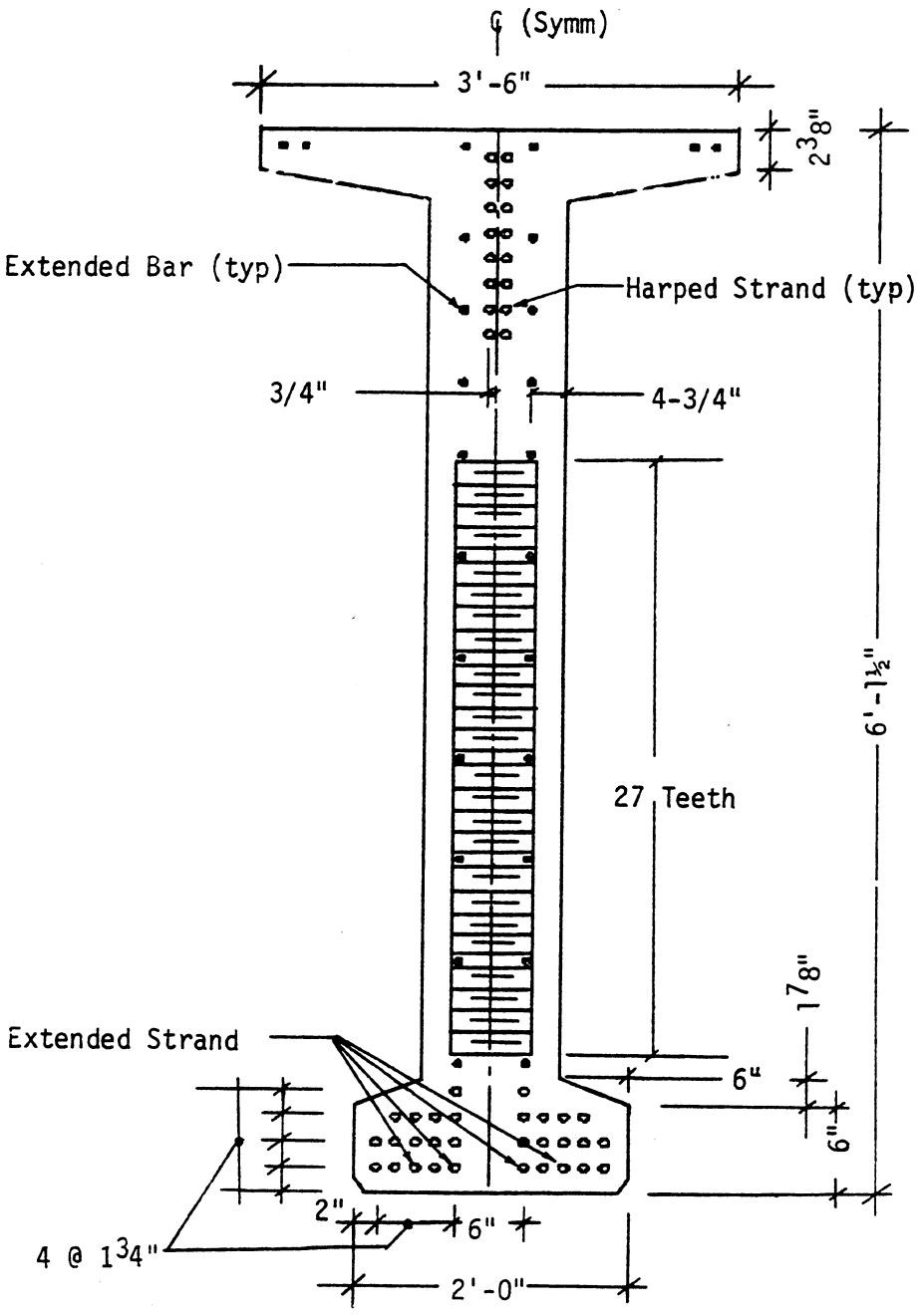

Figure 4.4 Field Test - View of the Continuous End of Girder 5D

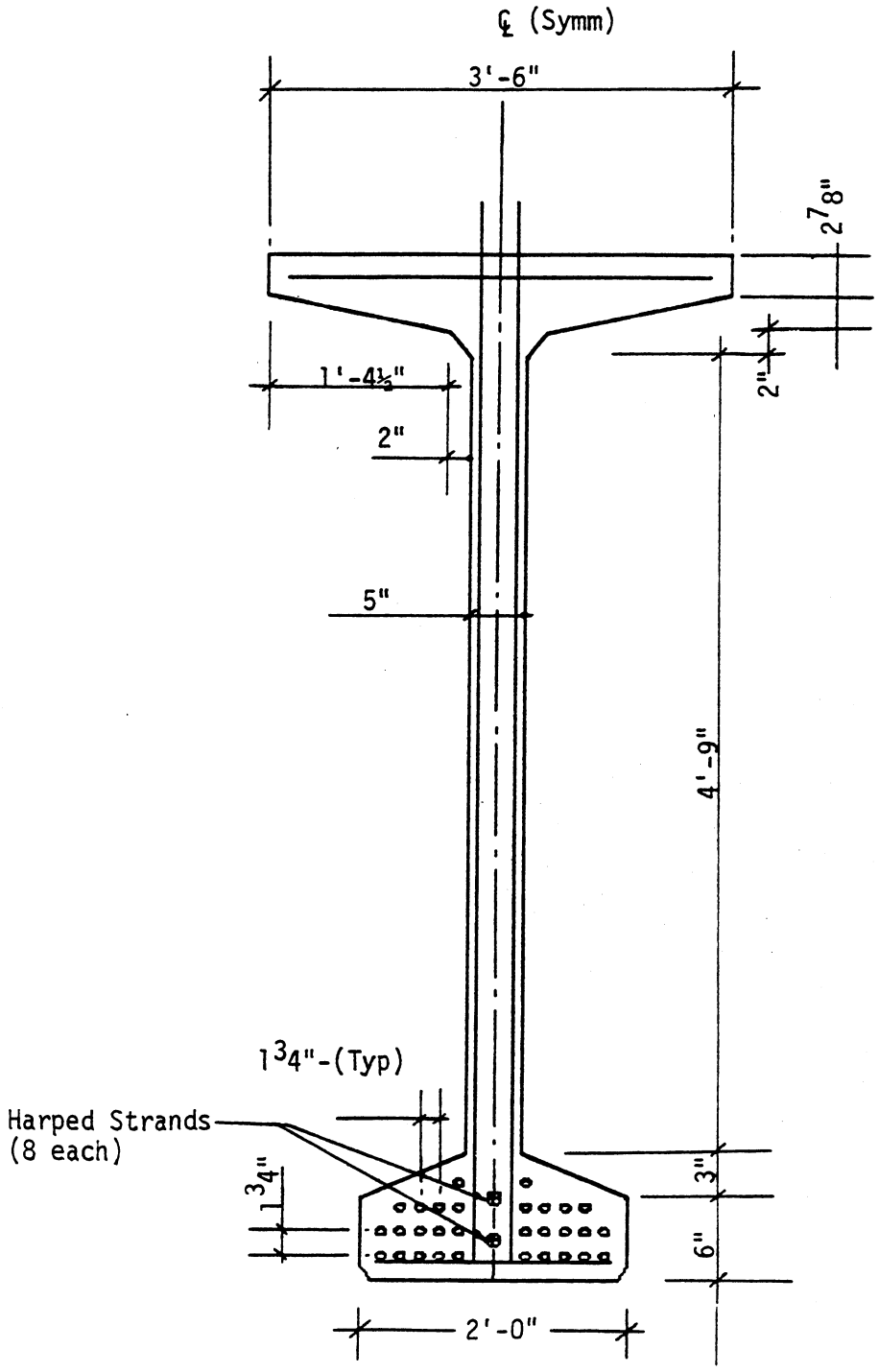

Figure 4.5 Field Test - Section through Mid-span of Girder 5D

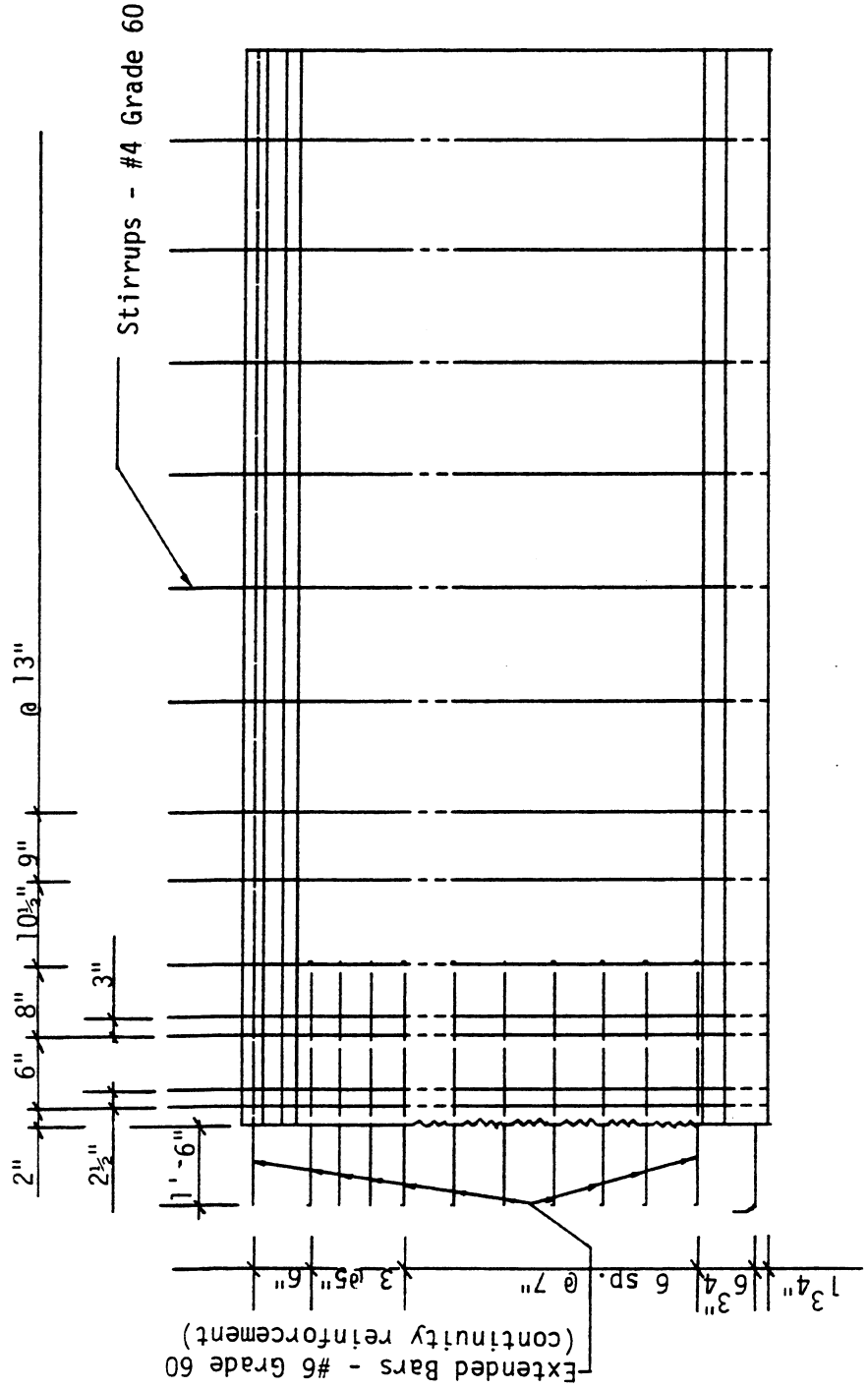

Figure 4.6 Field Test - Shear and Continuity Reinforcement in Girder 5D

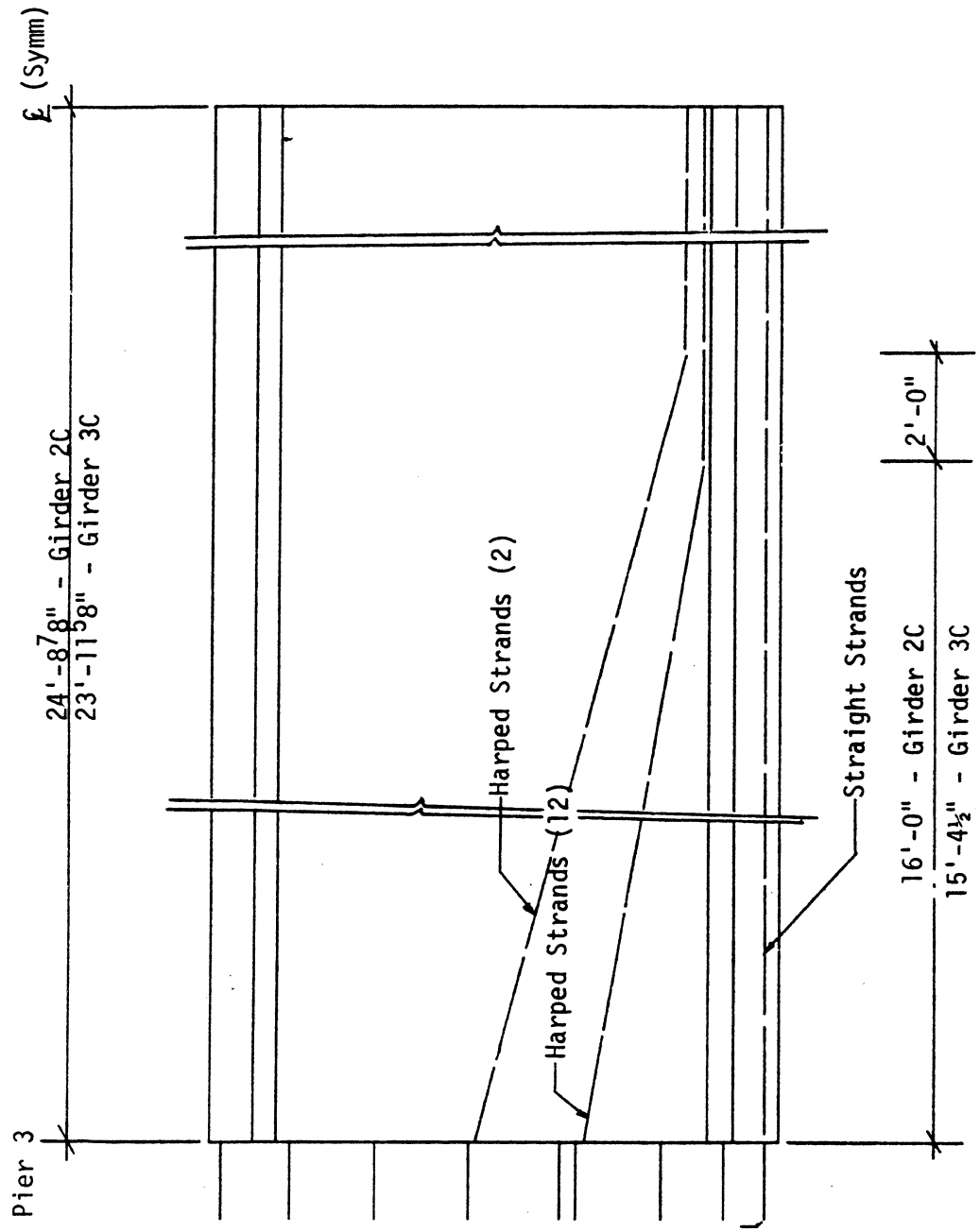

Figure 4.7 Field Test - Elevation of Girder 2C and 3C

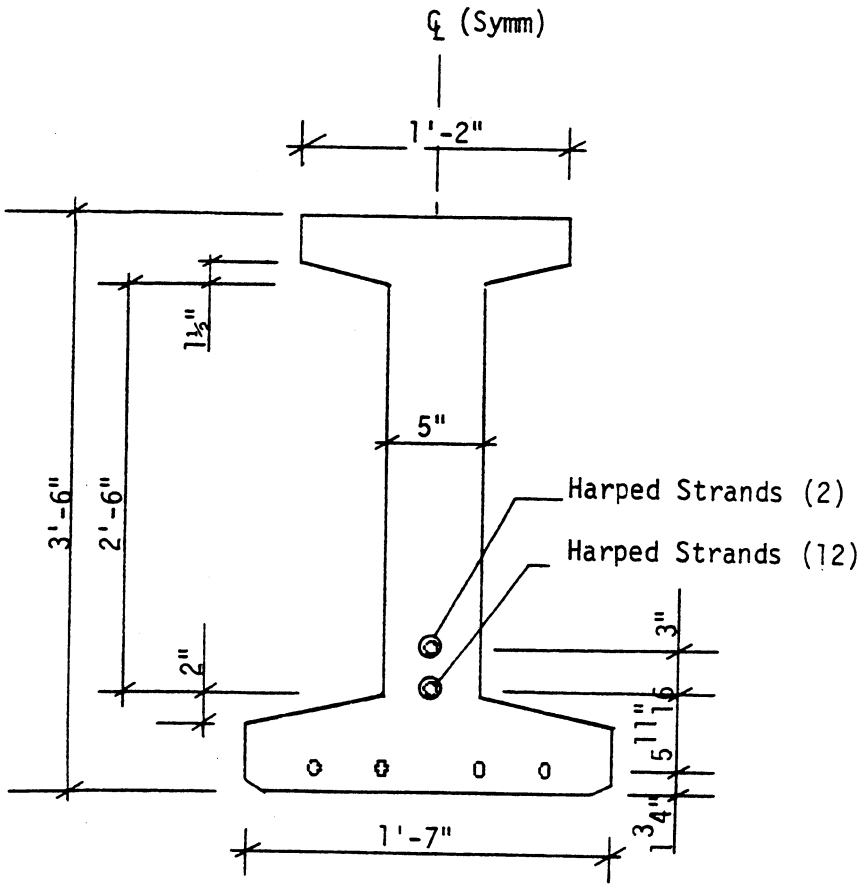

Figure 4.8 Field Test - View of Girders 2C and 3C at the Continuous End

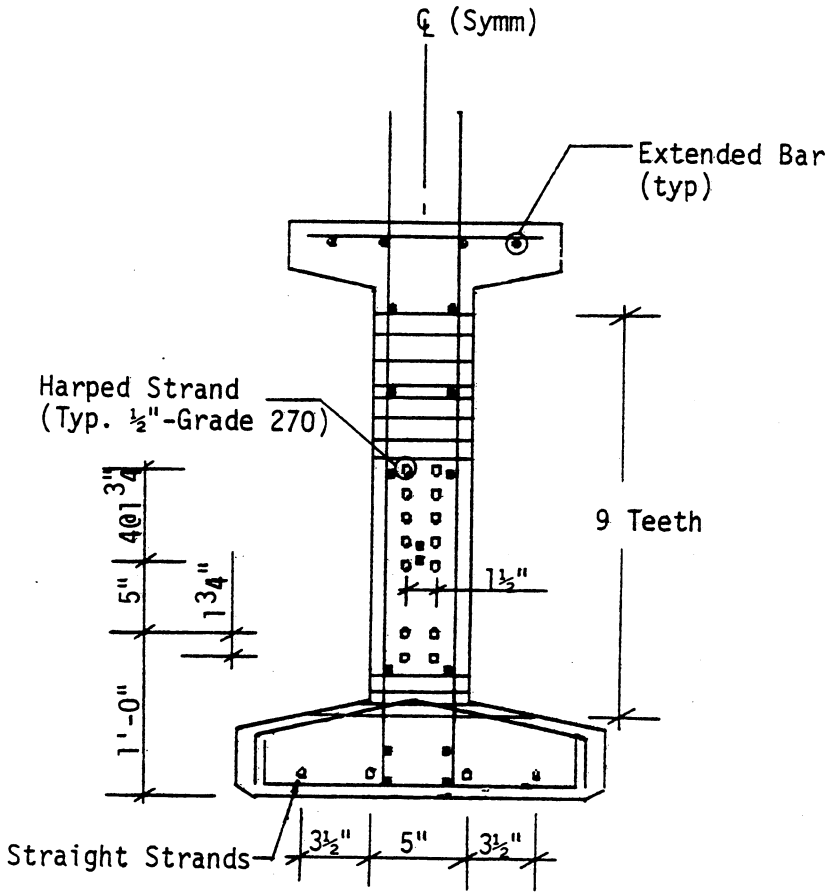

Figure 4.9 Field Test - Section through Mid-span of Girders 2C and 3C

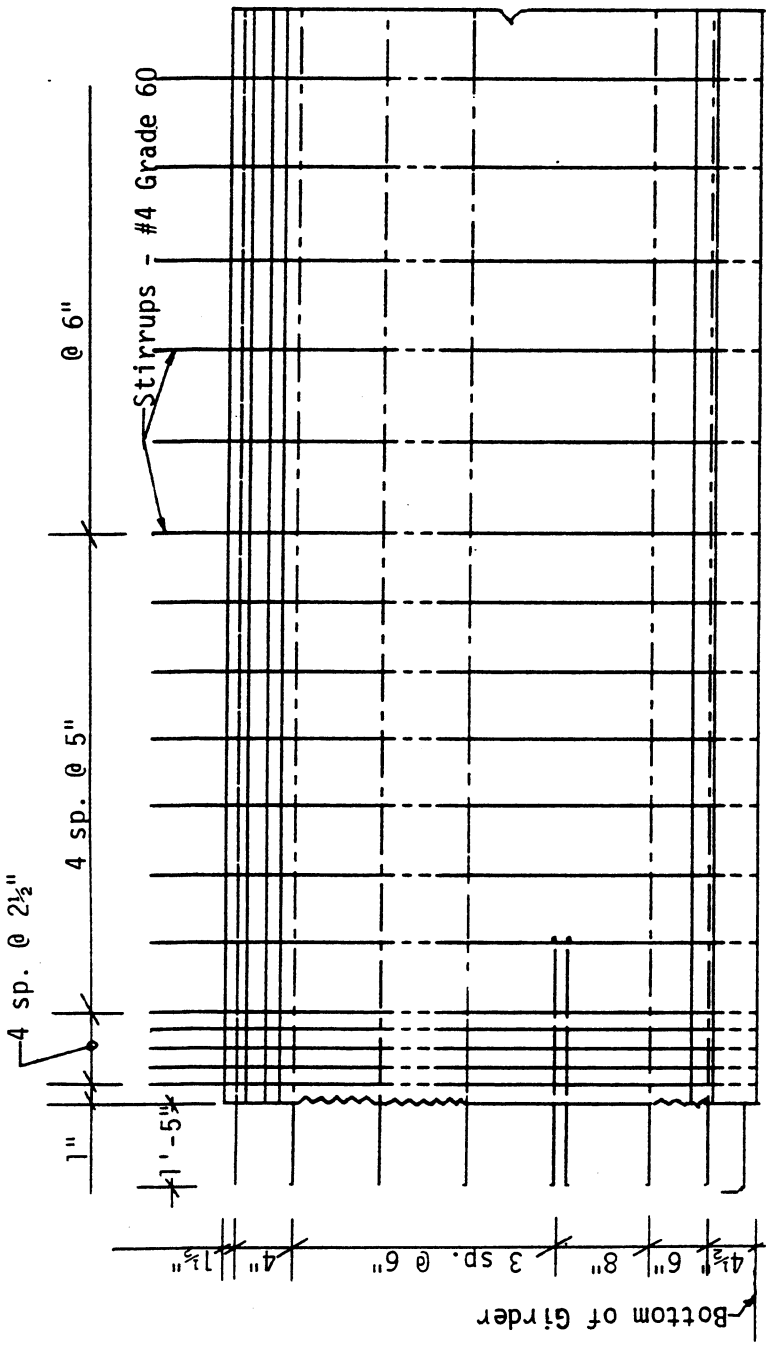

Figure 4.10 Field Test - Shear and Continuity Reinforcement in Girders 2C and 3C

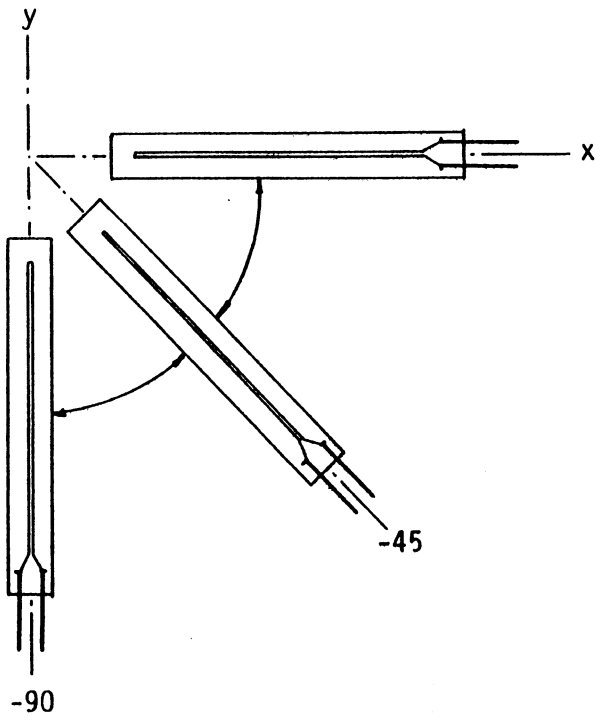

Strain Gages on the Surface of Concrete forming a rosette

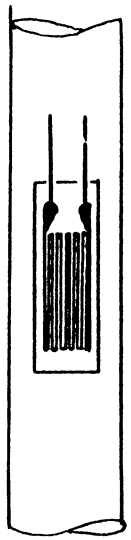

Strain Gage on Steel

Note - Refer Appendix A for Details

Figure 4.11 Field Test - Strain Gages

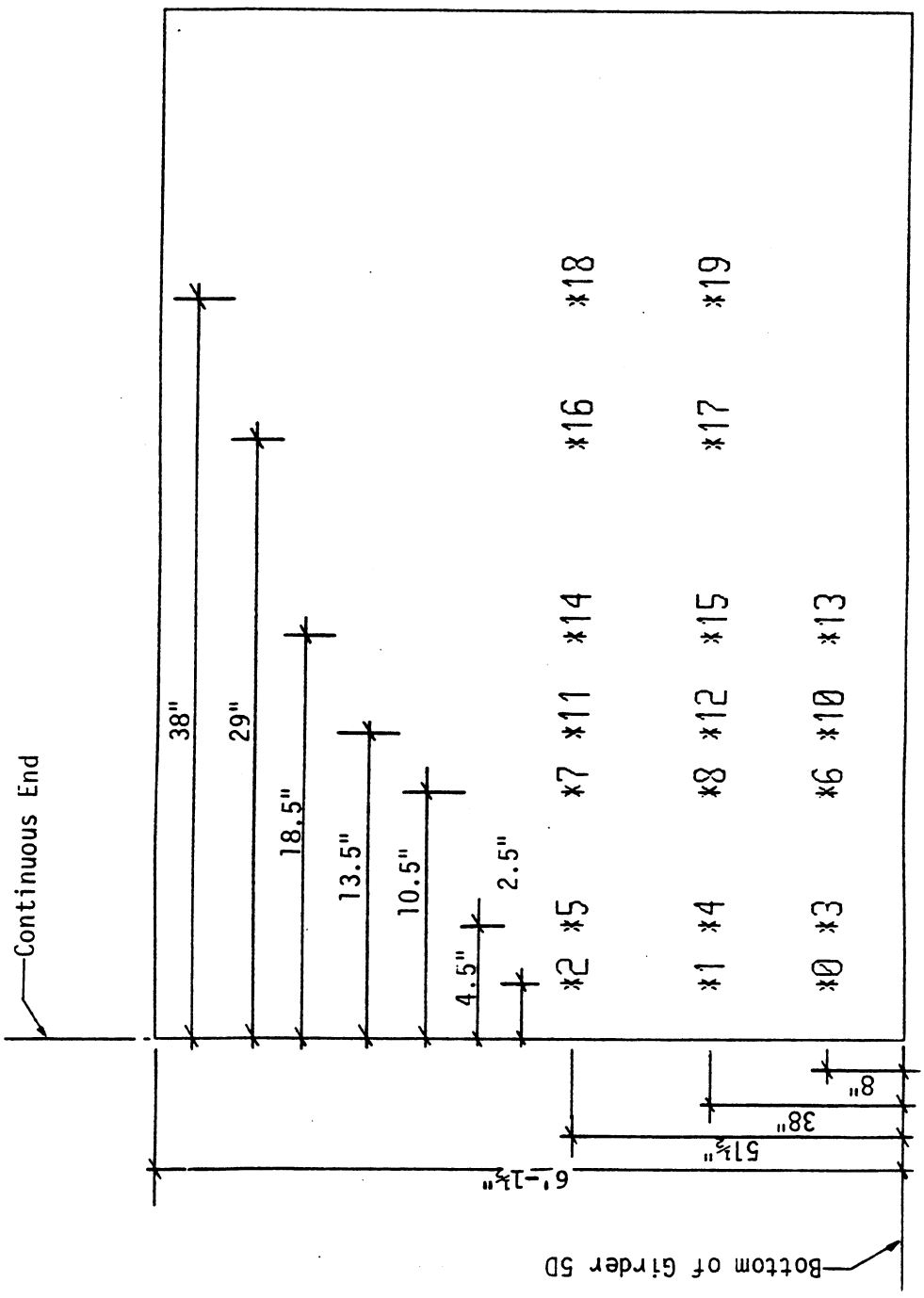

Figure 4.12.a Field Test - Configuration of Strain Gages on Stirrups of Girder 5D

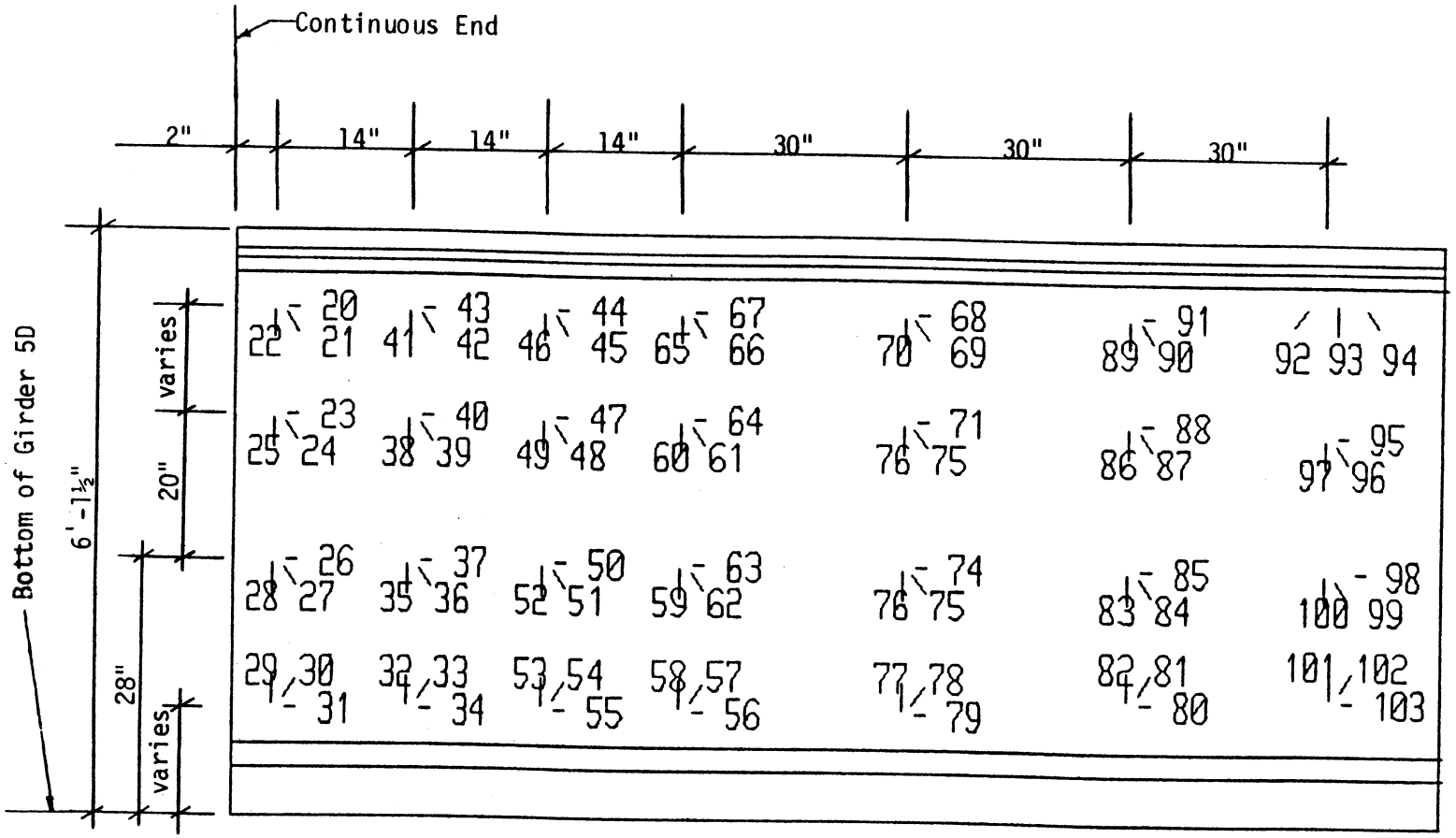

Figure 4.12.b Field Test - Configuration of Strain Gages on the Web Surface of Girder 5D

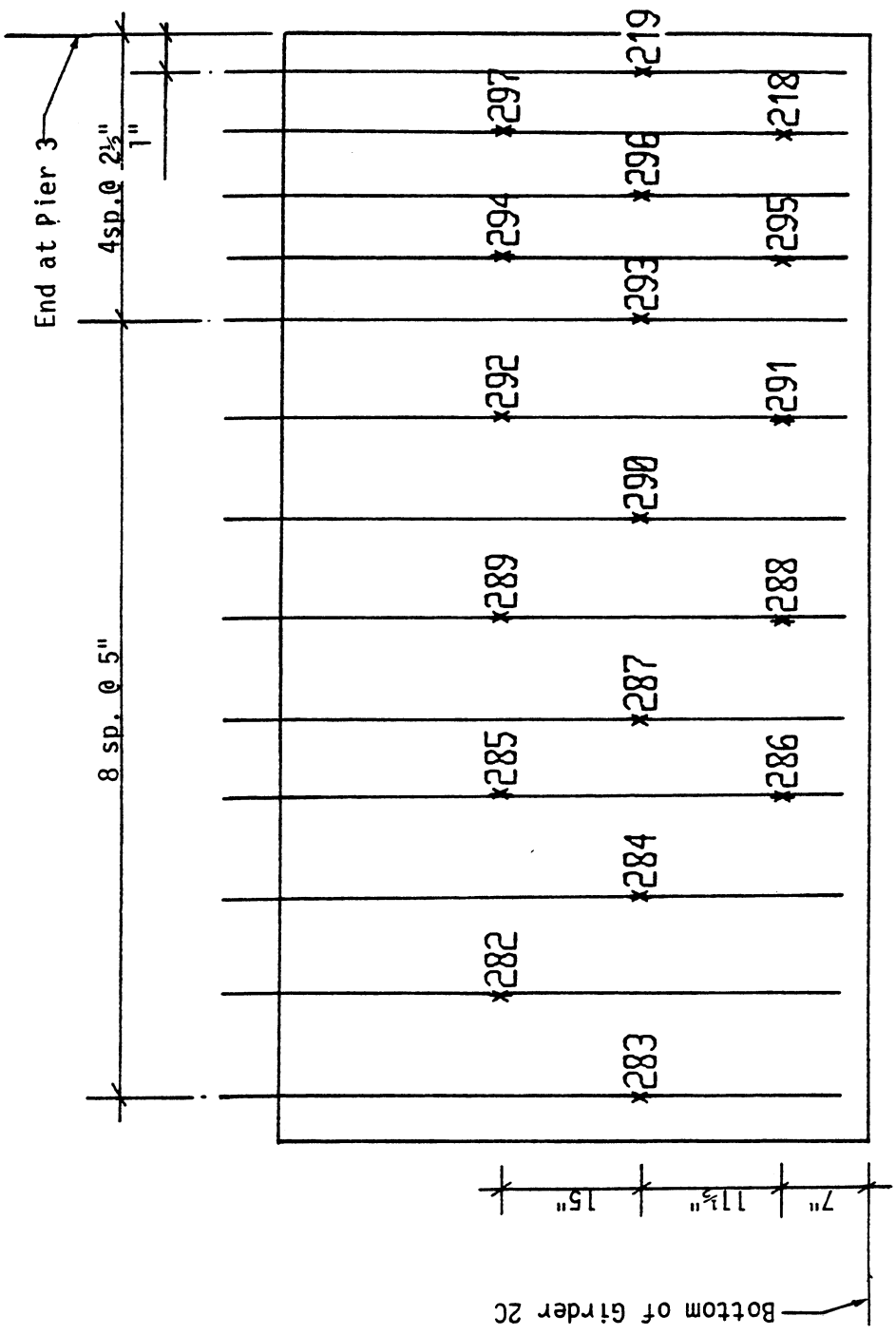

Figure 4.13.a Field Test - Configuration of Strain Gages on Stirrups of Girder 2C

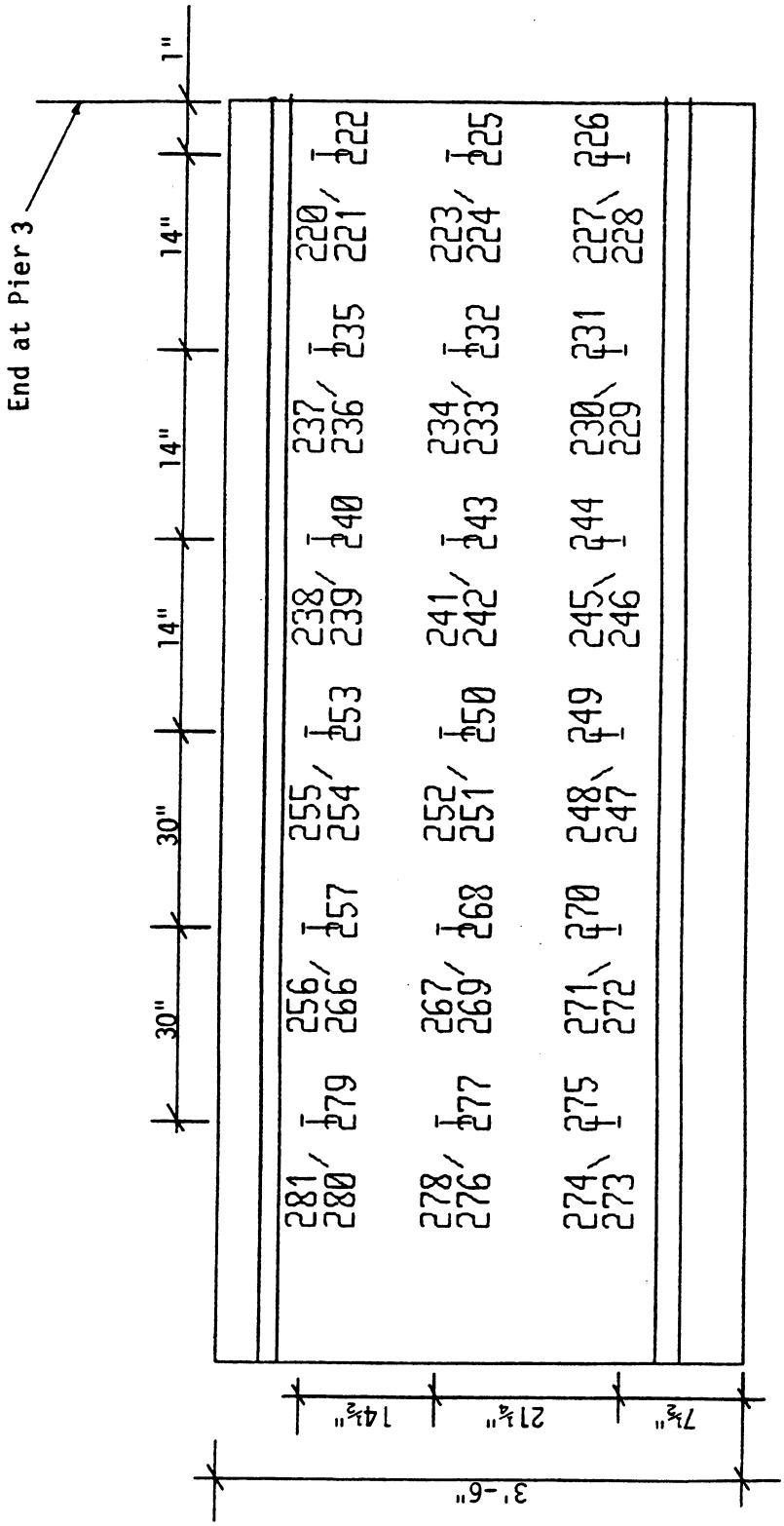

Figure 4.13.b Field Test - Configuration of Strain Gages on the Web Surface of Girder 2C

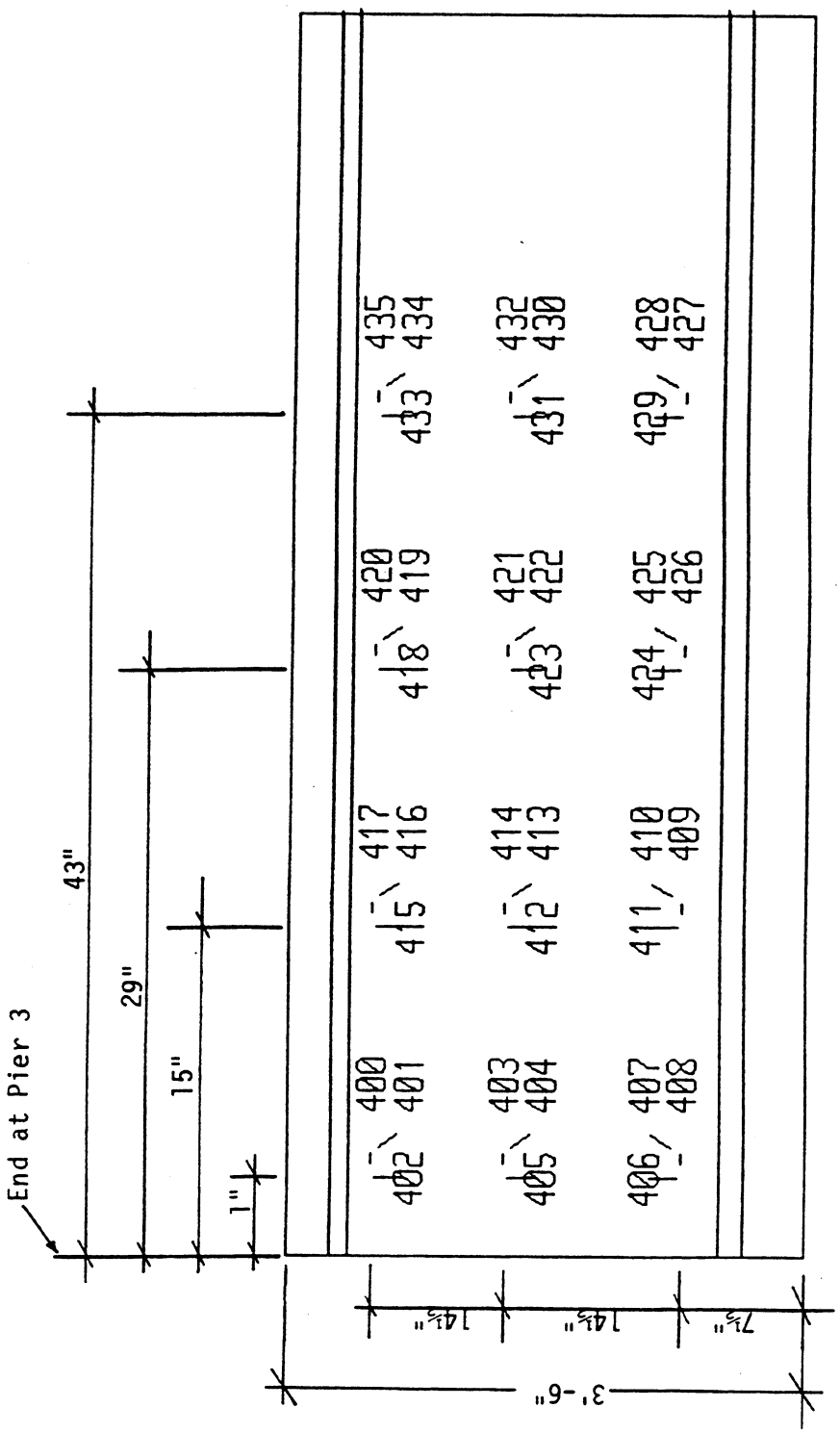

Figure 4.14 Field Test - Configuration of Strain Gages on the Web Surface of Girder 3C

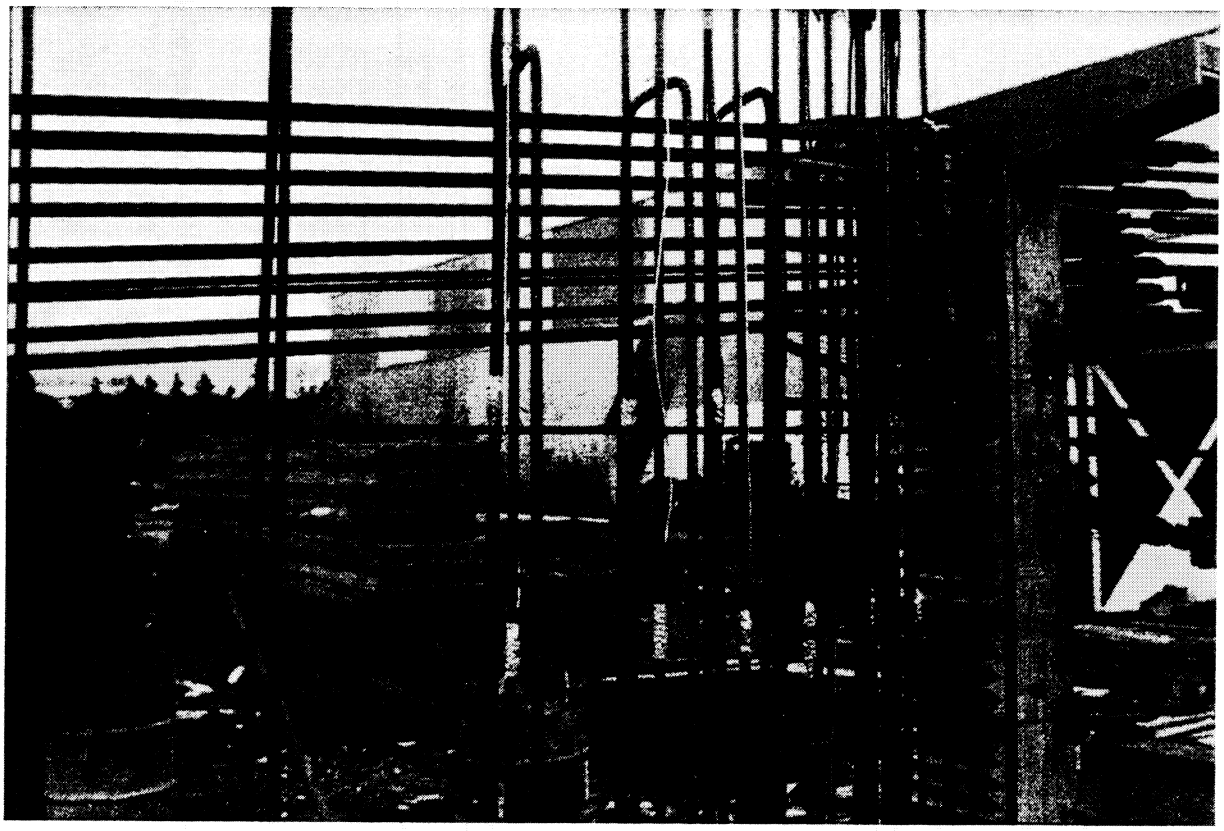

Figure 4.15 Field Test - Arranging the Stirrups for Manufacturing Girder 5D

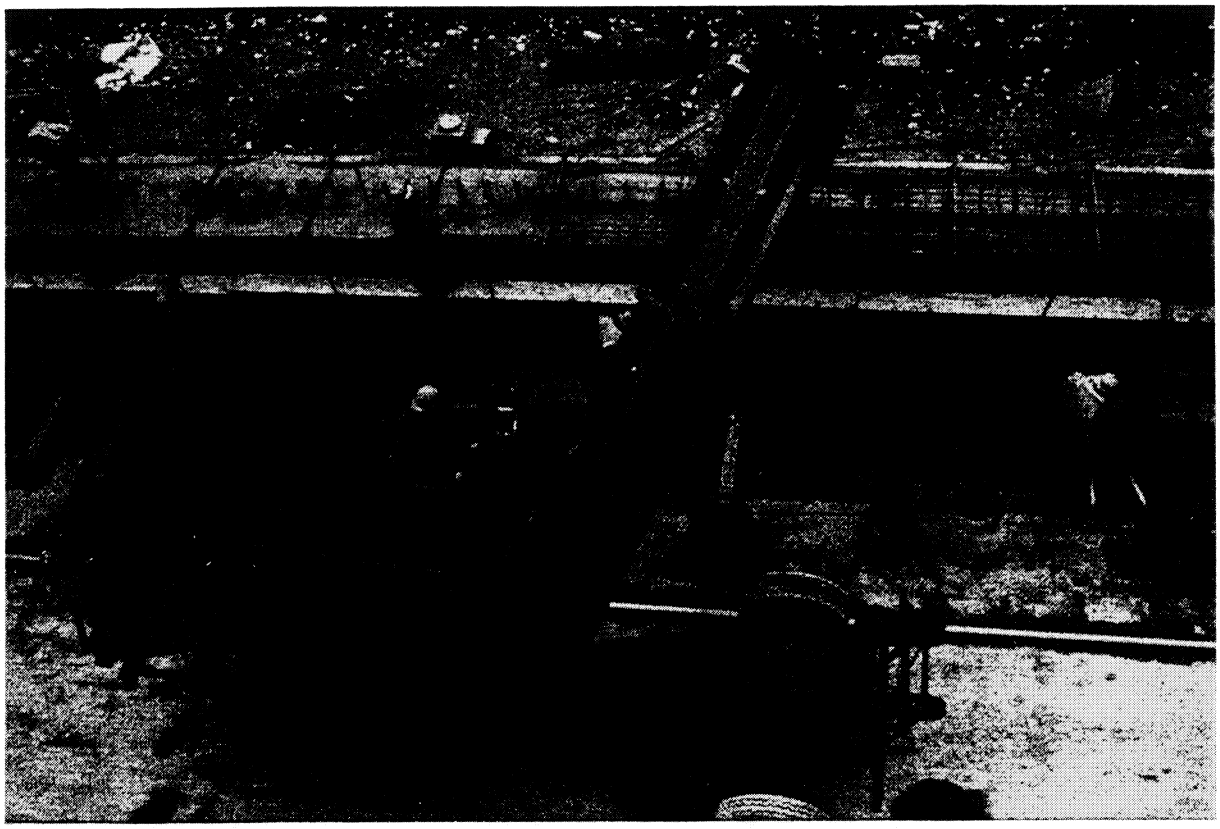

Figure 4.16 Field Test - Placing Concrete in the Forms of Girder 5D

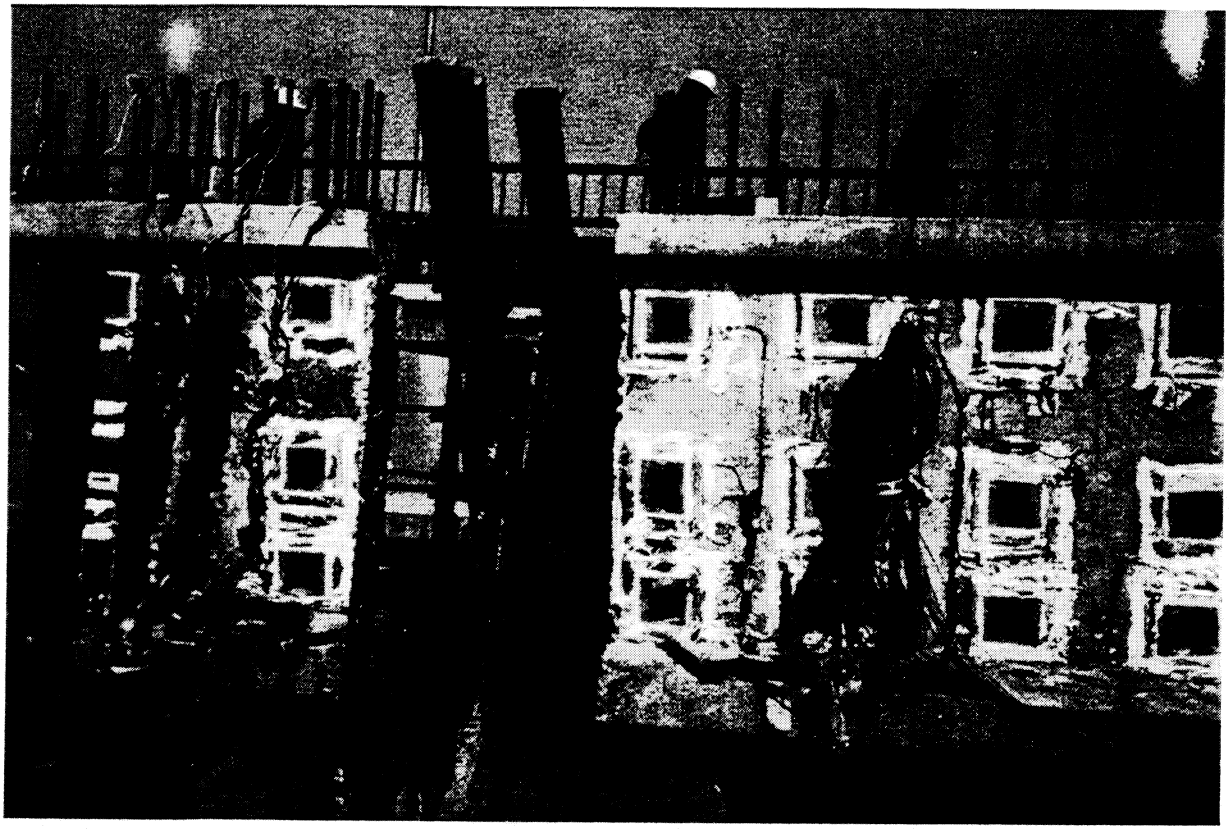

Figure 4.17 Field Test - Erection of Girders 2C and 3C (portion near pier 3 can be seen)

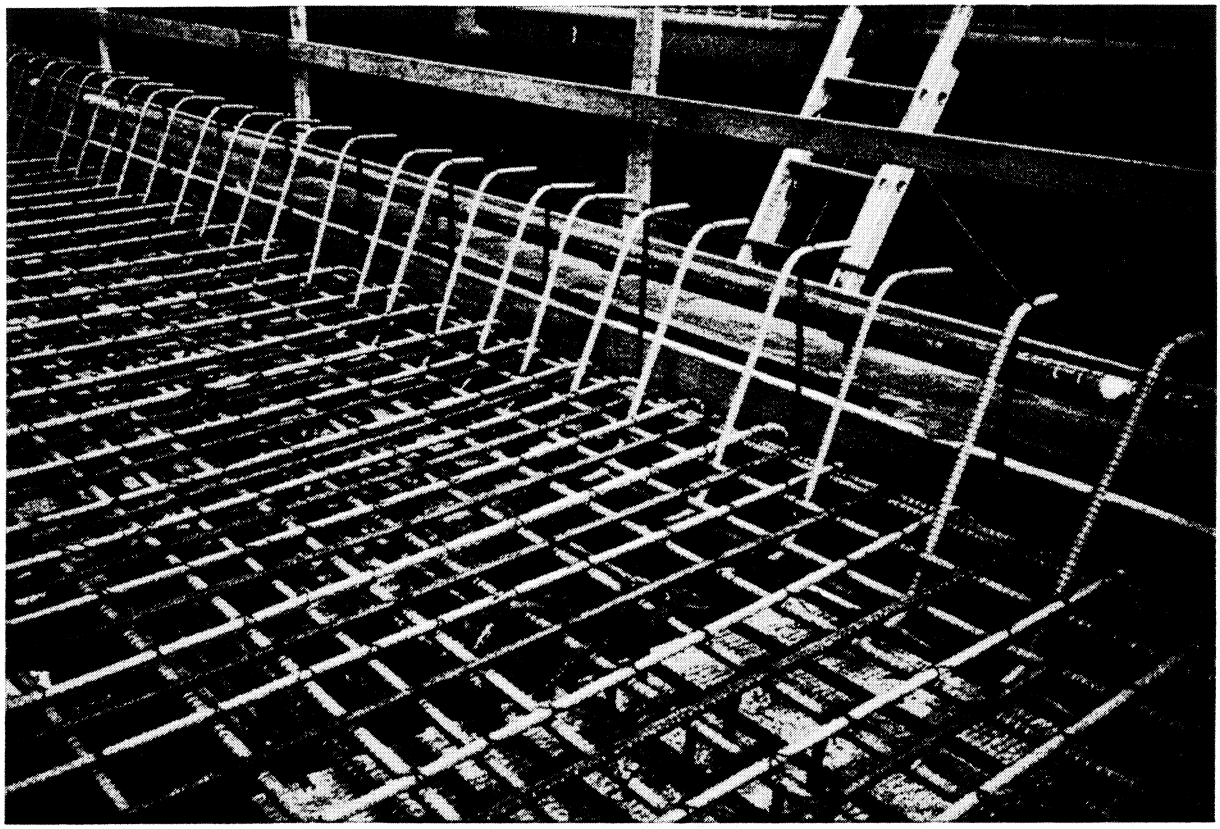

Figure 4.18 Field Test - Reinforcement in the Roadway Slab (portion of it can be seen)

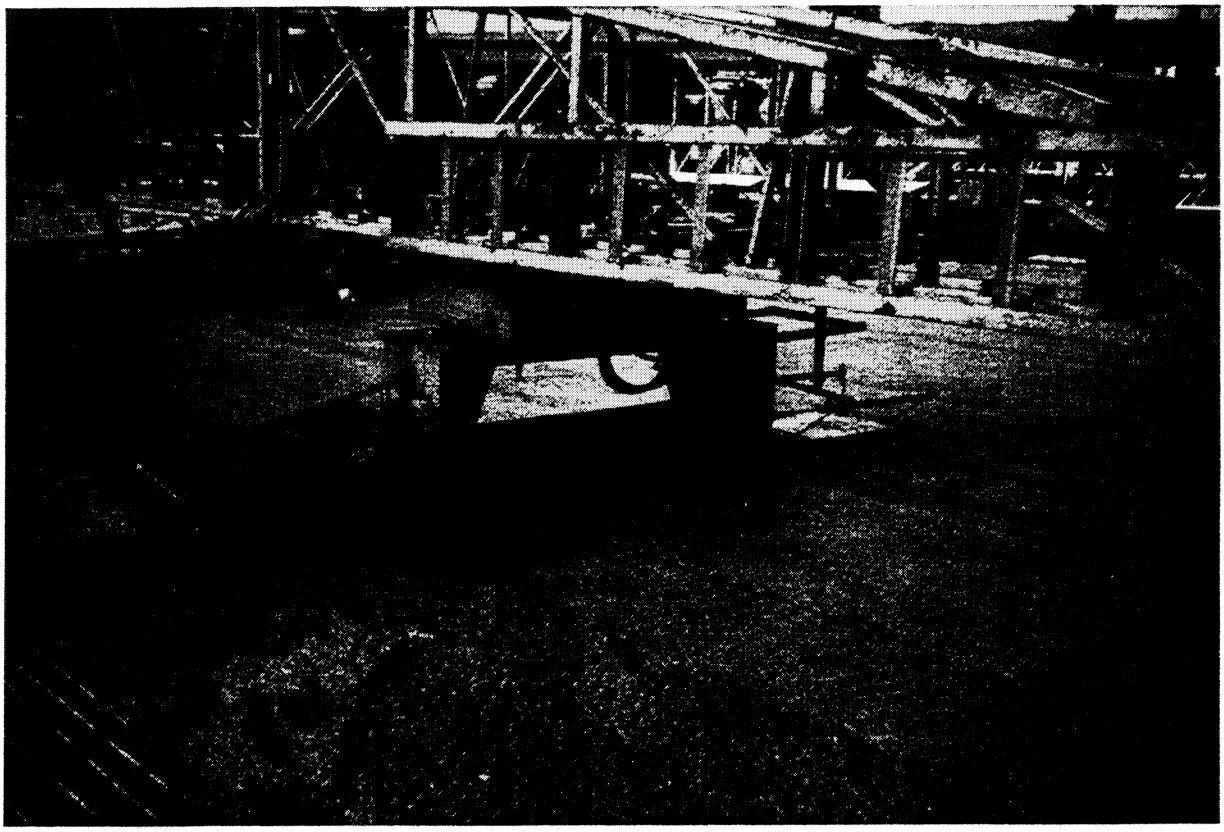

Figure 4.19 Field Test - Placing Concrete in the Roadway Slab

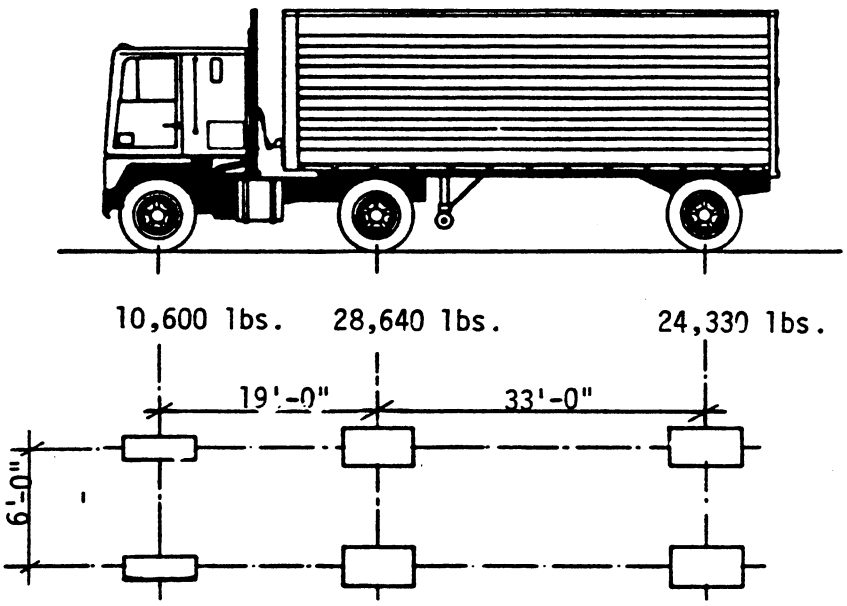

Figure 4.20 Field Test - The Truckload

CHAPTER 5

RESULTS OF THE FIELD TEST

As described in Chapter 4, the field test began with monitoring of the strains in the end regions of girders 5D, 3C, and 2C after the prestress transfer and concluded with recording of the strains under a superimposed truck load.

This chapter deals with the results of the data collected during the different phases of construction. First, the strains and stresses recorded after the prestress transfer are discussed, while the next section focuses on the strains and stresses resulting from the combined effect of the prestressing and casting of the slab and diaphragms. The last section deals with conclusions.

The truck load, which was approximately equal to the HS20-44 loading, produced average strains of about 10 microstrains. The readings were scattered. The main source affecting the readings was the noise due to the traffic on the adjacent bridge, the railroad traffic, the electrical network, and the generator. The strain readings were reliable but the values were small. Therefore, the results from the live-load test are not presented.

At the Prestress Transfer

Girders 5D, 2C, and 3C were monitored for strains in their end regions after detensioning. In the following sections the results are presented.

Stresses in Girder 5D

Strain gages were used on the stirrups and on the surface of the web near pier 5. The allowable stresses in the concrete and the steel measured after the prestress transfer are given in Table 5.1.

Table 5.4 shows the stresses in the stirrups measured after detensioning. Figure 5.1 shows the variation in the stresses along the centroidal axis versus the locations of stirrups. The maximum amount of stress in a stirrup was 32 ksi. With this exception, the maximum amount of stress in a stirrup varied between 0 to 10 ksi. The curve in Figure 5.1 is similar to that presented by Itani and Sarles [38]. The stirrups were in tension because bursting and the spalling stresses were present in this region.

Table 5.5 shows the principal stresses on the surface of the web measured after detensioning. The maximum compressive stress was 1984 psi and was less than the allowable value of 3645 psi (Table 5.1). It occurred at a distance of 30 in. from the end of the girder and near the junction of the bottom flange and the web. The location of the maximum stress was beyond the transfer length of 25 in. The prestressing combined with the cambering effect produced compression in the region.

The table shows that at two locations which were a distance of 2 in. from the end, the tensile stresses exceeded the modulus of rupture. The allowable tensile stress was about 50 percent of the modulus rupture of the concrete.

Stresses in Girder 2C

Girder 2C was instrumented with strain gages on the web surface. The end was adjacent to pier 3. Table 5.2 indicates the allowable stresses in the concrete and steel after the stress transfer.

Table 5.6 shows the stresses in the stirrups. The maximum stress was 8 ksi, and it occurred 11 in. from the end along the centroidal axis of the girder.

Figure 5.2 shows the variation of the stresses in the stirrups along the centroidal axis of the girder. The plot is similar to that in Figure 5.1

Table 5.7 indicates the principal stresses on the surface of the web. The maximum compressive stress was 2466 psi, which was less than the allowable compression of 4320 psi. It occurred well beyond the transfer length of 25 in. The allowable stress and strength of the concrete in tension were 228 and 570 psi, respectively. The strength was exceeded at a distance of 43 in. along the centroidal axis and at a distance of 15 in. near the junction of the web and the bottom flange which indicated the formation of microcracks.

Stresses in girder 3C

Twelve rosettes were installed on the surface of the web and the stirrups were not provided with strain gages.

The allowable stresses in the concrete are given in Table 5.3.

Table 5.8 presents the principal stresses in the web measured after the prestress transfer. The maximum compressive stress was 1568 psi and was within the allowable limit of 2430 psi. The maximum tensile stress was 2175 psi, while the tensile strength was 522 psi. The locations

where the tensile strength was exceeded was near the junction of the bottom flange and the web. It reflected the presence of microcracks in the region.

Stresses in the girders after the casting of the slab and the diaphragms

In this section stresses resulting from the casting of the roadway slab and the diaphragms are discussed. Losses in prestressing force were assumed to be about 25 percent. Another assumption was that the strains recorded during detensioning varied linearly with the prestressing force. Therefore, the strains due to the effective prestressing force were assumed to be 75 percent of the strains recorded during detensioning. The effective strains were added to the strains that were recorded after the slab and the diaphragms were poured. The resultant stresses were computed from these resultant strains.

Stresses in girder 5D

The allowable stresses at this stage are listed in Table 5.1.

The stresses in the stirrups of girder 5D are presented in Table 5.9. Stresses of 17 and 29 ksi along the centroidal axis occurred at a distance of 2 in. and 10.5 in. from the end of the girder. The term NG indicates that the strain gage did not function at that stage.

Figure 5.3 shows the maximum amount of stress in the stirrups along the centroidal axis versus the distance along the length of the girder. Except for the stress of 29 ksi, the stress decreases as the distance increases.

The principal stresses on the surface of the web are shown in Table 5.10. The maximum compressive stress was 1794 psi, which is less than the allowable stress of 3220 psi. It occurred near the junction of the

web and the bottom flange at 30 in. from the end of the girder. The principal tensile stress exceeded the tensile strength of 673 psi, which indicated the presence of microcracks.

Stresses in girder 2C

The allowable stresses in the steel and the concrete are given in Table 5.2.

Table 5.11 shows the stresses in the stirrups of girder 2C after the slab and diaphragms were in place. The stress of 13 ksi at 3.5 in. from the end indicates concrete cracking.

The principal stresses on the surface of the concrete are presented in Table 5.12 Tensile stresses of more than 636 psi indicate the presence of microcracks. The allowable compression is 2880 psi, which is greater than the maximum compressive stress of 1980 psi. Note that microcracks were present in the concrete adjacent to the end of the girder.

Stresses in girder 3C

Table 5.3 shows the allowable stresses in the concrete and steel. The principal stresses at various locations on the surface of the web are presented in Table 5.13. The maximum compressive stress was 1494 psi and was less than the allowable stress of 2920 psi. The tensile stresses greater than 641 psi represented the locations of microcracks. Tensile stresses were more than the tensile strength in the concrete near the end of the girder.

Conclusions

After the prestress transfer, except for two locations, the stresses on the concrete surface of girder 5D were within allowable limits. In the case of the stirrups of girder 5D, the variation in the stresses after the addition of the slab depended on the location of the gage. The compressive stresses on the concrete surface of girders 2C and 3C after the prestress transfer and after the slab was placed were within the allowable limits.

Table 5.1

Design Parameters: Girder 5D

Parameters	At Detensioning	At time of casting the deck
1. Nominal Cylindrical Strength of Concrete (psi)	6075	8050
2. Allowable Compression in Concrete (psi) (AASHTO Sect 9.15.2)	3645	3220
3. Allowable Tension in Concrete (psi) (AASHTO Sect.9.15.2)	234	270
4. Modulus of Rupture of Concrete (psi) ($7.5\sqrt{f'c}$)	585	673
5. Modulus of Elasticity of Concrete (psi) ($E_c = 63700\sqrt{f'c}$)	4964924	5715278
6. Minimum Shear Stress in Concrete (psi) ($2\sqrt{f'c}$)	156	179
7. Allowable Principal Tension in Concrete (psi) ($4\sqrt{f'c}$)	312	358
8. Yield Strength of Nonprestressed Steel (ksi)	60	60
9. Tension in Stirrups at Cracking of Concrete (ksi) ($7.5\sqrt{f'c}\cdot Es/Ec$)	3.5	3.5

Table 5.2

Design Parameters: Girder 2C

Parameters	At Detensioning	At time of casting the deck
1. Nominal Cylindrical Strength of Concrete (psi)	5775	7200
2. Allowable Compression in Concrete (psi) (AASHTO Sect 9.15.2)	3645	2880
3. Allowable Tension in Concrete (psi) (AASHTO Sect.9.15.2)	228	255
4. Modulus of Rupture of Concrete (psi) ($7.5\sqrt{f'c}$)	570	636
5. Modulus of Elasticity of Concrete (psi) ($E_c = 63700\sqrt{f'c}$)	4840781	5405124
6. Minimum Shear Stress in Concrete (psi) ($2\sqrt{f'c}$)	152	170
7. Allowable Principal Tension in Concrete (psi) ($4\sqrt{f'c}$)	304	340
8. Yield Strength of Nonprestressed Steel (ksi)	60	60
9. Tension in Stirrups at Cracking of Concrete (ksi) ($7.5\sqrt{f'c}\cdot Es/Ec$)	3.5	3.5

Table 5.3

Design Parameters: Girder 3C

Parameters	At Detensioning	At time of casting the deck
1. Nominal Cylindrical Strength of Concrete (psi)	4850	7300
2. Allowable Compression in Concrete (psi) (AASHTO Sect 9.15.2)	2910	2920
3. Allowable Tension in Concrete (psi) (AASHTO Sect.9.15.2)	209	256
4. Modulus of Rupture of Concrete (psi) ($7.5\sqrt{f'c}$)	522	641
5. Modulus of Elasticity of Concrete (psi) ($E_c = 63700\sqrt{f'c}$)	4436192	5442530
6. Minimum Shear Stress in Concrete (psi) ($2\sqrt{f'c}$)	139	171
7. Allowable Principal Tension in Concrete (psi) ($4\sqrt{f'c}$)	278	342
8. Yield Strength of Nonprestressed Steel (ksi)	60	60
9. Tension in Stirrups at Cracking of Concrete (ksi) ($7.5\sqrt{f'c}\cdot Es/Ec$)	3.5	3.5

Table 5.4

Stresses (ksi) in Stirrups of Girder 5D after Prestress Transfer

y	x						
	2.0	4.5	10.5	13.5	18.5	29.0	38.0
51.5	2	1	8	NF	NF	1	0
38.0	4	10	32	NF	2	1	4
8.0	4	2	4	4	1	-	-

x = Distance of a stirrup to the end of the girder in inches

y = Distance of the gages from the bottom of the girder in inches

NF = The gage did not function.

Table 5.5

Principal Stresses on the Web Surface of Girder 5D after Prestress Transfer (psi)

		x						
		2.0	16.0	30.0	44.0	74.0	104.0	134.0
T	σ_{p1}	168	-	277	-624	226	124	114
	σ_{p2}	-202	NG	-366	-1675	-65	-1357	-464
	θ	-35	-	-26	-38	-26	19	14
47	σ_{p1}	489	254	-157	-	122	207	163
	σ_{p2}	11	-474	-1081	NG	-433	-712	-546
	θ	-11	-25	15	-	-1	-7	-43
29	σ_{p1}	6939	704	-67	266	-31	51	128
	σ_{p2}	198	-104	-627	-77	-802	-845	-1044
	θ	-22	-1	17	26	1	7	-7
B	σ_{p1}	3239	-	-93	-180	-58	64	-92
	σ_{p2}	504	NG	-1984	-1947	-1575	-1525	-936
	θ	18	-	8	-1	-9	-6	-3

x = Distance of a rosette from the end of the girders in inches.

y = Distance of a rosette from the bottom of the girders in inches.

σ_{p1} σ_{p2} = Principal stresses on the concrete in psi.

θ = Orientation of the principal stresses in degrees.

NG = Not Good

T = Junction of the top flange and the web

B = Junction of the bottom flange and the web

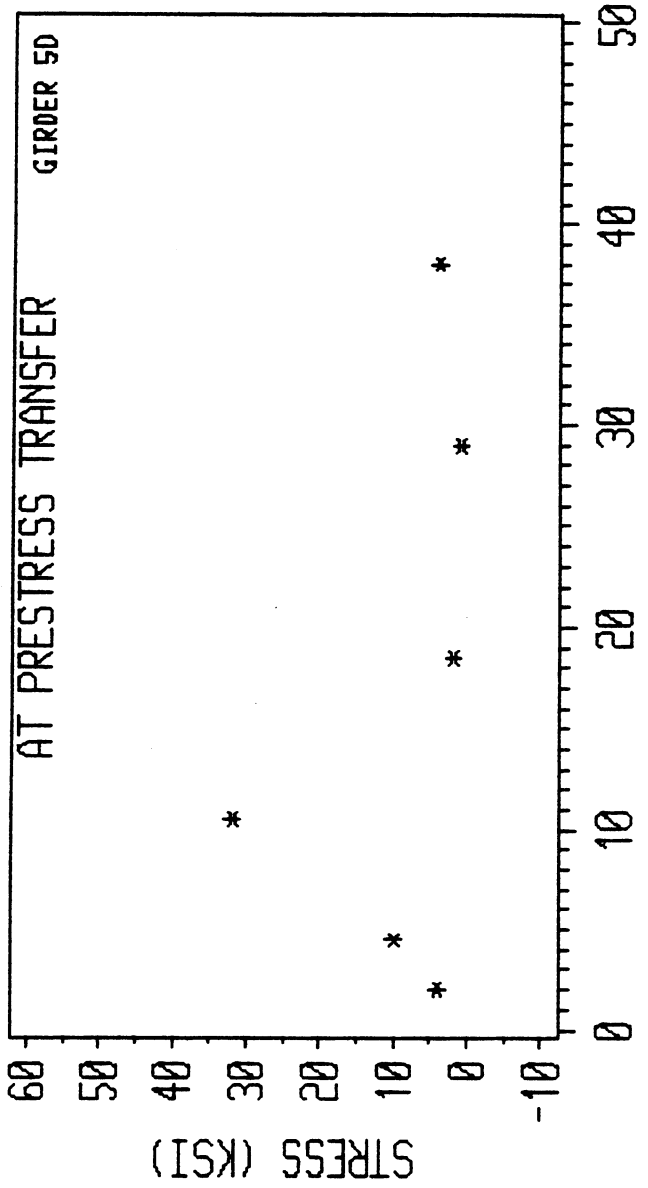

Figure 5.1 Field Test - Stresses in Stirrups at Prestress Transfer versus Distance from the Continuous End : Girder 5D

Table 5.6

Stresses (ksi) in Stirrups of Girder 2C after Prestress Transfer

	y		
X	7.0	18.5	33.5
1.0	-	2	-
3.5	0	-	2
6.0	-	5	-
8.5	NF	-	2
11.0	-	8	-
16.0	3	-	1
21.0	-	7	-
26	4	-	0
31.0	-	NF	-
36.0	7	-	1
41.0	-	1	-
46.0	-	-	0
52.0	-	6	-

x = Distance of a stirrup to the end of the girder in inches.

y = Distance of the gages from the bottom of the girder in inches.

NF = The gage did not function.

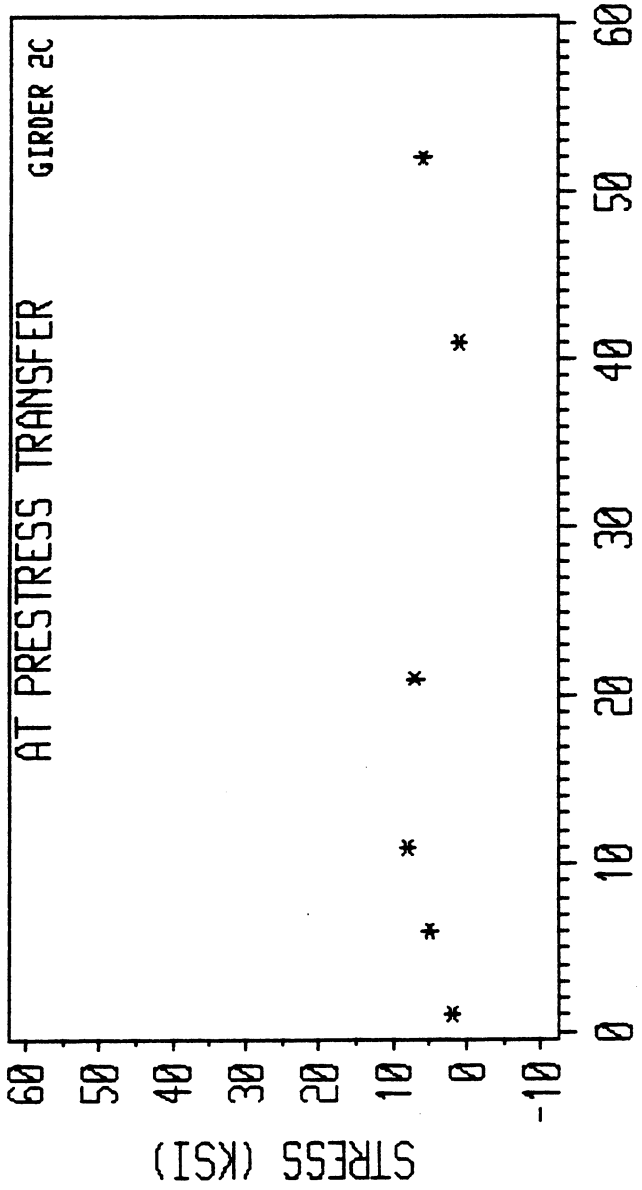

Figure 5.2 Field Test - Stresses in Stirrups at Prestress Transfer versus Distance from the Continuous End : Girder 2C

Table 5.7

Principal Stresses on the Web Surface of Girder 2C after Prestress Transfer

y		x = 1.0	15.0	29.0	43.0	73.0	103.0
36.5	σ_{p1}	-1	50	-12	44	-229	107
	σ_{p2}	-25	-507	-623	-710	-1062	-442
	θ	-23	21	6	4	31	-14
22.0	σ_{p1}	11	372	483	3154	-165	-158
	σ_{p2}	-656	-824	-529	-152	-2466	-2387
	θ	39	10	-7	36	38	39
7.5	σ_{p1}	174	2202	532	-	-8	58
	σ_{p2}	-1128	-1288	-1593	NG	-1851	-1780
	θ	-44	-21	-15	-	-1	-13

x = Distance of a rosette from the end of the girders in inches.

y = Distance of a rosette from the bottom of the girders in inches.

σ_{p1} σ_{p2} = Principal stresses on the concrete in psi.

θ° = Orientation of the principal stresses in degrees.

NG = Not Good

Table 5.8

Principal Stresses on the Web Surface of Girder 3C after Prestress Transfer

		x			
		1.0	15.0	29.0	43.0
36.5	σ_{p1}	119	110	151	277
	σ_{p2}	-101	-287	-533	-58
	θ^{p2}	11	18	15	-17
22.0	σ_{p1}	-35	265	274	194
	σ_{p2}	-524	-726	-958	-1111
	θ^{p2}	-37	1	8	6
7.5	σ_{p1}	341	2175	816	227
	σ_{p2}	-635	-1370	-1262	-1567
	θ^{p2}	-42	-29	-24	-15

x = Distance of a rosette from the end of the girders in inches.

y = Distance of a rosette from the bottom of the girders in inches.

σ_{p1} σ_{p2} = Principal stresses on the concrete in psi.

θ° = Orientation of the principal stresses in degrees.

NG = Not Good

Table 5.9

Stresses (ksi) in Stirrups of Girder 5D Load Combination: Effective Prestress Plus Weight of the Roadway Slab

	x						
y	2.0	4.5	10.5	13.5	18.5	29.0	38.0
51.5	5	7	NG	NF	NF	NG	3
38.0	17	9	29	NG	1	4	NG
8.0	4	2	9	8	NG	-	-

x = Distance of a stirrup to the end of the girder in inches

y = Distance of the gages from the bottom of the girder in inches

NF = The gage did not function.

NG = The gage did not function.

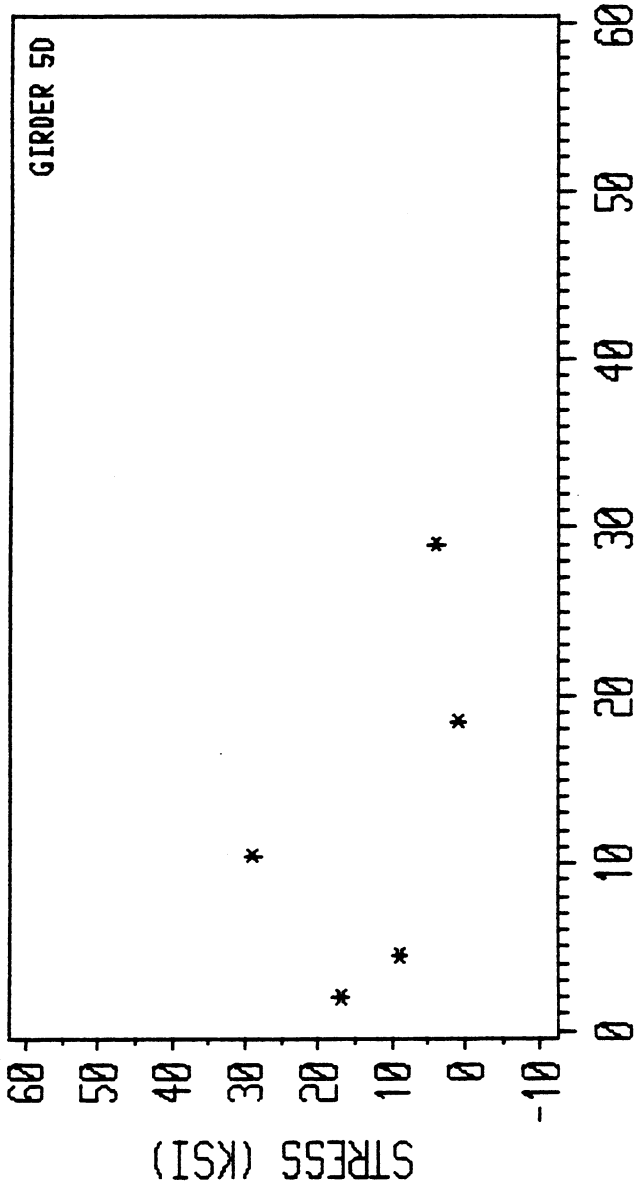

Figure 5.3 Field Test - Stresses in Stirrups after Placing Slab versus Distance from the Continuous End

Table 5.10

Principal Stresses on the Web Surface of Girder 5D
Load Combination: Effective Prestress Plus Weight of the Roadway Slab

		x						
		2.0	16.0	30.0	44.0	74.0	104.0	134.0
T	σ_{p1}	778	NG	NG	-525	1303	-74	1263
	σ_{p2}	194	NG	NG	-1208	-361	-1609	168
	θ	45	NG	NG	-36	-36	36	-27
47	σ_{p1}	887	1563	NG	NG	1929	-143	740
	σ_{p2}	121	-233	NG	NG	489	1121	-669
	θ	-12	-19	NG	NG	-1	-13	-41
29	σ_{p1}	NG	NG	360	425	-59	193	NG
	σ_{p2}	NG	NG	-911	-34	-714	-1526	NG
	θ	NG	NG	17	41	2	28	NG
B	σ_{p1}	NG	NG	-150	NG	-74	NG	NG
	σ_{p2}	NG	NG	-1794	NG	-1449	NG	NG
	θ	NG	NG	6	NG	-8	NG	NG

x = Distance of a rosette from the end of the girders in inches.

y = Distance of a rosette from the bottom of the girders in inches.

σ_{p1} σ_{p2} = Principal stresses on the concrete in psi.

θ = Orientation of the principal stresses in degrees.

NG = Not Good

T = Junction of the top flange and the web

B = Junction of the bottom flange and the web

Table 5.11

Stresses (ksi) in Stirrups of Girder 2C
Load Combination: Effective Prestress Plus Weight of the Roadway Slab

	y		
X	7.0	18.5	33.5
1.0	-	NG	-
3.5	5	-	13
6.0	-	NG	-
8.5	NF	-	2
11.0	-	5	-
16.0	1	-	0
21.0	-	6	-
26.0	2	-	1
31.0	-	NG	-
36.0	6	-	1
41.0	-	0	-
46.0	-	-	1
52.0	-	5	1

x = Distance of a stirrup to the end of the girder in inches

y = Distance of the gages from the bottom of the girder in inches

NF = The gage did not function.

NG = Not good

Table 5.12

Principal Stresses on the Web Surface of Girder 2C
Load Combination: Effective Prestress Plus Weight of the Roadway Slab

y		x = 1.0	15.0	29.0	43.0	73.0	103.0
36.5	σ_{p1}	-25	-67	104	-263	66	NG
	σ_{p2}	-330	-385	-723	-1155	-546	NG
	θ	21	5	18	35	-4	NG
22.0	σ_{p1}	318	285	472		-98	-85
	σ_{p2}	-229	-641	-465	NG	-1980	-1922
	θ	44	17	16		36	37
7.5	σ_{p1}		1413	389		-10	31
	σ_{p2}	NG	-1090	-790	NG	-1479	-1326
	θ		-19	-5		1	-9

x = Distance of a rosette from the end of the girders in inches.

y = Distance of a rosette from the bottom of the girders in inches.

σ_{p1} σ_{p2} = Principal stresses on the concrete in psi.

θ = Orientation of the principal stresses in degrees.

NG = Not Good

Table 5.13

Principal Stresses on the Web Surface of Girder 3C
Load Combination: Effective Prestress Plus Weight of the Roadway Slab

		x			
		1.0	15.0	29.0	43.0
36.5	σ_{p1}	75	-136	155	158
	σ_{p2}	--154	-2175	-463	16
	θ	33	-28	18	-20
22.0	σ_{p1}	2015	23	136	179
	σ_{p2}	-127	-1808	-1014	-1176
	θ	15	13	19	11
7.5	σ_{p1}	1054		684	185
	σ_{p2}	-332	NG	-1177	-1494
	θ	4		-21	-129

x = Distance of a rosette from the end of the girders in inches.

y = Distance of a rosette from the bottom of the girders in inches.

σ_{p1} σ_{p2} = Principal stresses on the concrete in psi.

θ = Orientation of the principal stresses in degrees.

NG = Not Good

CHAPTER 6

THE LABORATORY TEST

The elimination of the end blocks from girders reduces the area of the cross-section of the girders. Therefore, the area available for shear transfer at the interface of the girder and the adjoining diaphragm is less than that available in girders with end blocks. The purpose of the destructive laboratory test was to study the effect of the elimination of end blocks from continuous series 14 girders. This chapter describes in detail the setup for the laboratory test.

Details of the Girders

Two 20-ft., series 14 girders without end blocks were manufactured. The girders were designed for a nominal shear capacity of 400 kips, with the assumption that the nominal strength of the concrete would be 6000 psi. The choice of the length was mainly dictated by the following factors.

Depth of the Girders

To prevent diagonal tension from causing strutting action and to avoid failure of the continuous joint in the diaphragm, a load should be a distance at least equal to twice the depth of the girder from the face of the diaphragm. Since a series 14 girder is 73-1/2 in. deep, a 20-ft. girder was adequate to satisfy the minimum length requirement.

The Point of Contraflexure Consideration

A standard construction sequence is followed in a bridge consisting of these types of girders and a cast-in-situ roadway slab (Fig. 1.1).

The girders act as continuous beams under superimposed loads and experience reversal in curvature. Although the points of contraflexure depend on the applied loads, they usually fall within a distance of 1/8 to 1/3 of the span length from the continuous support. The objective in the experimental setup was to simulate conditions similar to the continuous joint at pier 5 (Chapter 4), assuming that there was a point of inflection on each side of the pier. Since girder 5D was 132 ft. 10 in. long, the point of contraflexure would fall at a distance of 20 ft. from the diaphragm. Hence the choice of a 20-ft. girder could be justified (Fig. 6.1).

The next step was to simulate conditions similar to those at the continuous joint over pier 5 of the BNRR overcrossing. Therefore, a pedestal with design and detailing identical to that of the cross beam at pier 5 was selected (Fig. 6.2). The pedestal was 3 ft. 9 in. wide so that a diaphragm 3 ft. 6 in. wide could be poured in place. The profile and number of strands, their material characteristics and positioning were selected to be identical to that of girder 5D. At the continuous end, reinforcing bars and strands were extended into the connection (Fig. 6.1). The standard sawteeth detailing was modified to account for the reduction in the area of the cross-section, and additional sawteeth were provided in the flange areas of the continuous end (Fig. 6.3).

Since at the continuous joint a slab is in tension, the concrete in the slab is expected to crack. As a result, only the reinforcement in the slab contributes to the moment resistance. This justified the reduction of a slab width to that of the flange of the girder. The effective width of the deck that would participate in the composite action of the roadway slab and girder 5D was computed according to the

section 8.10 of the AASHTO specifications [3]. In the experimental setup, the reinforcement in the slab was equivalent to the area of reinforcement in the effective width of the roadway slab.

Table 6.1 shows the design loads at pier 5. These loads defined the design criteria for the test girders and the slab. In Figure 6.1 the spacing of the stirrups at 2 in. on the center was dictated by section 9.21.3 of the AASHTO specifications. Figure 6.4 shows the view of a test girder at the discontinuous end.

Instrumentation of the Girders

The girders were instrumented with strain gages on the stirrups and strain rosettes on the concrete surface of the web.

Twenty-four stirrups with strain gages at 10 in., 25 in., and 38 in. from the bottom were provided in each girder. These stirrups were located at 1.5 in., 5.5 in., 9.5 in., 13.5 in., 17.5 in., 25.5 in., 33.5 in., and 41.5 in. from the continuous end. Each girder was provided with a #4 steel bar in the bottom flange which was located at the center and 3 in. from the bottom fiber. The bar was 5 ft. 11 in. long and extended 17 in. beyond the continuous end of a girder. Figures 6.5.a and 6.6.a show the locations and the channel numbers of the gages on the stirrups and the steel bar.

The gages on the concrete were 2-3/8 in. long, forming 45 degree-rosettes. The rosettes formed a rectangular grid on the surface of the web concrete. In Figures 6.5.b and 6.6.b the configuration of the gages and the channel numbers are shown.

The procedures for mounting the gages were similar to those described in Appendix A.

Experimental Setup

The test was carried out at the Research and Technology Park of Washington State University. The testing bed consisted of an embedded beam of 5 ft. x 6 ft. x 48 ft. A 44-ft. long steel plate with provisions for holddowns was anchored into the concrete bed.

The procedures followed for the experimental setup were similar to the construction sequence of the BNRRC bridge.

Manufacturing of the Girders

The girders were manufactured by the Central Pre-Mix Concrete Co. at its prestressing plant in Spokane. Because of the particular arrangement of the harped cables, a unique setup for the manufacturing of the girders was followed. This allowed both of the girders to be manufactured in one prestressing operation. Figure 6.7 shows the continuous ends of the girders before detensioning and the strain gages forming the rosettes.

The strands were tensioned to 189 ksi (70 percent of their ultimate tensile strength). The stirrups with the gages were installed at the predetermined locations. The remaining stirrups and reinforcement were placed as mandated by the design and calculations. The form work was erected and the concrete was placed. External vibrators as well as internal vibrators were used. The 5-in. webs and the electric wires from the strain-gages limited the use of internal vibrators to a minimum. More emphasis was given to the use of external vibrators. After the concrete was steam cured for about 24 hours, the form work was removed and the rosettes were installed.

On September 18 at about 3 P.M. the detensioning of the strands was started. The strain gages were initialized to zero. First the harped strands were detensioned. The strands were cut with a torch at the north end and then at the south end, followed by detensioning at the holddown. The bottom strands were then cut off and strains were recorded after detensioning had been completed.

Each girder weighed 14.6 kips, which was about one 1/6 of girder 5D. However, the longitudinal thrust caused by detensioning was the same in both cases. As a result, instead of a cambering effect longitudinal movement of the girders was observed. It was about 1 in.

The strains recorded at this stage are referred to as the strains measured after the prestress transfer or detensioning in Chapter 7.

Erection of the Girders

Before the girders were transported to the laboratory, a concrete pedestal was cast. Figure 6.8 shows the reinforcement in the pedestal, which was welded to a steel plate. The plate was 4 ft. 6 in. x 3 ft. 9 in. x 1/4 in. thick and was bolted to the test floor. The form work was built, and concrete with a nominal strength of 3000 psi was placed. The pedestal was provided with the shear key and the hinge bars (Fig. 6.2).

In Figure 6.9 the erection of a girder on the pedestal can be seen. The other end of the girder rested on a temporary support. Figure 6.10 shows the continuous end and the pedestal. The #10 hinge bars, the shear key and the girders resting on 4-in. x 4-in. wooden blocks can be seen in the figure.

Construction of the Deck Slab and the Diaphragm

The form work for the 7-1/2 in. slab and the 18-in. wide diaphragm was erected. The slab was provided with longitudinal reinforcement in two layers that were 12-#7 x 39 ft. 10 in. long at the top and bottom (Fig. 6.11). The transverse reinforcement in the slab consisted of a #5 bars placed 9 in. on center at the top and bottom. All the strain gages were initialized to zero. Concrete with a nominal strength of 4000 psi was placed in the diaphragm and the slab (Fig. 6.12). Strain measurements were taken after the concrete was poured. The form work was removed after a week.

Loading Mechanism

Two actuators of 300 kips capacity each were used for loading the girder (Fig. 6.13). Each actuator had a base of 3 ft. x 3 ft. x 1 ft. 6 in. and the two opposite faces of the base had ten 1-1/2 in. bolt holes. Two W24 x 62 x 9 ft. 6 in. beams were used to support the two actuators. The beams were anchored to the floor with sixteen A324 1-1/4 in. bolts. A holddown was provided at a distance of 13 ft. 10 in. from the diaphragm. This consisted of two W24 x 68 x 8 ft. beams, which were anchored to the floor with sixteen A324 1-1/4 in. bolts.

A cross beam consisting of two W24 x 68 x 7 ft. 6 in. was placed on the slab. This was located at a distance of 13 ft. 10 in. from the diaphragm. A similar crossbeam was provided on the actuator side. High strength, heat treated bars of 2-1/2 in. were connected to the actuator heads and the ends of the cross beams. Similar bars were used to link the holddown beam and the corresponding cross beam. In one of the links

between the actuator head and the end of the cross beam, a load cell with a capacity of 300 kips of tension was installed.

Lateral supports consisting of 4-in. rubber wheels were provided near the loading point and the holddown location to prevent lateral movement and to ensure that the deflection was vertical. Two dial gages were installed on either side of the web at the actuator end to observe any twist of the end of the girder. The deflection of the girder at the point of load application was recorded with the help of a transit and a scale mounted on the surface of the web. Figure 6.14 shows the experimental setup before testing commenced. The figure shows that the temporary wooden supports were removed at this stage so that each girder behaved as a cantilever. As the loading began, the end of the girder that was toward the actuator was free to deflect, while the holddown prevented the upward movement of the other end.

The Destructive Test

The test was conducted on April 23, 1987. The data logger was initialized, and all the strain readings were set at zero. A load of 12 kips, corresponding to a hydraulic pressure of 3000 psi, was applied and then removed to ensure against slack in the mechanical connections. The data logger was initialized again and the deflection reading was recorded. The beam was then loaded with 30 kips. Thereafter, the load was increased in steps of 60 kips up to a load of 210 kips. Beyond that, the girder was loaded in increments of 30 kips. At every load, the step strains and deflections were recorded. Cracks were observed and marked and at each end of the cracks the applied load was recorded. Load levels were noted on the cracks as they developed.

The final load was 480 kips. The connections of the beams supporting the actuators were designed for 500 kips. At 510 kips, one of the connections failed. Therefore, further loading was not possible. Because of the high level of loading reached, the objectives of the test were satisfied.

At this applied load, strain and deflection readings were taken. The load was then reduced gradually to zero and the permanent deflection was recorded.

The maximum deflection at the applied level of 480 kips was 3.3 in. The permanent deflection was 0.9 in. The load was reduced steadily to zero. The recovery after removal of the load was recorded.

Table 6.1

Design Loads at Pier 5

Case	Maximum Moment Case (ft-kips)	Maximum Shear Case (kips)
Vdl	99.5	99.5
VDL cont.	35.7	35.7
Vll	34.2	45.2
Vu	250.	274.
Mdl	-952.	-952.
Mll	-1067.	-804.
Mu	-3554.	-2980.

DL (Uniform Continuous) = 0.43 K/ft.
Impact = 1.194
Distribution = .955
Span = 132.8 ft.

Where, Vdl = factored dead load, kips

Vdl cont. = factored uniform continums dead load, kips

Vll = factored live load, kips

Vu = design factored load, kips

Mdl = factored moment due to dead load, ft-kips

Mll = factored moment due to live load, ft-kips

Mu = design factored moment, ft-kips

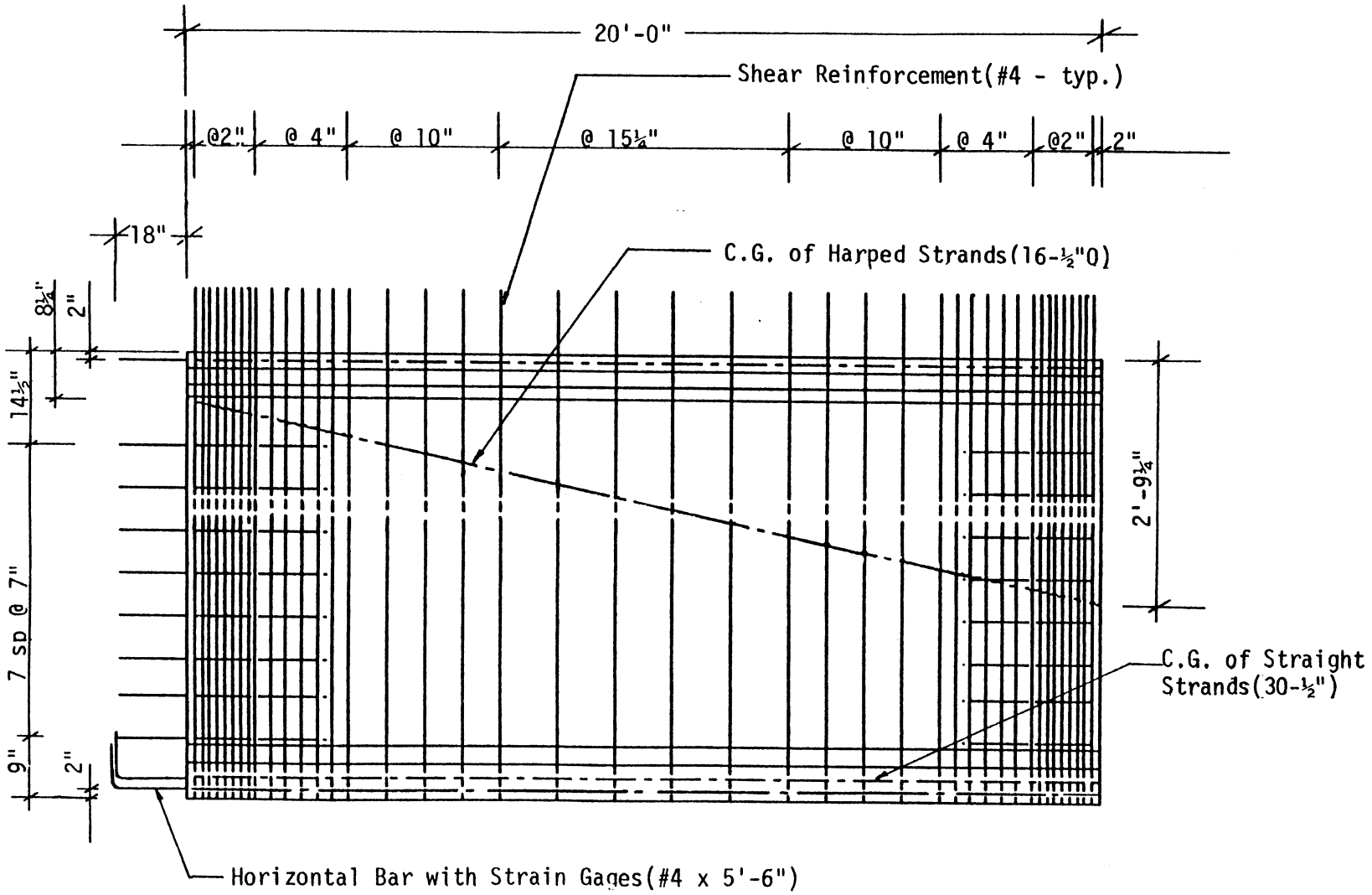

Figure 6.1 Laboratory Test - Longitudinal Section of a Test Girder

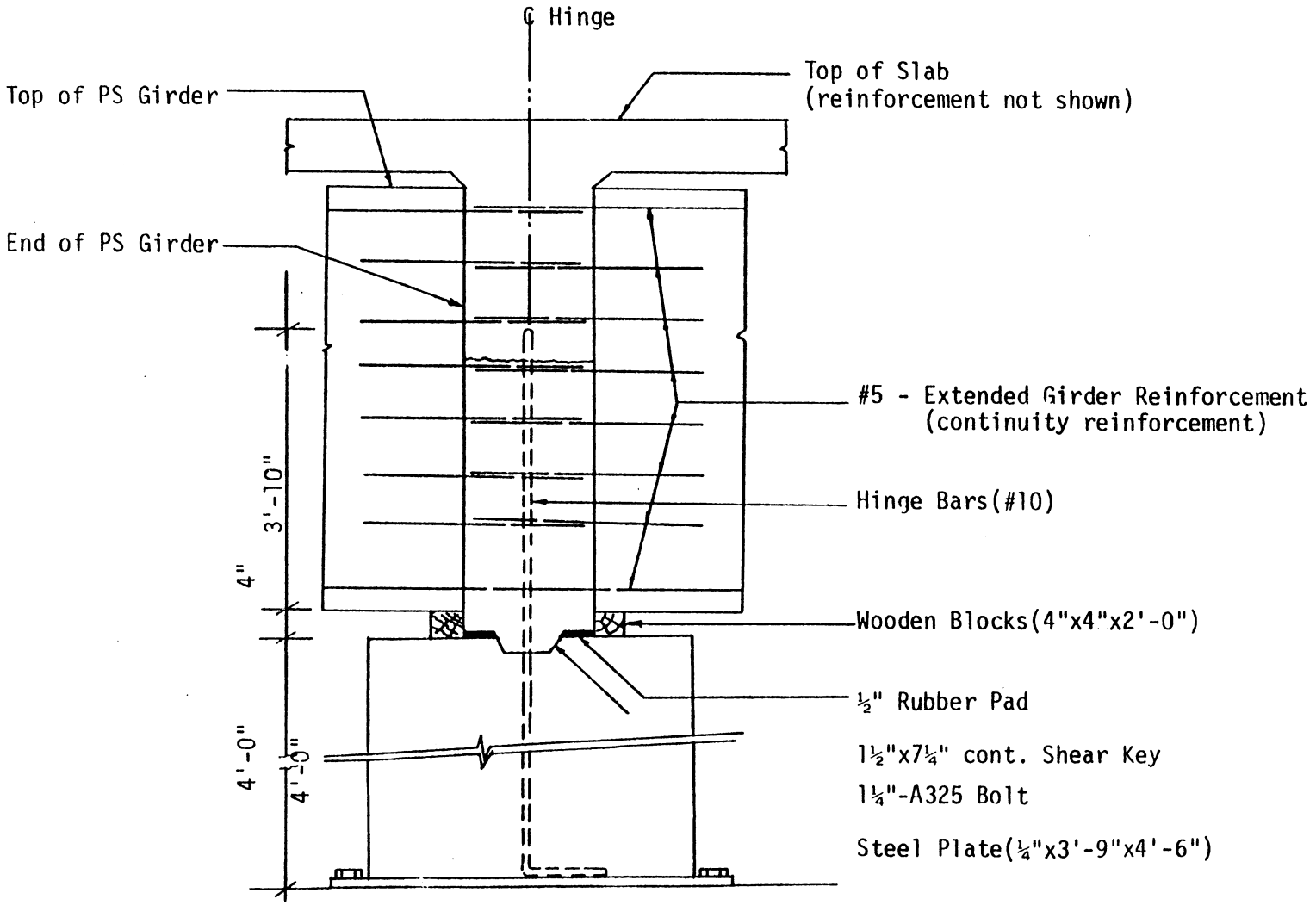

Figure 6.2 Laboratory Test - Continuity Joint (typ. hinge section)

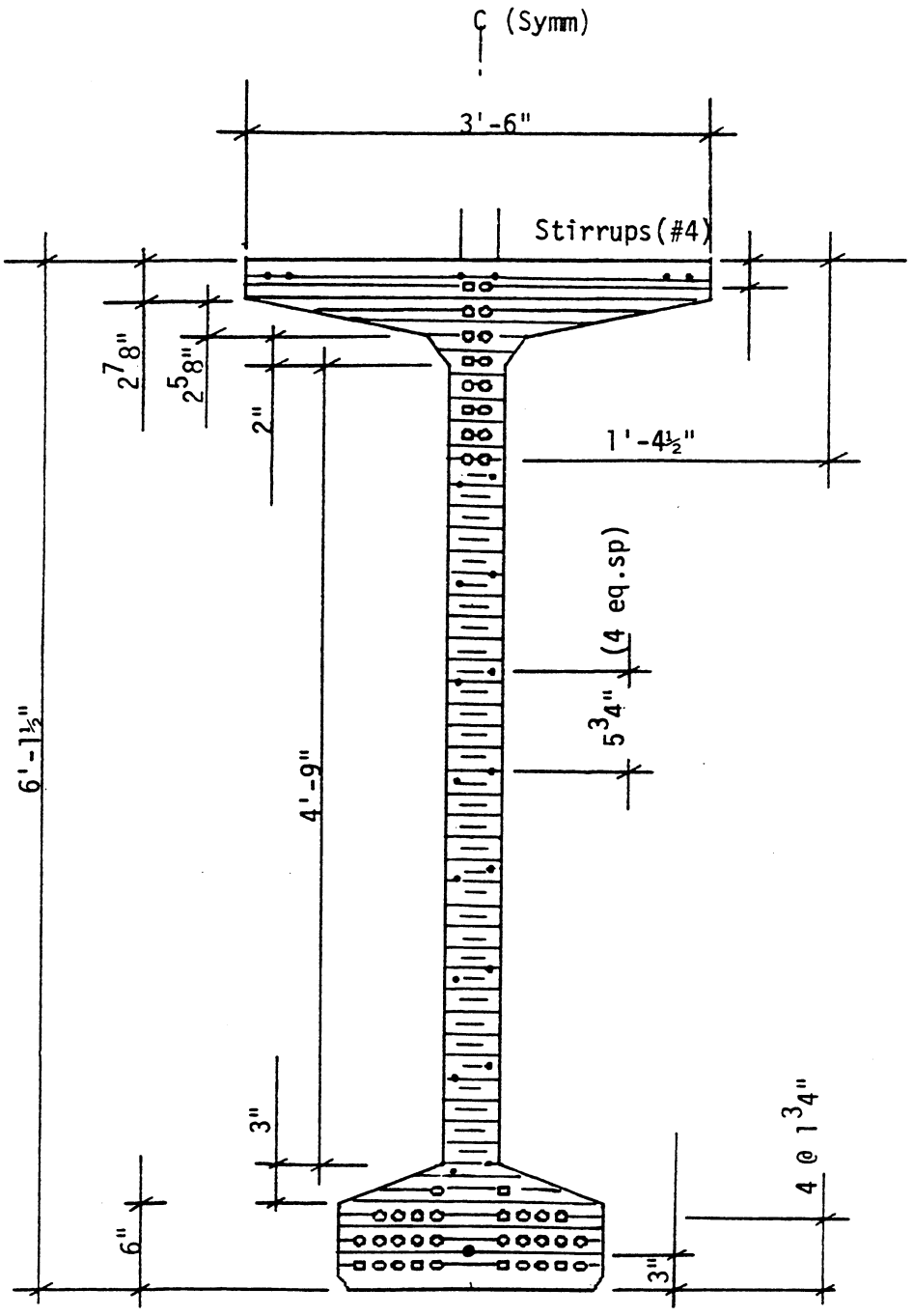

Figure 6.3 Laboratory Test - View of the Continuous End of a Test Girder

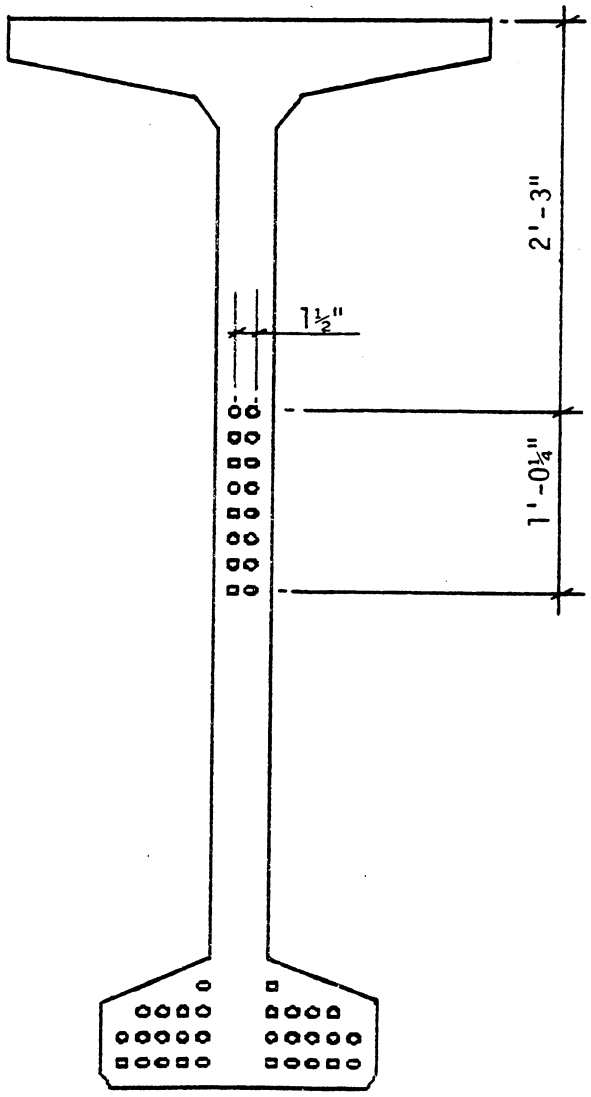

Figure 6.4 Laboratory Test - View of the Discontinuous End of a Test Girder

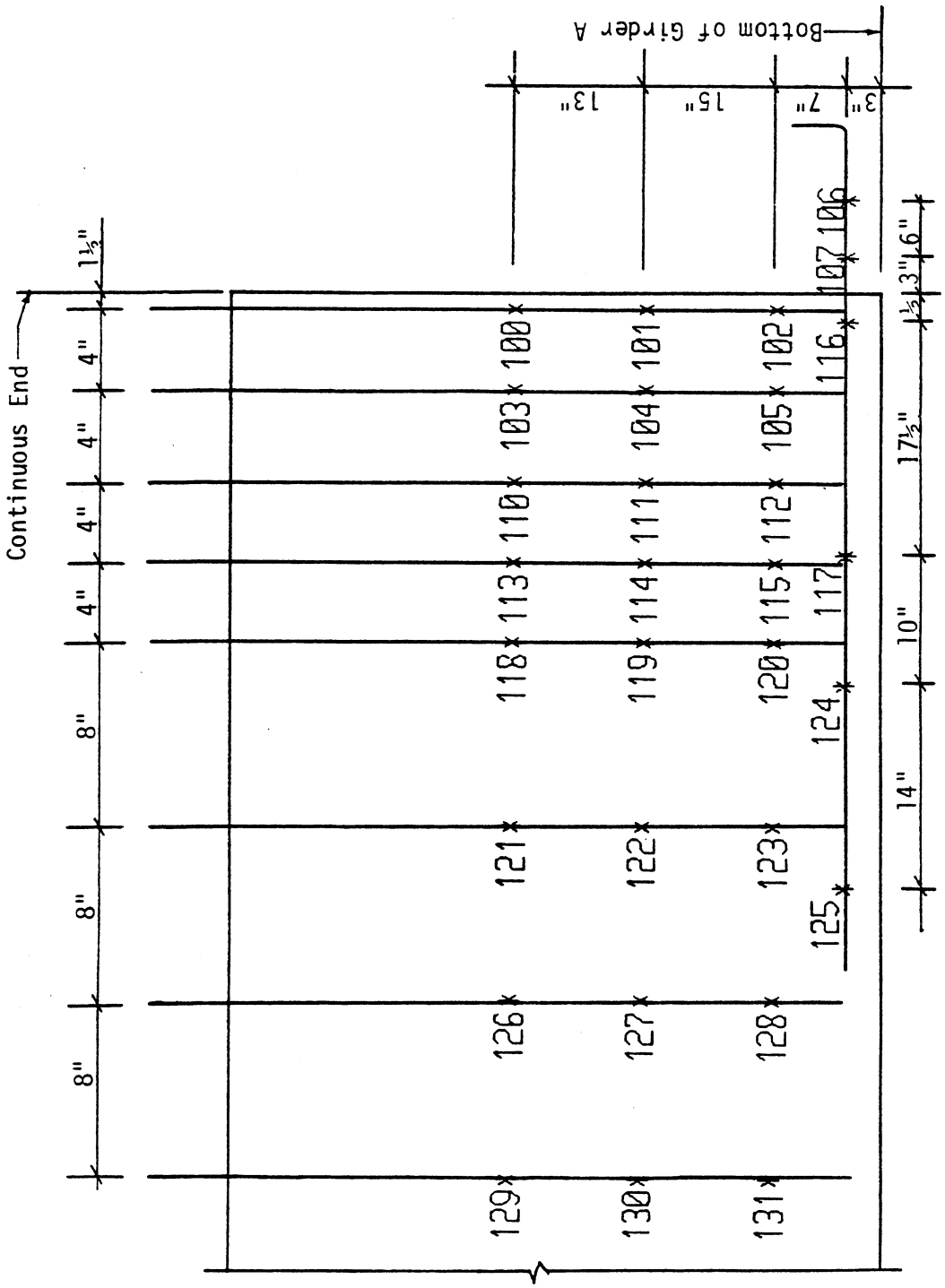

Figure 6.5.a Laboratory Test - Configuration of Strain Gages on Stirrups of Girder A

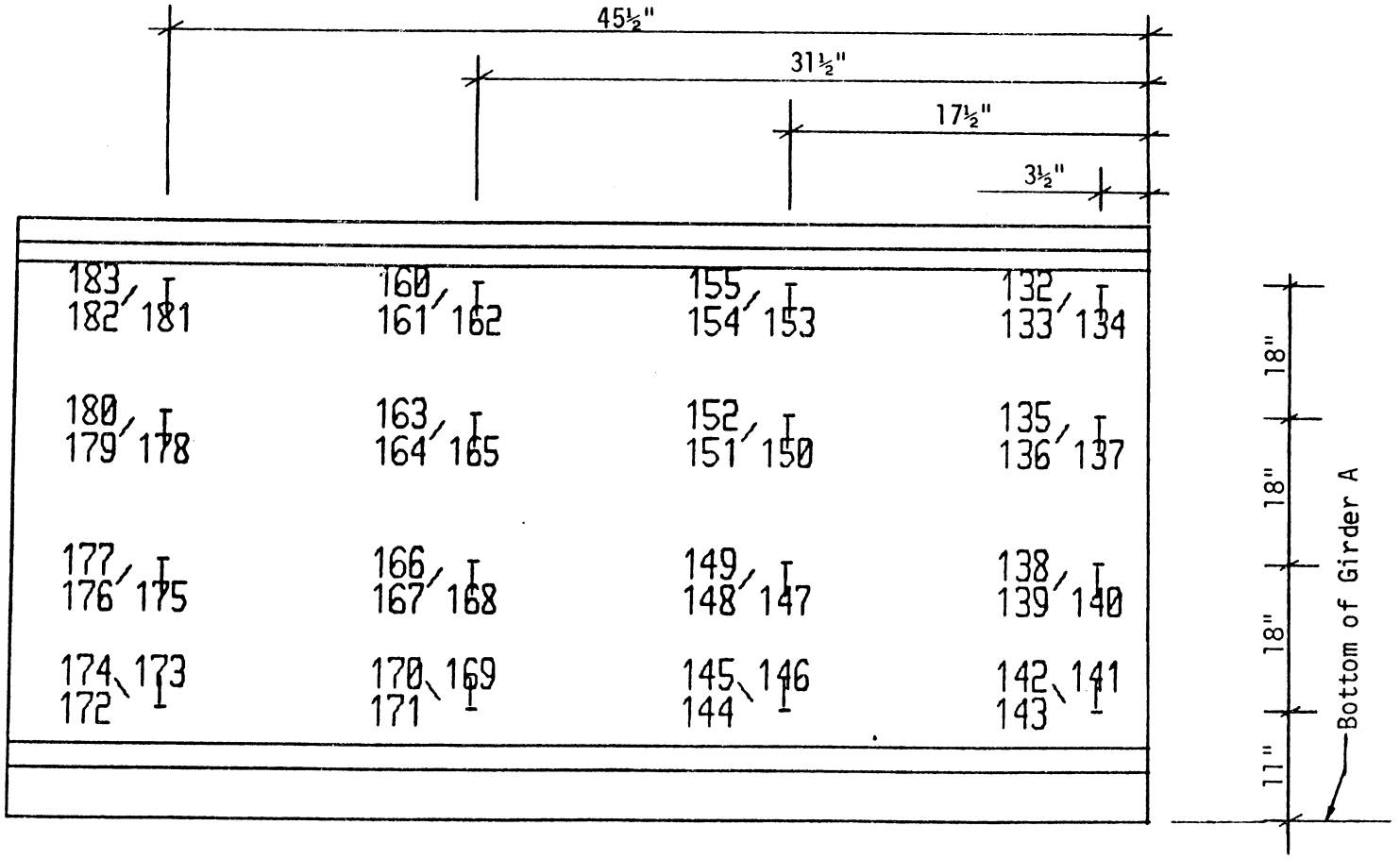

Figure 6.5.b Laboratory Test - Configuration of Strain Gages on the Web Surface of Girder A

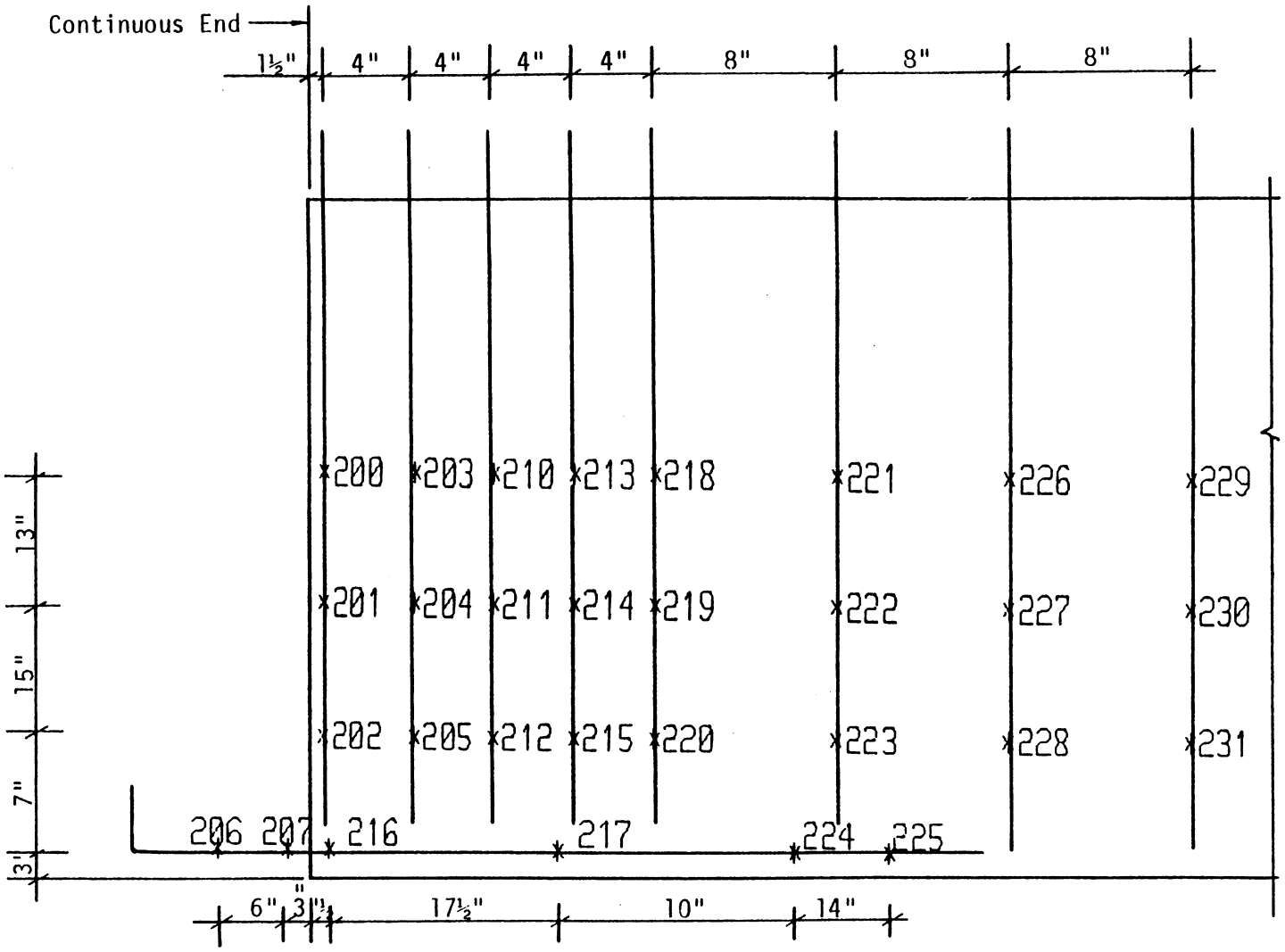

Figure 6.6.a Laboratory Test - Configuration of Strain Gages on Stirrups of Girder B

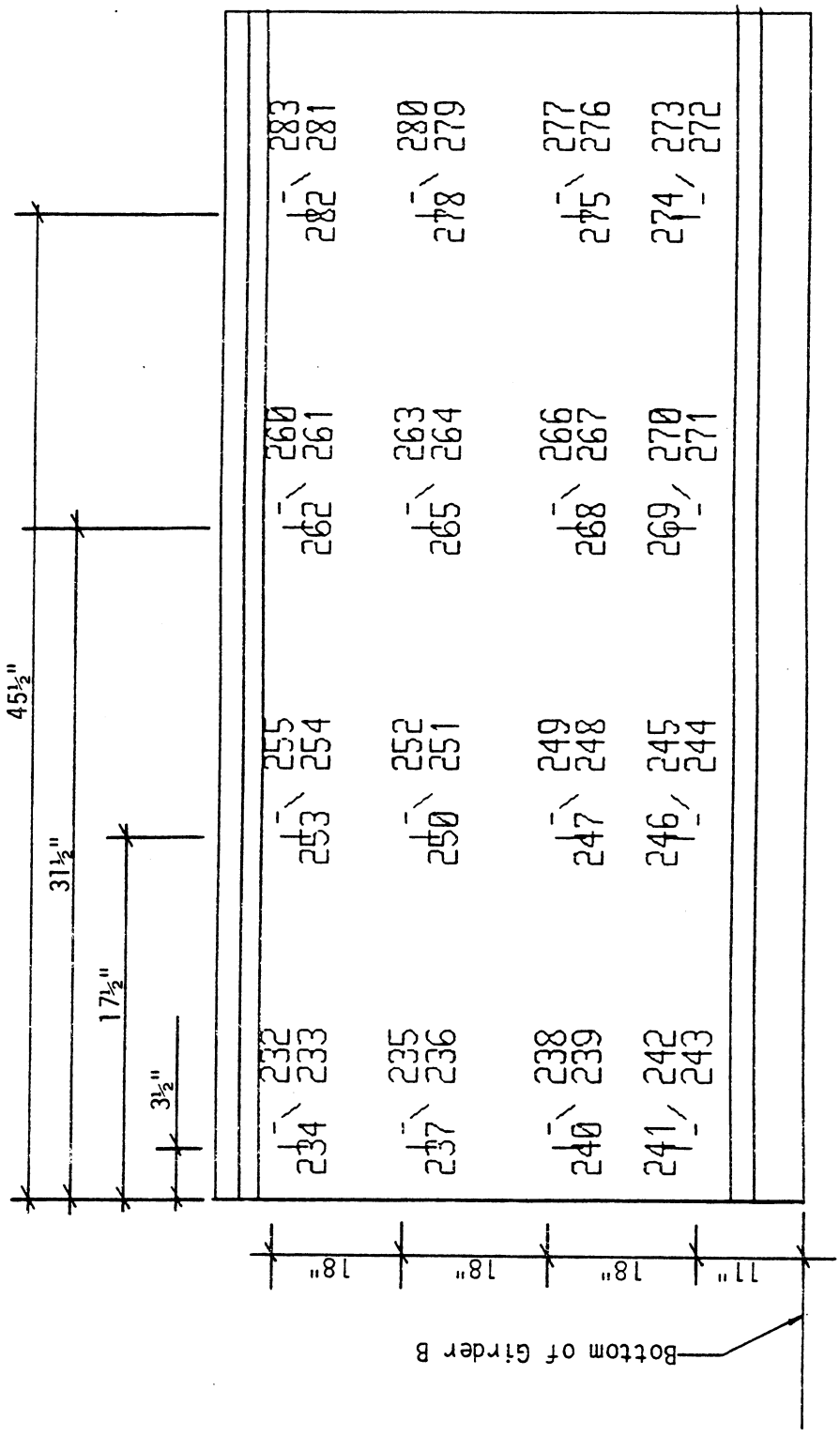

Figure 6.6.b Laboratory Test - Configuration of Strain Gages on the Web Surface of Girder B

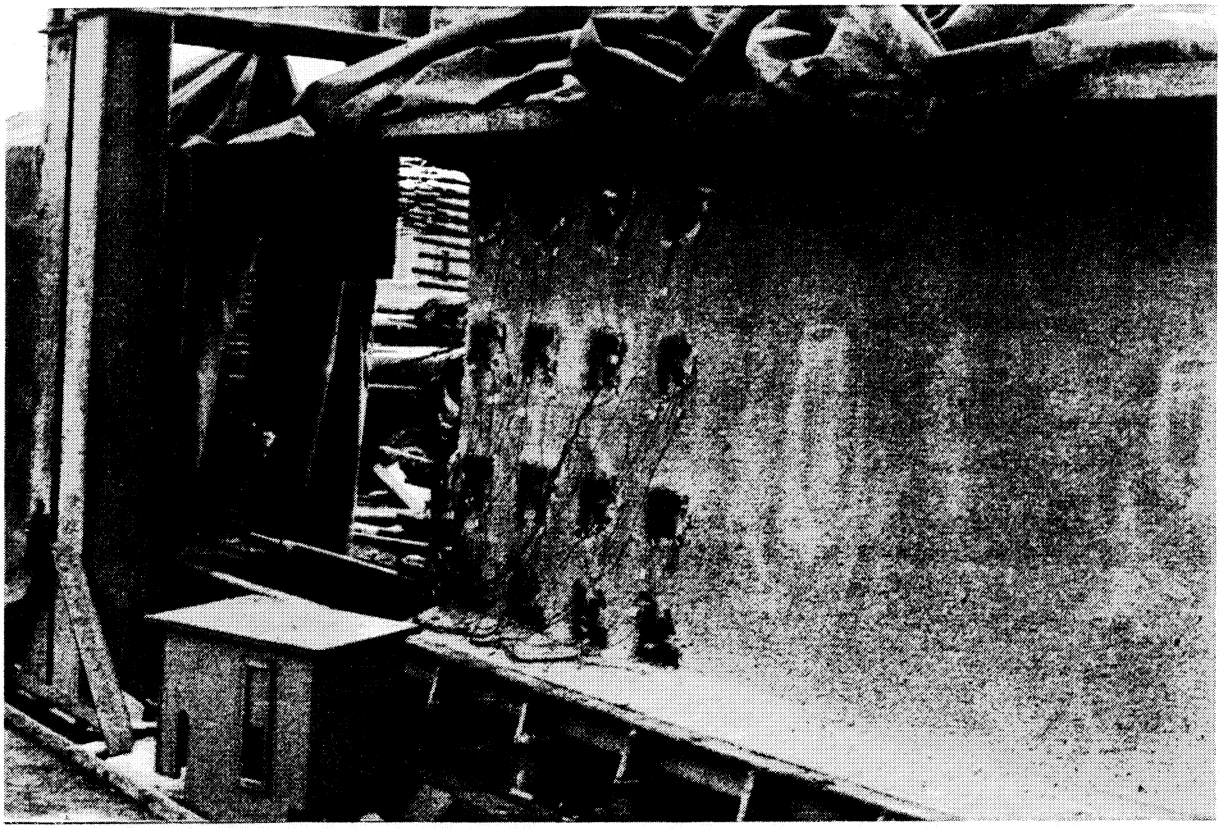

Figure 6.7 Laboratory Test - Portion of Girders A and B at the Continuous End Prior to Detensioning

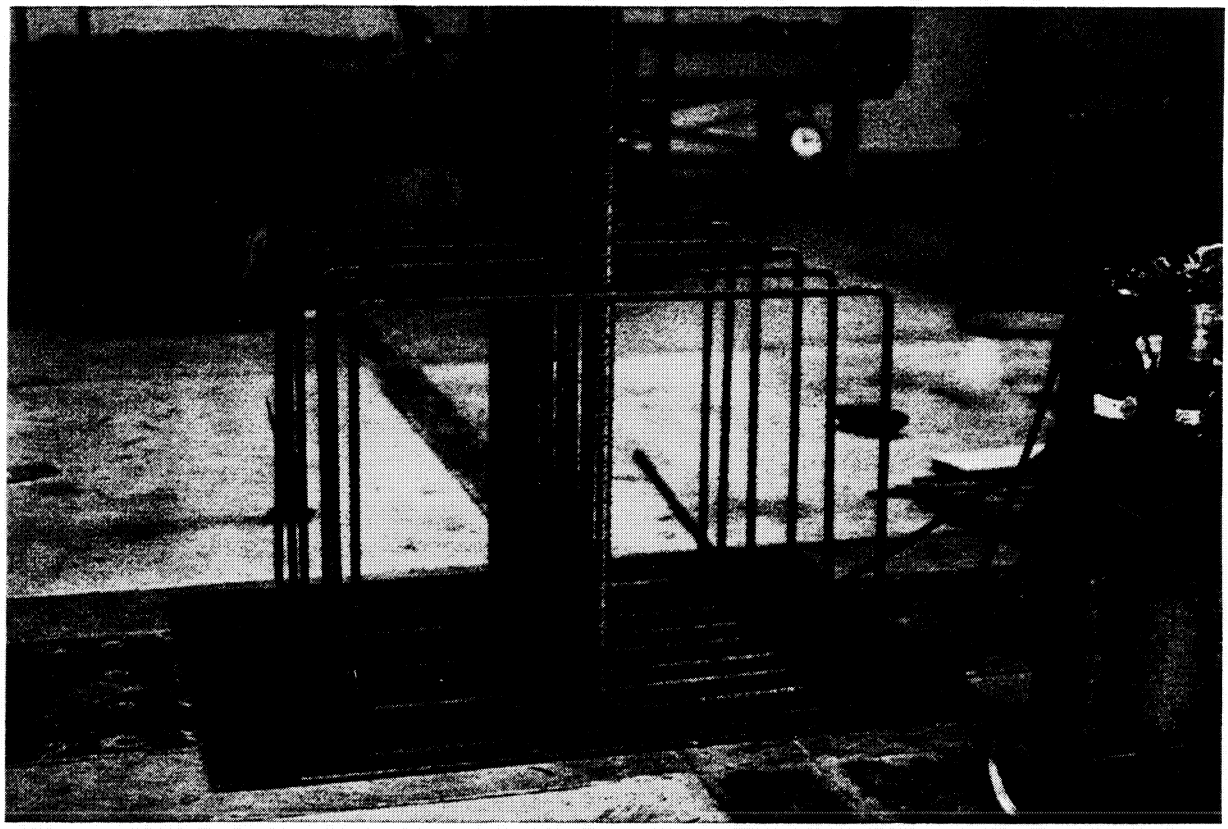

Figure 6.8 Laboratory Test - Reinforcement in the Pedestal and the Hinge Bars

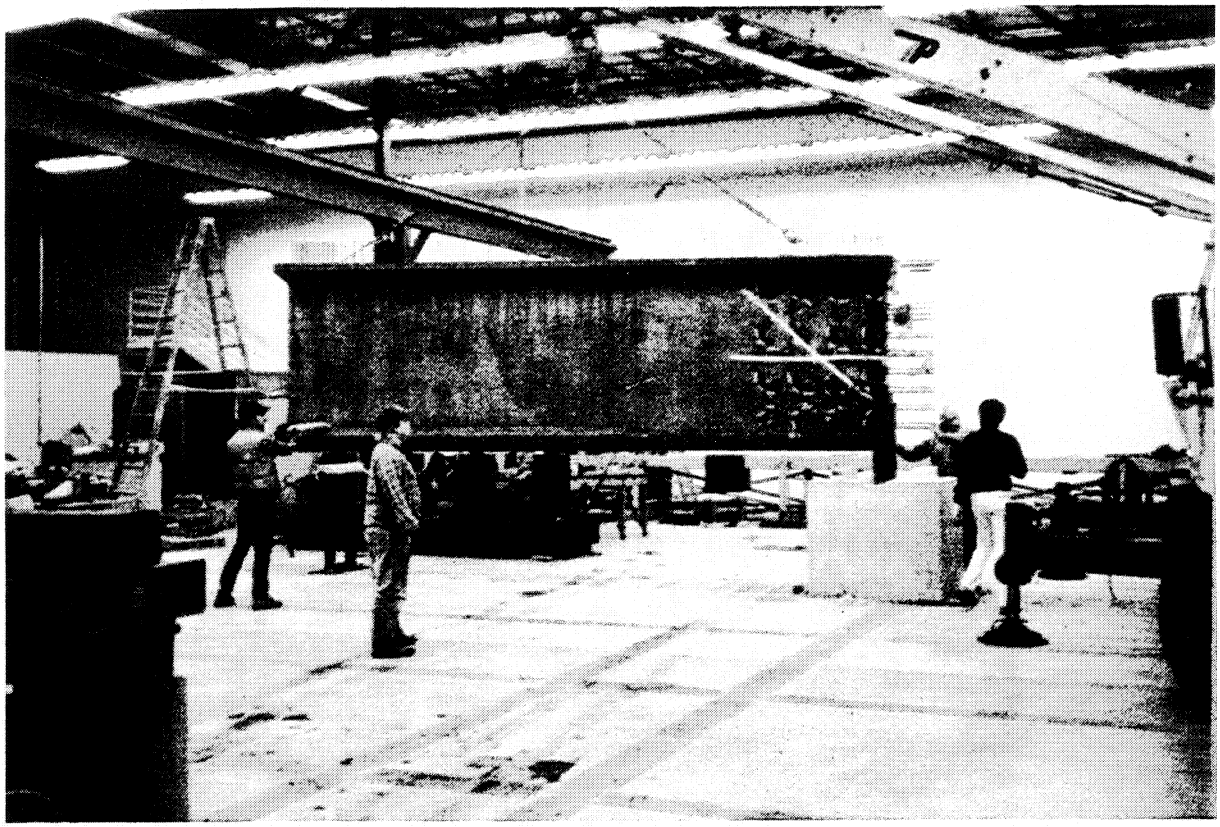

Figure 6.9 Laboratory Test - Erection of Girder A on the Pedestal

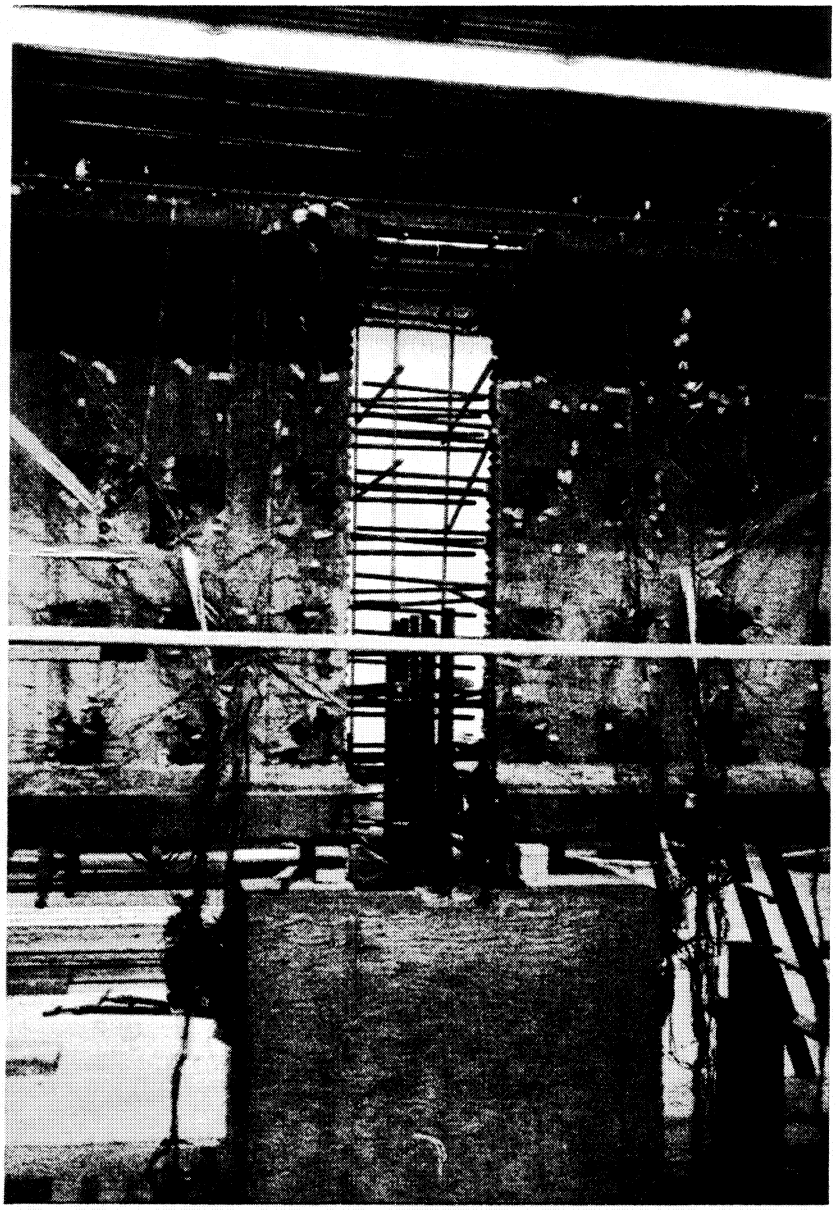

Figure 6.10 Laboratory Test - Portion of the Continuity Connection

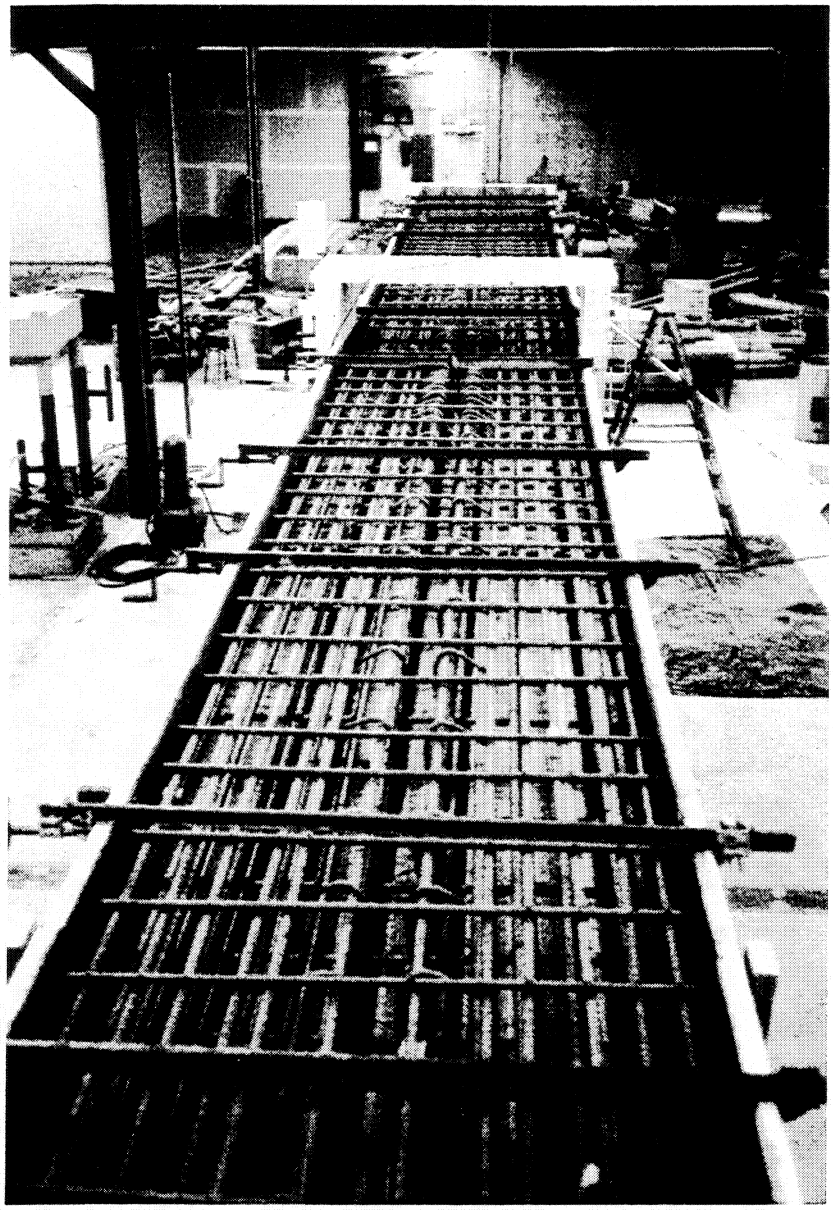

Figure 6.11 Laboratory Test - Reinforcement in the Slab

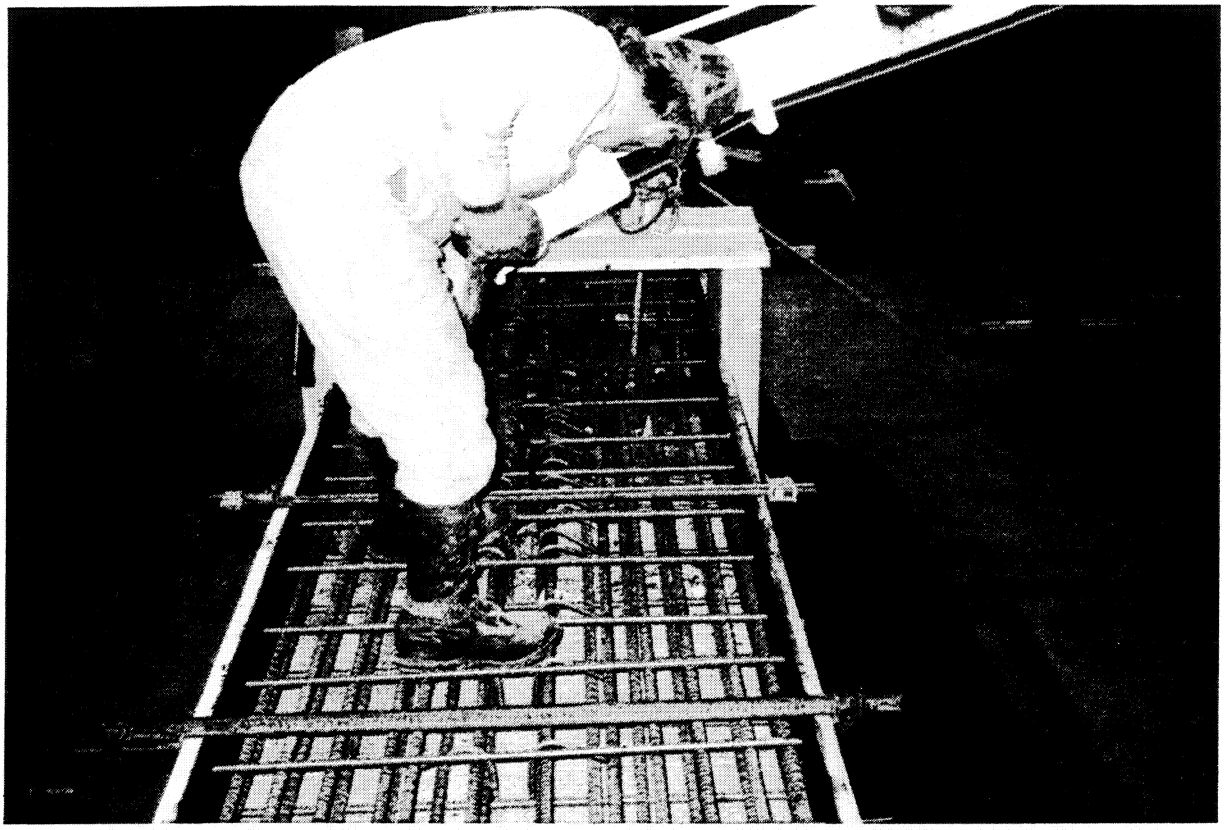

Figure 6.12 Laboratory Test - Placing Concrete in the Forms

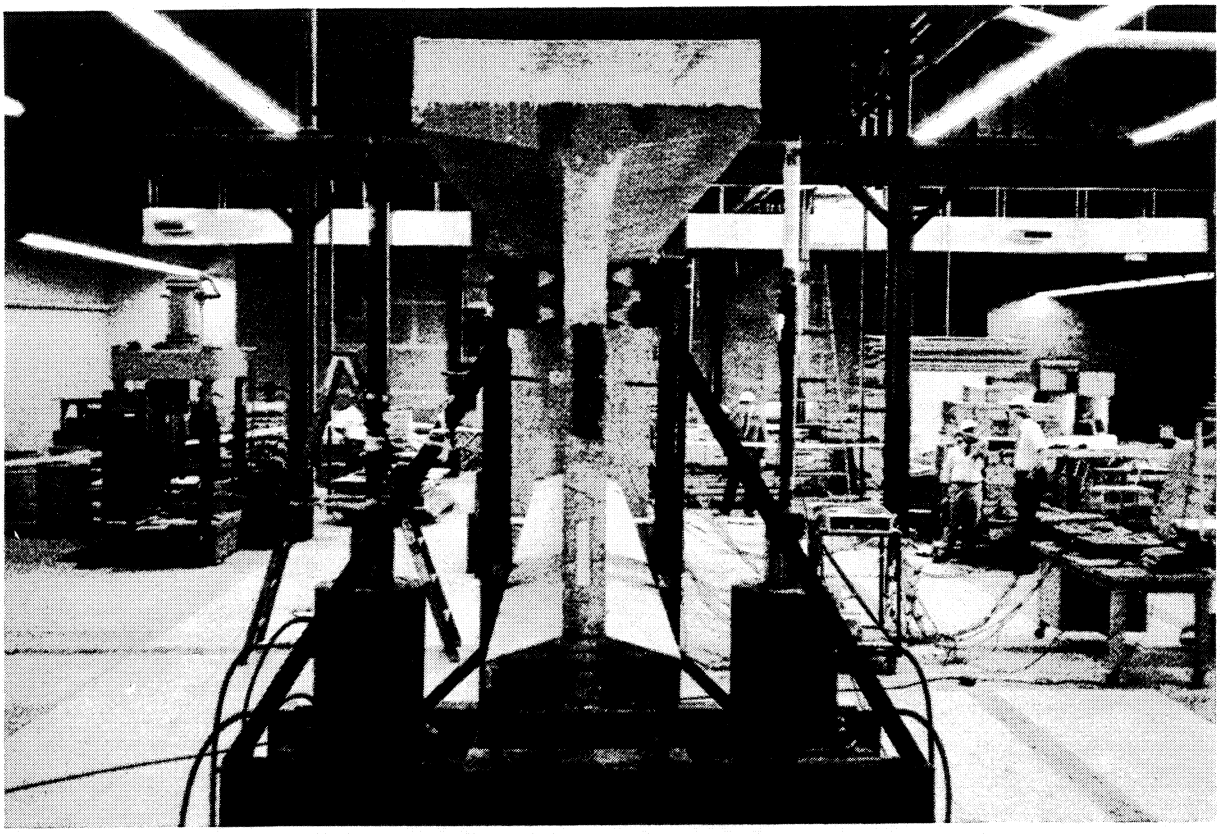

Figure 6.13 Laboratory Test - The Actuators (endview)

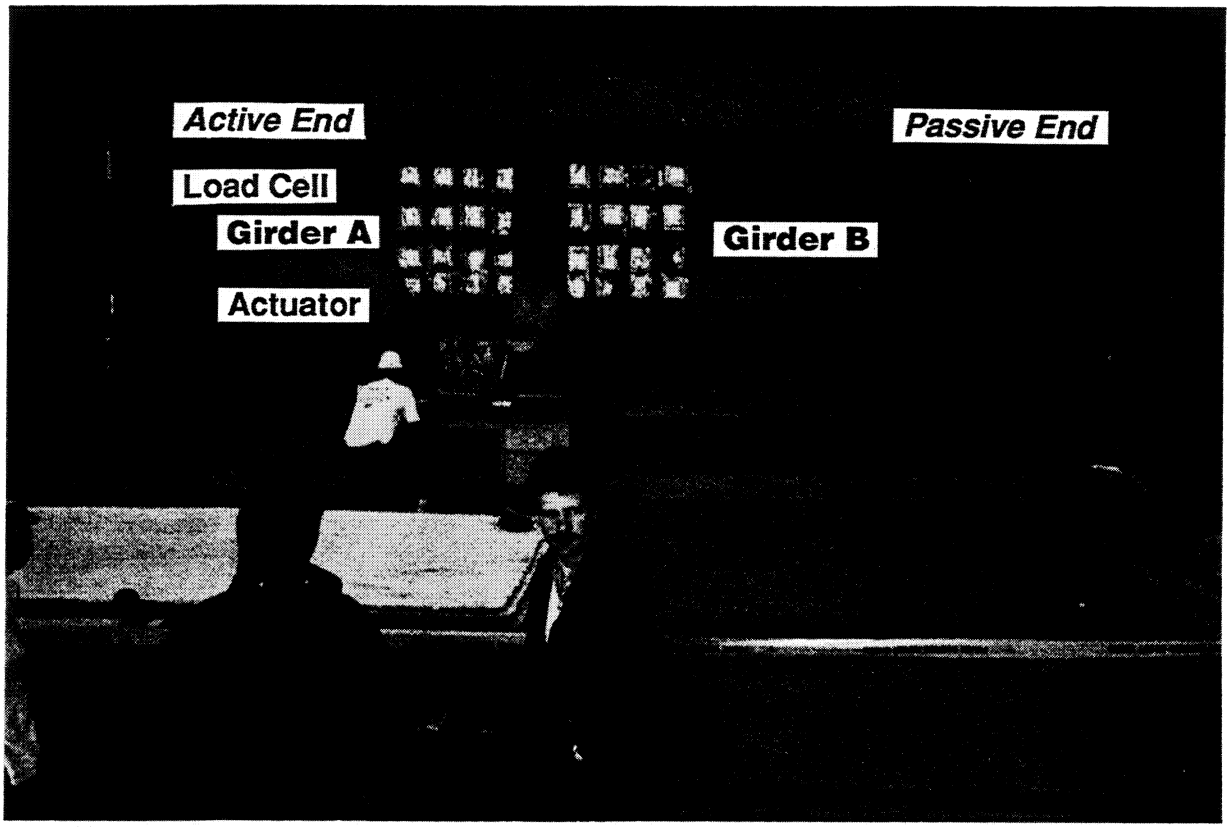

Figure 6.14 Laboratory Test - Elevation of the Experimental Setup

CHAPTER 7

OBSERVATIONS AND RESULTS OF THE LABORATORY TEST

In this chapter, the observations and results of the laboratory test are discussed. The first section deals with the stresses and the strains present after the prestress transfer. The stresses and the strains due to the applied loads are discussed in the next section. Then, the stresses and the strains due to the combined effects of detensioning, casting of the slab and the diaphragm, and the applied loads are presented. The strains in the slab and the diaphragm showed little change after the prestress transfer. Therefore, the stresses due to the combined effects of detensioning, and the slab and the diaphragm's weight are not discussed. The cracking pattern is compared with the theory in the following section. Then the load versus the deflection curve is discussed. Finally, the findings of the destructive test are summarized.

Table 7.1 gives material properties useful for design and analysis.

After the Prestress Transfer

The stresses in the stirrups and the steel bar, which was specially provided to measure strains in the bottom flange, were obtained by multiplying the strains by the modulus of elasticity of steel (E = 29000 ksi). The Tables 7.2 (a-c) and Figures 7.1 (a-c) show the variation in the stresses along the length of the girders. The following observations can be made from the tables and figures.

1. The stress in the stirrups decreased with an increase in the distance from the ends of girders A and B because the bursting and the spalling zones were located in the end zones.
2. At the levels of the centroidal axis, the resultant prestressing force, and the junction of the web and the bottom flange, the stresses near the end were 20, 23, and 23 ksi, respectively. The stresses decreased with an increase in the distance, except at gages 230, 123, 223, 131, and 231, where the stresses varied from 20 ksi to 29 ksi.
3. In Tables 7.2 (a-c) stresses more than 3.5 ksi indicated the presence of microcracks. The value 3.5 ksi was based on the assumption that the tensile strength of concrete is $7.5\sqrt{f'c}$ and the modulus of elasticity of concrete is $33\, w^{1.5}\sqrt{f'c}$ (Table 7.1)
4. Girders A and B agreed well. This supports the validity of the results. There were differences in the stresses (Table 7.2.c) at the junction of the web and the bottom flange because the region was highly susceptible to microcracking and because of the subsequent non-uniform behavior of concrete.

The above observations are consistent with the study by Itani and Galbreith [13]. In their experimental study of the WSDOT series 14 girders without end blocks, they monitored strains in the end zones.

As previously indicated, a #4 steel bar was placed horizontally at the center of the bottom flange and 3 in. from the bottom in each girder. Table 7.3 and Figure 7.2 show the stresses in the steel bar at different locations along the length of the bar. The tensile stresses varied between 2 to 4 ksi and were considerably lower than the stresses in the stirrups because the bar was away from the spalling and the

bursting zones and at the same time, the bar was oriented in the direction of cracks caused by spalling and bursting effects. The compressive zone began at a distance of 28 in., which was beyond the transition zone of 25 in. from the end (Table 7.3).

The data from the gages on the surface of the web concrete are given in Tables 7.4, 7.5, and 7.6. There was no correlation between the data from girders A and B except at a distance of 45.5 in. from the end of the girders. There was considerable difference within the transition zone of 25 in. One of the reasons is the nonuniform behavior of the concrete. Concrete is a nonhomogeneous and anisotropic material. As a result, the formation of microcracks need not be identical in two girders. The behavior of concrete after the formation of cracks is nonuniform because cracking is a localized phenomenon attributed to the microstructure of the concrete. The transition zone is highly susceptible to the formation of microcracks. In addition, there may be shrinkage cracks, which are often invisible. The locations of these gages on the concrete surface did not match with the gages on the stirrups.

In Table 7.7, the principal stresses on the surface of the web are presented. In computing the principal stresses, the following assumptions were made:

1. Concrete acts as a linearly elastic, homogeneous, and isotropic material.
2. Concrete remains uncracked.
3. A plane stress condition exists.

Table 7.7 shows that the maximum tensile stress is 3206 psi, which indicates cracking of concrete. The maximum compressive stress was

2879 psi, which is less than the allowable compressive stress of 4128 psi.

If one or more legs of a rosette becomes nonfunctional, the results for the rosette become redundant. The principal stresses computed are then not good. In Table 7.7, redundant rosettes are singled out as NG (not good).

The Load Application

In this section the results from the destructive tests are discussed. These results are independent of the strains recorded after detensioning and during casting of the slab and diaphragm.

The Cracking Pattern

Figure 7.3 shows cracking in girder A after applying a load of 270 kips. This corresponds to a maximum shear of 291 kips, which includes the dead load and the applied load. The maximum design shear, Vu was 274 kips. The figure also shows that flexural and flexural-shear cracks were more prominent than web-shear cracks. Shear cracks were located in the web near the top fillet and away from the diaphragm. These were inclined at an angle of 30 degrees. The flexural cracks in the slabs were caused by a load of 210 kips. Some of these cracks propagated into the top flange and web as the load increased.

Figure 7.4 shows the condition of girder B at an applied load of 360 kips. The observations made in Figure 7.3 agree with the cracking seen here. A load of 300 kips resulted in propagation of the cracks formed at 270 kips. The propagation was toward the bottom flange and was restricted to the web. A load of 330 kips caused cracks in the web

at an angle of 30 degrees. These cracks were an extension of earlier shear cracks and extended over a considerable portion of the web.

Figure 7.5 shows girder A at a load of 360 kips. Loads of 300, 330, and 360 kips caused cracks, which were inclined at an angle of about 30 to 35 degrees. As the load increased there was an extension of earlier cracks, as well as the development of new cracks. The cracks were equally spaced and were located away from the diaphragm.

Figure 7.6 shows girder B at an applied load of 450 kips. There were flexural cracks in the slab and top flange, and flexural cracks in the portion of the web toward the diaphragm. Cracks due to web-shear appeared at loads higher than 300 kips. These cracks appeared parallel to each other, equally spaced and extended throughout the web.

Figure 7.7 shows the similarity in the cracking pattern of both the girders. Cracks were not observed in the diaphragm.

The observations can be summarized as follows:

1. Cracks in the slab and top flange were due to flexural tensile stresses. The first visible flexural crack appeared at an applied load of 210 kips.
2. At an applied load of 270, the cracks were mainly due to flexural-shear. These were located generally on the tension side of the web and fell within a distance of h/4 from the girder, where h is the overall depth of a composite section. The applied load of 270 kips corresponded to a maximum shear of 291 kips, which was higher than the maximum design shear of 274 kips.
3. Cracks located within a distance h/2 from the face of the diaphragm were inclined at varying angles, depending on their location with respect to the neutral axis. Cracks located in the tension zone

were inclined at an angle between 40 to 50 degrees to the horizontal. Cracks in the compression zone were inclined at an angle of 25 to 30 degrees. Thus in the tensile region, flexural-shear cracks occurred, while in the compression region cracks were due to shear stresses combined with direct and flexural compressive stresses.

4. For cracks located at a distance greater than h/2, the angle of inclination varied from 25 to 30 degrees. These cracks were due to loads of more than 270 kips. Cracks due to loads of 270, 360, 390, 420, 450 and 480 kips were located at a distance of 1 ft 6 in., 3 ft., 3 ft. 8 in., 6 ft. 3 in., 10 ft., and 10 ft. 3 in. from the face of the diaphragm along the centroidal axis. The corresponding angles of inclination at these locations were 65, 50, 35, 30, 29, and 25 degrees.
5. Most of the web-shear cracks originated at the junction of the top flange and web and propogated towards the bottom flange at an angle about 30 degrees. The web-shear cracking was observed at loads higher than 300 kips.

The strains recorded during the destructive test were due to the applied loads only, because the gages were initialized before the load application. A gage showing irregular readings or a sudden jump in strains indicated formation of cracks in the vicinity of the gage. A gage on a stirrup experienced a sudden increase in strain due to cracking of the concrete and the subsequent transfer of loads to the stirrup. Until then, the gage exhibited strains consistent with the state of stress in the concrete surrounding the gage. If a crack

crossed a gage on the concrete surface, the gage may have ceased to function due to excessively large strains.

Figure 7.8 shows that cracks due to applied loads did cross the gages installed on the surface of the web. Thus, if a crack crossed a rosette, the corresponding principal stresses became unreliable. In the figure, the cracks that were away from the diaphragm appear to be parallel. The angle of inclination varied from 28 to 34 degrees.

Strains versus Applied Loads

The variation of strains in the gages as the applied load increased from 30 to 480 kips is discussed in the following sections.

Gages on the Stirrups. In Figures 7.9, and 7.10 strains versus applied loads are plotted for the gages that are located at 38 in. from the bottom of the girders on the stirrups.

In Figure 7.9, gages 100 and 200 show the presence of microcracks at a load of 150 kips. For loads of more than 150 kips, the strain increased. Gages 113 and 213 indicated the formation of microcracks at a load of 270 kips. The gages in Figure 7.9 were located below the centroidal axis of the composite section.

Figure 7.10 shows that gages 118 and 218 behaved linearly up to a load of 300 kips. while gages 129 and 229 showed a linear response up to 360 kips. At loads of more than 300 and 360 kips, respectively, concrete cracking transferred the load to the stirrups.

The response of the stirrups at the level of the prestressing force, i.e., at 25 in. from the bottom of the girders, can be seen in Figures 7.11 and 7.12.

Figure 7.11 shows that deviation occurred at a load of 270 kips. In the case of gages 114 and 214, there was a transition from a compressive strain to a tensile strain. For gages 122 and 222, instead of a sudden increase in strain, deviation from linearity occurred at a load of 360 kips.

For gages 127 and 227 (Fig. 7.12), the cracking load was 360 kips. Gage 130 indicated a linear increase in tensile strains up to 390 kips and then deviated from linearity. Gage 230 did not function.

The strains in the gages at the junction of the web and the bottom flange are plotted in Figures 7.13 and 7.14.

Gages 105 and 205, shown in Figure 7.13, indicated compressive strain, while gages 115 and 215 showed negligible strains up to a load of 300 kips. Beyond this point, the strains became increasingly tensile. Figure 7.14 shows that gage 123 behaved linearly up to a load of 480 kips, while gage 223 deviated from linearity at 360 kips. The steady increase of tensile strains in the gages was due to the strutting behavior of the concrete. Strutting action causes the stirrups to be in tension. The resultsagree with the cracks observed near the web and the bottom flange (Fig. 6.5).

The following conclusions can be drawn from the strains in the stirrups.

1. Loads at which the strains versus loads curve deviates from linearity increased further away from the diaphragm.
2. Gages located up to a distance of 13.5 in. showed irregularity at either 270 or 300 kips.
3. Gages located beyond a distance of 13.5 in. behaved linearly for loads between 300 to 390 kips.

Gages on the Longitudinal Steel Bar at the Center of the Bottom Flange. Strains in the steel bar located at 3 in. above and along the centerline of the bottom flange are presented in Figures 7.15 to 7.17.

Gages 106, 206, 107, and 207 were located within the diaphragm. Hence they indicated compressive strains (Fig. 7.15). Figures 7.16 (a-b) shows a comparison between the experimental values and the theoretical values.

The theoretical values were based on the assumptions that concrete acts as a homogeneous and linearly elastic material. Theoretical results were obtained with the flexural equation. In obtaining the theoretical results, the tensile reinforcement in the slab was transformed into an equivalent area of concrete. The deviation of the experimental values from the theoretical results began at a load of 270 kips.

Figure 7.17 shows that gages 124 and 224 showed development of cracks at a load of 330 kips. Gage 225 did not function. Gage 125 showed deviation from linearity at a load of 270 kips. The gages showed negligible strains before deviating from linearity, and later they showed tensile strains.

The strains in the steel bar lead to the following conclusions.

1. The maximum compressive strain at the mid-section of the diaphragm was 0.0017, which is about 50 percent of the maximum compressive strain that concrete can sustain.
2. The tension in gages 124, 224, and 125 can be explained on the basis of the compression strut theory. The formation of cracks in the web near the bottom flange results in a strutting action in the web. The horizontal component of the force in the strut is

resisted by the bottom flange, which behaves as a tension member. Thus, the gages on the steel bar indicated tensile strain.

Gages on the Bottom Flange. Figures 7.18 (a-d) show gages 156 through 159 and gages 256 through 259, which were located 3 in. from the bottom flange and at distances of 3.5, 17.5, 33.5, and 45.5 in. from the face of the diaphragm. The strains in these gages were compressive due to the applied negative moment.

The following conclusions are drawn from Figures 7.18 (a-d).

1. The gages showed compressive strain and hence, indicated no correlation with the gages along the centerline of the bottom flange.
2. The experimental results compared well with the computations that were based on the assumptions mentioned earlier.

Gages on the Surface of the Concrete. In Figure 7.19, the results from gages 134, 234, 153, and 253 can be seen. Gage 234 showed the formation of cracks due to excessive tension at a load of 270 kips. Gage 134 showed deviation from linearity at 270 kips and experienced a tensile strain of 364 microstrains at a load of 480 kips. Gage 253 ceased functioning at a load of 300 kips and indicated a sudden change from a compressive strain of -381 microstrains to a tensile strain of 95 microstrains. At a load of 390 kips, gage 153 stopped functioning and recorded a strain of 808 microstrains.

Figure 7.20 presents the performance of inclined gages 133, 233, 154, and 254. Deviation is shown in gages 133 and 233 at a load of 270 kips after they had attained a strain level of 192 microstrains. The figure indicates that at a load of 240 kips, gage 254 showed the

presence of cracks, while at a load of 390 kips, gage 154 indicated the formation of cracks.

In Figure 7.21, gage 237 did not function, while gage 137 indicated a maximum strain of 41 microstrains. Gage 250 deviated from linearity at a load of 330 kips, and gage 150 showed an increase in compressive strain as the load increased. It reached a maximum compressive strain of 359 microstrains at 360 kips. At this stage, it indicated the initiation of cracks, resulting in a decrease in the compressive strain.

Figure 7.22 indicates the nonuniform responses of gages 136 and 251 at 270 kips. Gage 236 reached a strain of 48 microstrains at a load 480 kips. Gage 151 showed a sudden increase in strain at a load of 150 kips, followed by nonuniform behavior at 300 kips.

The rosettes consisting of gages 178, 179, 180 and 278, 279, 280 (Fig. 7.23) reflected cracking at a load of 360 kips. These rosettes were located 47 in. above the bottom of the girder and 45.5 in. from the face of the diaphragm. The cracks in this region were almost parallel.

Figure 7.24 shows the gages forming the rosette at 29 in. from the bottom and 45.5 in. from the face of the diaphragm. The rosettes continued to function up to a load of 300 kips.

Figure 7.25 shows that the rosette on girder A became unreliable after a load of 300 kips was reached. At 300 kips, the horizontal leg of the rosette indicated deviation. The results agree with the cracks observed in Figure 6.5. The corresponding rosette on girder B was redundant because the vertical leg did not function.

In Figure 7.26, the gages forming a rosette 45.5 in. from the diaphragm can be seen. The vertical leg of the rosette recorded strains up to a load of 480 kips.

The conclusions from the above discussion are as follows.

1. The response of the gages on the surface of the concrete cannot be predicted after the formation of a crack.
2. The minimum load at which the deviation of strains occurred was 270 kips. The corresponding gages were nearer to the diaphragm than the gages indicating deviation at higher loads.
3. The performance of individual gages indicated that cracking does not take place at a particular load or at a particular strain.

Effective Strains and Stresses

It may be observed that the compressive stresses exceeded the allowable compression of 3952 psi. These stresses were higher because they were recorded adjacent to the harped strands. In the previous section, the strains and stresses caused by applied loads and corresponding moments were studied. This section presents the combined strains resulting from the effective prestressing force and the slab. The effective prestressing force is assumed to be 75 percent of the initial prestressing force. Assuming that there is a linear relationship between this force and the corresponding data, the data resulting from the effective prestressing force are also assumed to be 75 percent of the strains recorded after the prestress transfer.

Effective Stresses in the Surface of Concrete

In Table 7.8, the results of the rosette consisting of gages 141, 142, and 143 are presented. The table shows that the principal tensile stress was 1433 psi at an applied load of 30 kips. It decreased with an increase in the load. At 360 kips, the principal tension suddenly increased to 2745 psi. At this point, the shear strain was 764

microstrains. The angle of 35 degrees (Table 7.8) at a load of 330 kips agrees with the cracks observed.

Table 7.9 shows the effective strains and corresponding stresses as measured by a rosette. At detensioning stresses have shown the formation of microcracks (Table 7.7). Subsequent application of loads causes the closure of these microcracks. Therefore, the table shows increasing tension in x-direction and compression in y-direction. Stresses obtained from this rosette do not show the actual state of stress in the concrete. As a result, it can be observed that the compressive stresses are more than the allowable limit.

Table 7.10 shows that at a load of 150 kips the tensile stress exceeds the modulus of rupture indicating the formation of cracks. Therefore, subsequent stress values do not represent the actual state of stress in the concrete. As the load is increased, a stage is reached when the strains exceed the capacity of the rosette, resulting in its failure.

Strain measurements on the surface of prestressed concrete should be carefully interpreted. Researchers usually evaluate stresses by placing an instrumented metal bar inside the concrete. In this study strain gages were placed on the surface of the web. Strain gages were initialized at the beginning of each phase of the test. Accordingly should a crack be formed in one phase, strains in the subsequent phases of loading may measure the closure or further opening in the cracks. Therefore, any further measurement of strains beyond the formation of a crack do not represent the actual strains in the concrete.

Table 7.11 presents the results from gages 175, 176, and 177. The cracking angle was 67 degrees, which is 10 to 15 degrees higher than the cracking angle observed in testing.

Effective Stresses in the Stirrups

Tables 7.12 to 7.14 show stresses in the stirrups due to the combined effect of prestressing, the weight of the slab, and the applied moment.

In Table 7.12, stresses that were 38 in. from the bottom of the girders are shown. At a load of 300 kips, the maximum stress in the stirrups was 20 ksi and it occurred at a distance of 1.5 in. from the diaphragm. Up to the applied load of 360 kips, stresses in the stirrups decreased as the distance of the stirrups from the diaphragm increased. For loads higher than 360 kips, stresses in the stirrups at distances greater than 17.5 increased. At a load of 480 kips, the first yielding occurred in the stirrup located 41.5 in. away.

Table 7.13 shows the stresses that were 25 in. from the bottom. Within a distance of 9.5 in., stresses increased as the distance from the diaphragm increased. The maximum stress at a load of 300 kips was 17 ksi and occurred at a distance of 25.5 in. Beyond this load, except at gages 222 and 127, the stresses decreased. At the maximum load of 480 kips, stresses in the stirrups located within the transfer length of 25 in. were about 50 percent of the yield strength. At the same load, yielding occurred in the stirrup located at 25.5 in. from the diaphragm.

At the junction of the web and the bottom flange, i.e., at 11 in. from the bottom, the maximum stress in the stirrups at a load of 300

kips was 17 ksi and occurred at 33.5 in. from the diaphragm. (Table 7.14). At the load of 480 kips, the stresses within a distance of 17.5 in. were within 50 percent of the yield strength and stresses in the stirrups 33.5 in. from the diaphragm were 57 ksi.

Table 7.15 shows the maximum stresses in the stirrups along the length of the girders. The following can be observed from the table.

1. The maximum stress at a load of 300 kips was 20 ksi and occurred at 1.5 in. from the face of the diaphragm. Thus, at an applied load of 300 kips, the maximum stresses are not more than 30 percent of the yield strength of the stirrups.
2. Within the transfer length of 25 in., the maximum stress caused by the applied load of 480 kips was 34 ksi, which is about 60 percent of the yield strength. For locations beyond the transfer length, the maximum stress at 480 kips was 60 ksi.
3. As the load increased from 300 kips to 480 kips, the stresses increased with the increase in distance from the diaphragm. This reflects the observations that at loads higher than 300 kips, cracking takes places away from the diaphragm and that the angle of inclination decreases to 30 degrees or less (Figs 7.3 and 7.4).

Cracking Pattern and Design Codes

The cracking pattern observed can be related to the ACI code (3) and commentary (2) and the AASHTO specifications (1). The ACI code defines V_{ci} and V_{cw} as follows :

$$V_{ci} = 0.6\sqrt{f'c}\, b_w\, d + V_d + V_i\, M_{cr}/M_{max}$$

$$V_{wc} = (3.5\sqrt{f'c} + 0.3\ fpc)\, b_w\, d + V_p$$

where,

$M_{cr} = \frac{I}{y_t} (6\sqrt{f'c} + f_{pe} - f_d)$

b_w = thickness of the web

d = the distance from the extreme compression fiber to the centroid of longitudinal tension reinforcement but need not be less than 0.80 h

$f'c$ = the strength of the concrete in psi

f_d = the stress due to unfactored dead loads, at the extreme fiber of section, where tensile stress is caused by externally applied loads, psi

f_{pc} = the compressive stress at the centroid of the composite section caused by both prestress and moments resisted by a precast member acting alone, psi

f_{pe} = compressive stress in concrete caused by effective prestress forces only (after allowance for all prestress losses) at the extreme fiber of sections where tensile stress is caused by externally applied loads, psi

h = the overall depth of the section, in.

I = the moment of inertia of the section resisting externally applied factored loads

M_{max} = the maximum factored moment at the section due to externally applied loads

V_{ci} = the nominal shear strength provided by concrete when diagonal cracking results from combined shear end moment

V_{cw} = the nominal shear strength provided by concrete when diagonal cracking results from excessive principal tensile stress in the web

V_d = the shear force at the section due to a factored dead load

V_i = the factored shear force at the section due to externally applied loads occurring simultaneously in Mmax

V_p = the vertical component of the effective prestress force at the sections

V_{ci} is the shear force that produces flexure-shear cracks, while V_{cw} is the shear force that causes web-shear because of excessive principal tension. The shear strength V_c is governed by the lesser of the two values. Depending on whether V_{ci} or V_{cw} governs, either flexure-shear or web-shear cracks may form.

In V_{ci}, the term $0.6\sqrt{f'c}\ b_w\ d$ is constant, regardless of the location of the section under consideration and the applied load. It is equal to 19.3 kips. V_d decreases as the distance of the section from the diaphragm increases. The cracking moment, M_{cr}, increases as the distance of the section increases. Since the dead load is negligible compared to the applied moment, M_{max}/V_i is the shear distance that decreases as the distance from the diaphragm increases. Thus, the term $V_i\ M_{cr}/M_{max}$ increases as the distance of the section from the diaphragm increases. The increase in this term is more than the decrease in V_d, because the dead load of the girder and slab amounts to only 1.06 kip per ft. As a result V_{ci} increases as the distance of the section from the diaphragm increases.

The code does not consider V_p in determining V_{ci}. However, in the present case, V_p is associated with high moments and hence cannot be ignored in computing V_{ci}.

The transfer length for the prestressing strand is assumed to be 50 times the diameter. In this case, it was 25 in. Within this distance,

since f_{pe} and V_p are insignificant, M_{cr} depends mainly on f'c and f_d. V_i/M_{max}, the lever arm, is at its maximum near the diaphragm. This reduces V_{ci} and results in V_{ci} being lower than V_{cw}. The difference between V_{ci} and V_{cw} decreases as the distance of the section from the diaphragm increases.

According to section 11.4.2.2 of the ACI code [3], V_{cw} may be computed as the shear force corresponding to the dead load plus the live load, which results in a principal tensile stress of $4\sqrt{f'c}$ at the centroidal axis of the member. This leads to the following equation:

$$V_{cw} = f_t \sqrt{1 + \frac{f_{pc}}{f_t}}\, b_w\, d$$

The above equation considers f_{pc} to be positive if it is compressive. If f_{pc} is a tensile stress, V_{cw} is given by the following equation

$$V_{cw} = f_t \sqrt{1 - \frac{f_{pc}}{f_t}}\, b_w\, d$$

In this case, f_{pc} is positive if it is tensile and cannot be higher than f_{pt}.

The value of f_{pc} becomes tensile with an increase in the applied load because the centroidal axis falls on the tension side. In the limiting case, V_{cw} equals zero. In such a case, V_{cw} can be taken as $2\sqrt{f'c}\, b_w\, d$, which is the minimum value of V_c specified by the code. Therefore, V_{cw} decreases with an increase in the applied load.

Hence, with an increase in the load, V_{cw} becomes less than V_{ci} and therefore governs. This leads to inclined web-shear cracking as the load increases.

This explains the pattern of cracks observed at loads higher than 300 kips. These were inclined at an angle of about 30 degrees. The web-shear cracks were observed near the junction of the top flange and web at a load of 270 kips. The flexural stresses combined with the shear stresses resulted in principal stresses that were higher than the allowable stress of $4\sqrt{f'c}$.

Most of the web-shear cracks originated near the top flange. The principal stresses in this location were higher than those near the centroidal axis due to higher flexural tensile stress.

This discussion supports the conclusion that the cracking pattern agrees with the theory. The code procedures to design for shear have shortcomings in the region of the negative moment, near an intermediate support.

The computations for V_{ci} and V_{cw} are given in Appendix C.

The Load Versus the Deflection Curve

The deflection of the active side was measured at the point of the application of the load.

Figure 7.27 shows the load versus the deflection curve. The curve is linear up to 270 kips of applied load. Thereafter, a steady increase in the deflection with an increase in the applied load can be seen. The maximum deflection was 3.3 in., whereas thedeflection at 270 kips was 1.2 in. The recovery after the removal of the load was 2.4 in., i.e., the net plastic deformation was 0.9 in.

Figure 7.28 indicates that the stress in the reinforcement of the slab varied linearly with the total load. The stress was computed at a distance of 4.72 in. from the diaphragm. The stress was 64 ksi at a

total load of 408 kips, which corresponds to an applied load of 387 kips. The total load included the dead load and the load exerted by the actuators. Thus, 408 kips was the limiting load at which the steel yielded. The corresponding nominal moment was equal to 5407 ft. kips.

The idealized moment-curvature relationship consists of an elastic portion and an ideal plastic portion. The actual relationship for reinforced concrete may be closer to be ideal if the capacity of the section is governed by yielding of the steel. In the present case when the steel yielded the maximum strain in the concrete was 0.000698, which is about 23 percent of the ultimate strain that concrete can sustain.

The above results are consistent with the characteristics of the load-deflection curve which deviated from linearity for loads that were higher than 270 kips. The computations for the curve in Figure 7.28 are presented in Appendix C.

Salient Points of the Observations and the Results

In this laboratory test the distance of the load from the diaphragm was 13 ft. 10 in. Thus, the x/d ratio, where x is the distance at which the load is applied and d is the effective depth of the section, was 2.56. The distance x is also referred as the shear distance. The value d is not less than 0.8 times the total depth of the section. This enables researchers to reach the maximum design moment and shear in a single test. The maximum moment is attained first and subsequently the maximum shear isreached. Earlier research [31] concluded that the contribution of stirrups to the shear strength decreases as the ratio x/d increases. The study also suggested that flexural-shear cracks develop within a distance of d and do not extend over the entire span of

the web. Furthermore, studies have concluded that cracks due to excessive principal tension extend over the entire length of the shear span and that x/d, if it is greater than 2, has no influence on the angle of inclination of the diagonal tension cracks. These findings agree with the observations of this test.

1. The limiting load at which the steel yield is 408 kips. The corresponding moment is 5407 ft.-kips. Excluding the dead load, the corresponding applied load is 387 kips. The girder was loaded beyond this point up to an applied load of 480 kips.
2. The cracking pattern due to flexure-shear and web-shear were consistent with the theory.
3. The deflection and the stresses in the slab reinforcement agreed.
4. The first visible crack occurred at an applied load of 210 kips. It was a flexural crack and was located in the slab.
5. Significant cracking of the web began at an applied load of 300 kips. Including the maximum unfactored dead load, it was equal to the total load of 321 kips. This is approximately equal to the desired nominal shear strength capacity.
6. The first yielding of the stirrups occurred at an applied load of 480 kips. The location of the yielding was beyond the transfer length. Since after the prestress transfer the stresses in the stirrups beyond the transfer length were less than those within, the yielding was caused by the web-shear cracking, which was caused by loads higher than 300 kips.

Table 7.1

Design Parameters for the Laboratory Test

Parameters	At Detensioning	At time of Loading
1. Nominal Cylindrical Strength of Concrete (psi)	6800	9880
2. Allowable Compression in Concrete (psi) (AASHTO Sect 9.15.2)	4080	3952
3. Allowable Tension in Concrete (psi) (AASHTO Sect.9.15.2)	247	298
4. Modulus of Rupture of Concrete (psi) ($7.5\sqrt{f'c}$)	618	745
5. Modulus of Elasticity of Concrete (psi) ($E_c = 63700\sqrt{f'c}$)	5252,837	6331,665
6. Minimum Shear Stress in Concrete (psi) ($2\sqrt{f'c}$)	165	198
7. Allowable Principal Tension in Concrete (psi) ($4\sqrt{f'c}$)	330	397
8. Yield Strength of Nonprestressed Steel (ksi)	60	60
9. Tension in Stirrups at Cracking of Concrete (ksi) ($7.5\sqrt{f'c}\ Es/Ec$)	3.5	3.5

Table 7.2.a

Stress in Stirrups at y=38 in. After the Prestress Transfer.

x	Girder A		Girder B	
	Gage No	Stress (ksi)	Gage No.	Stress (ksi)
1.5	100	20.0	200	20.0
5.5	103	16.0	203	13.0
9.5	110	8.0	210	8.0
13.5	113	3.0	213	3.0
17.5	118	3.0	218	23.0
25.5	121	2.0	221	1.0
33.5	126	N.F.	226	0.0
45.5	129	8.0	229	1.0

x = Distance of a stirrup from the end of the girders in inches.

y = Distance of the gages from the bottom of the girders in inches.

N.F. = The gage did not function

Table 7.2.b

Stress in Stirrups at y=25 in. After the Prestress Transfer.

x	Girder A		Girder B	
	Gage No	Stress (ksi)	Gage No.	Stress (ksi)
1.5	101	23.0	201	23.0
5.5	104	17.0	204	22.0
9.5	111	12.0	211	13.0
13.5	114	8.0	214	9.0
17.5	119	1.0	219	0.0
25.5	122	1.0	222	0.0
33.5	127	3.0	227	1.0
45.5	130	8.0	230	22.0

x = Distance of a stirrup from the end of the girders in inches.

y = Distance of the gages from the bottom of the girders in inches.

N.F. = The gage did not function

Table 7.2.c

Stress in Stirrups at y=10 in. After the Prestress Transfer.

x	Girder A		Girder B	
	Gage No	Stress (ksi)	Gage No.	Stress (ksi)
1.5	102	18.0	202	23.0
5.5	105	8.0	205	13.0
9.5	112	12.0	212	N.F.
13.5	115	8.0	215	3.0
17.5	120	0.0	220	0.0
25.5	123	23.0	223	29.0
33.5	128	2.0	228	1.0
45.5	131	22.0	231	20.0

x = Distance of a stirrup from the end of the girders in inches.

y = Distance the gages from the bottom of the girders in inches.

N.F. = The gage did not function.

Table 7.3

Stress in Steel Bar at y=3 in. After the Prestress Transfer.

	Girder A		Girder B	
x	Gage No	Stress (ksi)	Gage No.	Stress (ksi)
2	116	2.0	216	2.0
18	117	4.0	217	4.0
28	124	0.0	224	-2.0
42	125	-4.0	225	N.F.

x = Distance of a gage from the end of the girders in inches.

y = Distance of the gages from the bottom of the girders in inches.

N.F. = The gage did not function.

Table 7.4

Strains (microstrains) in the Horizontal Gages on the Surface of the Web. After Prestress Transfer

x	3.5		17.5		31.5		45.5	
	Girder A	Girder B	Girder A	Girder B	Girder A	Girder B	Girder A	Girder B
65	NF	NF	-100	-94	NF	NF	-167	-173
47	-225	-26	49	-42	371	-56	-141	-144
29	NF	-28	-56	-31	NF	-4414	-198	-159
11	-103	26	-4	-226	NF	NF	-397	-403

x = Distance of a gage from the end of the girders in inches.

y = Distance of a gage from the bottom of the girders in inches.

NF = The gage did not function

Table 7.5

Strains (microstrains) in the Vertical Gages on the Surface of the Web. After Prestress Transfer

x	3.5		17.5		31.5		45.5	
	Girder A	Girder B	Girder A	Girder B	Girder A	Girder B	Girder A	Girder B
65	-526	155	-46	193	743	42	-487	0
47	-128	6	24	33	594	-34	12	5
29	236	NF	-264	26	-15	-38	-11	NF
11	-127	2019	NF	56	NF	1384	2	-40

x = Distance of a gage from the end of the girders in inches.

y = Distance of a gage from the bottom of the girders in inches.

NF = The gage did not function

Table 7.6

Strains (microstrains) in the Inclined Gages on the Surface of the Web. After Prestress Transfer

x	3.5		17.5		31.5		45.5	
	Girder A	Girder B	Girder A	Girder B	Girder A	Girder B	Girder A	Girder B
65	-198	-30	-89	-675	583	-119	-142	-93
47	43	-8	-123	-113	NF	-184	-117	-188
29	-141	-56	-99	-39	223	-99	-230	-56
11	-156	-26	-31	-256	-323	-331	-257	-262

x = Distance of a gage from the end of the girders in inches.

y = Distance of a gage from the bottom of the girders in inches.

NF = The gage did not function

Table 7.7

Principal Stresses (in psi) on the Surface of the Web.
After Prestress Transfer

x		3.5		17.5		31.5		45.5	
		Girder		Girder		Girder		Girder	
y		A	B	A	B	A	B	A	B
65	σ_{p1}			-306	3206			-961	-169
	σ_{p2}	NG	NG	-553	-2618	NG	NG	-2879	-851
	θ			-15	-39			-24	-2
47	σ_{p1}	-144	2	837	426		283	-3	
	σ_{p2}	-1876	-124	-412	-481	NG	-812	-1974	NG
	θ	3	38	43	-35		-43	-27	
29	σ_{p1}			154	171			-13	139
	σ_{p2}	NG	NG	-2033	-198	NG	NG	-742	-960
	θ			-34	-26			-17	-29
11	σ_{p1}	-509	NG		373			-345	-579
	σ_{p2}	-841	344	NG	-1376	NG	NG	-1975	-2043
	θ	-35	23		25			8	6

x = Distance of a rosette from the end of the girders in inches.

y = Distance of a rosette from the bottom of the girders in inches.

σ_{p1} σ_{p2} = Principal stresses on the concrete.

θ = Orientation of the principal stresses in degrees.

NG = Not Good

Table 7.8

Principal Stresses (in psi) on the Surface of the Web at x=3.5 in and y=11 in. Load Combination: Effective Prestress Plus Weight of the Slab Plus the Applied Load

Applied Load (kips)	$\epsilon_x * 10^{-6}$	$\epsilon_y * 10^{-6}$	$\gamma_{xy} * 10^{-6}$	σ_{p1} (psi)	σ_{p2} (psi)	θ
30	-84	66	501	1433	-1584	-37
90	-144	52	411	1016	-1577	-32
150	-193	27	290	532	-1545	-26
110	-229	-4	173	99	-1518	-19
240	-250	-16	125	-55	-1565	-14
270	-264	-31	68	-208	-1589	-8
300	-241	-65	-51	-410	-1456	8
330	-167	-104	-166	-321	-1333	35
360	198	-48	-764	2745	-1829	-36
The Rossette Failed						

x = distance of the rosette from the face of the diaphragm

y = distance of the rosette from the bottom of girder A

ϵ_x = strain in x direction

ϵ_y = strain in y direction

γ_{xy} = shear strain

σ_{p1}, σ_{p2} = principal stress in the concrete

θ = orientation of the prinicipal stresses in degrees

Table 7.9

Principal Stresses (in psi) on the Surface of the Web at x=17.5 in. and y=47 in Load Combination: Effective Prestress Plus Weight of the Slab Plus the Applied Load

Applied Load (kips)	$\epsilon_x * 10^{-6}$	$\epsilon_y * 10^{-6}$	$\gamma_{xy} * 10^{-6}$	σ_{p1} (psi)	σ_{p2} (psi)	θ
30	-519	-617	287	-2641	-4353*	36
90	-508	-628	248	-2684	-4253	32
150	-484	-644	213	-2683	-4203	27
210	219	-764	-324	1290	-4616	-9
240	-450	-857	-1499	4429	-6913	-24
270	The Rossette Failed					

*Crack formation resulted immediately after detensioning

x = distance of the rosette from the face of the diaphragm

y = distance of the rosette from the bottom of girder A

ϵ_x = strain in x direction

ϵ_y = strain in y direction

γ_{xy} = shear strain

σ_{p1}, σ_{p2} = principal stress in the concrete

θ = orientation of the prinicipal stresses in degrees

Table 7.10

Principal Stresses (in psi) on the Surface of the Web at x=17.5 in. and y=29 in Load Combination: Effective Prestress Plus Weight of the Slab Plus the Applied Load

Applied Load (kips)	$\epsilon_x * 10^{-6}$	$\epsilon_y * 10^{-6}$	$\gamma_{xy} * 10^{-6}$	σ_{p1} (psi)	σ_{p2} (psi)	θ
30	-48	-233	-431	480	-2191	-33
90	-58	-289	-548	636	-2753	-34
150	-52	-350	-679	890*	-3339	-33
210	-43	-404	-787	1103*	-3834	-33
240	-34	-417	-834	1240*	-3993	-33
270	-30	-437	-850	1261*	-4112	-32
300	-69	-469	-934	1254*	-4539	-33
330	-107	-429	-991	1338*	-4608	-36
The Rossette Failed						

*Exceeds the modulus of rupture of the concrete

x = distance of the rosette from the face of the diaphragm

y = distance of the rosette from the bottom of girder A

ϵ_x = strain in x direction

ϵ_y = strain in y direction

γ_{xy} = shear strain

σ_{p1}, σ_{p2} = principal stress in the concrete

θ = orientation of the prinicipal stresses in degrees

Table 7.11

Principal Stresses (in psi) on the Surface of the Web at x=45.5 in. and y=29 in. Load Combination: Effective Prestress Plus Weight of the Slab Plus the Applied Load

Applied Load (kips)	ϵ_x*10^{-6}	ϵ_y*10^{-6}	$\gamma_{xy}*10^{-6}$	σ_{p1} (psi)	σ_{p2} (psi)	θ
30	-213	43	123	292	-1328	-13
90	-228	41	61	217	-1356	-6
150	-239	35	-6	157	-1405	1
210	-250	31	-83	166	-1506	8
240	-258	37	-124	235	-1586	11
270	-231	38	-122	251	-1430	12
300	-219	44	-187	386	-1456	18
330	-315	-8	-244	134	-2104	-19.2
360	-224	-6525	-6670			-23
		The Rossette Failed				

x = distance of the rosette from the face of the diaphragm

y = distance of the rosette from the bottom of girder A

ϵ_x = strain in x direction

ϵ_y = strain in y direction

γ_{xy} = shear strain

σ_{p1}, σ_{p2} = principal stress in the concrete

θ° = orientation of the prinicipal stresses in degrees

Table 7.12

Stresses (ksi) in Stirrups at y=38 in. Load Combination: Effective Prestress Plus Weight of the Slab Plus the Applied Load

	x															
	1.5		5.5		9.5		13.5		17.5		25.5		33.5		41.5	
	Girder															
	A	B	A	B	A	B	A	B	A	B	A	B	A	B	A	B
	Gage No.															
Load (kips)	100	200	103	203	110	210	113	213	118	218	121	221	125	226	129	229
30	10	10	9	7		5		1	2		1	-1			6	
90	14	13	1	3		2		1	2		1	-1			6	
150	14	13	1	3		2		1	2		2	0			7	
210	17	14	0	-1		2		1	2		3	0			7	
240	18	14	-2	-2		3		1	3		3	1			8	
270	19	15	-3	-4	NG	2	NG	6	3	NG	4	1	NG	NG	8	NG
300	20	15	-3	-4		3		9	7		8	3			9	
330	20	15	-3	-5		4		11	8		12	8			11	
360	21	15	-2	-4		7		13	15		19	9			11	
390	21	15	-2	-2		10		16	21		27	18			16	
420	21	15	-1	-3		11		17	23		29	29			20	
450	22	15	-1	-5		13		18	26		33	37			27	
480	23	16	-2	-5		15		19	34		44	43			60	

x = distance of a stirrup from the face of the diaphragm in inches

y = distance of the gases from the bottom of girder A and girder B

NG = Not Good

Table 7.13

Stresses (ksi) in Stirrups at y=29 in.

Load Combination: Effective Prestress Plus Weight of the Slab Plus the Applied Load

	x															
	1.5		5.5		9.5		13.5		17.5		25.5		33.5		41.5	
	Girder															
	A	B	A	B	A	B	A	B	A	B	A	B	A	B	A	B
Load (kips)	Gage No.															
	101	201	104	204	111	211	114	213	119	219	122	222	127	227	130	230
30	7		11	11	10	8	6	6	-1	-1	-6	1	-2			
90	5		9	10	8	7	4	5	-1	-2	-6	3	-2			
150	2		7	7	6	6	4	4	-1	-3	-5	6	-3			
210	1		5	6	4	5	2	2	-2	-5	-5	10	-3			
240	1		4	5	2	4	1	2	-2	-5	-3	12	-3			
270	2	NG	4	4	3	10	3	0	-2	-8	-3	14	-3			
300	2		5	4	7	14	7	2	0	1	-1	17	-2			
330	3		6	5	9	16	9	12	8	5	-1	20	-1			
360	5		6	5	9	17	13	13	13	5	1	23	10			
390	7		7	9	10	20	15	18	15	8	4	27	19			
420	8		8	11	10	21	19	21	17	13	6	30	24			
450	9		8	13	11	23	20	25	18	17	8	33	29			
480	10		9	15	13	25	22	28	20	19	12	60	42			

x = distance of a stirrup from the face of the diaphragm in inches

y = distance of the gases from the bottom of girder A and girder B

NG = Not Good

Table 7.14

Stresses (ksi) in Stirrups at y=11 in.

Load Combination: Effective Prestress Plus Weight of the Slab Plus the Applied Load

	x															
	1.5		5.5		9.5		13.5		17.5		25.5		33.5		41.5	
	Girder															
	A	B	A	B	A	B	A	B	A	B	A	B	A	B	A	B
Load	Gage No.															
(kips)	102	202	105	205	112	212	115	215	120	220	123	223	128	228	131	231
30	11	14	5	9	8		6	1	0	-13			2	-1		
90	10	14	5	9	8		6	1	0	-13			2	-1		
150	8	13	3	8	7		5	1	-1	-14			2	-1		
210	5	11	2	7	7		5	1	-1	-14			2	-1		
240	4	10	2	7	6		5	1	-1	-14			1	-1		
270	3	9	1	7	6	NG	5	1	-1	-14	NG	NG	1	-1	NG	NG
300	3	9	0	7	5		6	2	-1	-15			17	-1		
330	4	9	2	10	8		10	6	-1	2			40	18		
360	5	11	6	14	12		15	14	1	3			38	38		
390	6	12	8	18	13		19	21	18	11			41	41		
420	7	13	10	21	15		21	22	20	14			44	45		
450	6	14	11	25	16		24	28	24	22			49	52		
480	6	15	14	27	20	28	31	30	27	57			57	57		

x = distance of a stirrup from the face of the diaphragm in inches

y = distance of the gases from the bottom of girder A and girder B

NG = Not Good

Table 7.15

Maximum Stresses (ksi) in the Stirrups

X	1.5	5.5	9.5	13.5	17.5	25.5	33.5	41.5
Load (kips)								
30	14	11	10	6	2	1	2	6
90	14	10	8	6	2	3	2	6
150	14	8	7	5	2	6	2	7
210	17	7	7	5	2	10	2	7
240	18	7	7	5	2	10	2	7
270	19	7	10	6	3	14	1	8
300	20	7	14	9	7	17	17	9
330	20	10	16	11	8	20	40	11
360	21	14	17	15	15	23	38	11
390	21	18	20	19	21	27	41	16
420	21	21	21	21	23	30	44	20
450	22	25	23	24	26	33	49	27
480	23	27	25	28	31	36	52	60

x = Distance from the face of the diaphragm

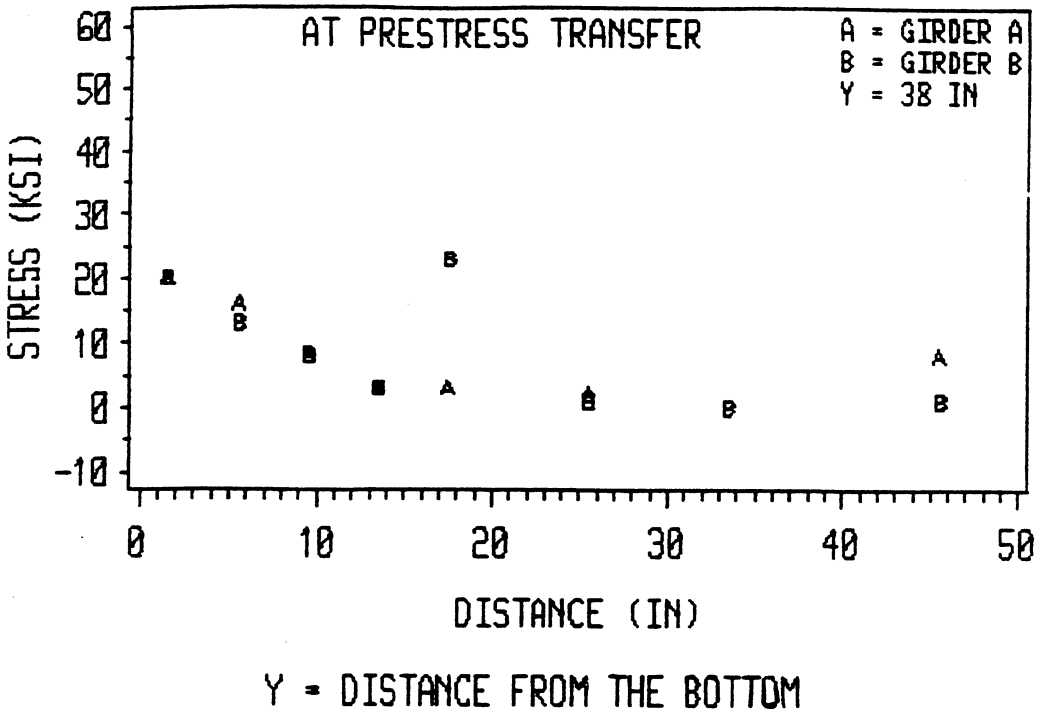

Figure 7.1.a Laboratory Test - Stresses in Stirrups versus Distance from the Continuous End

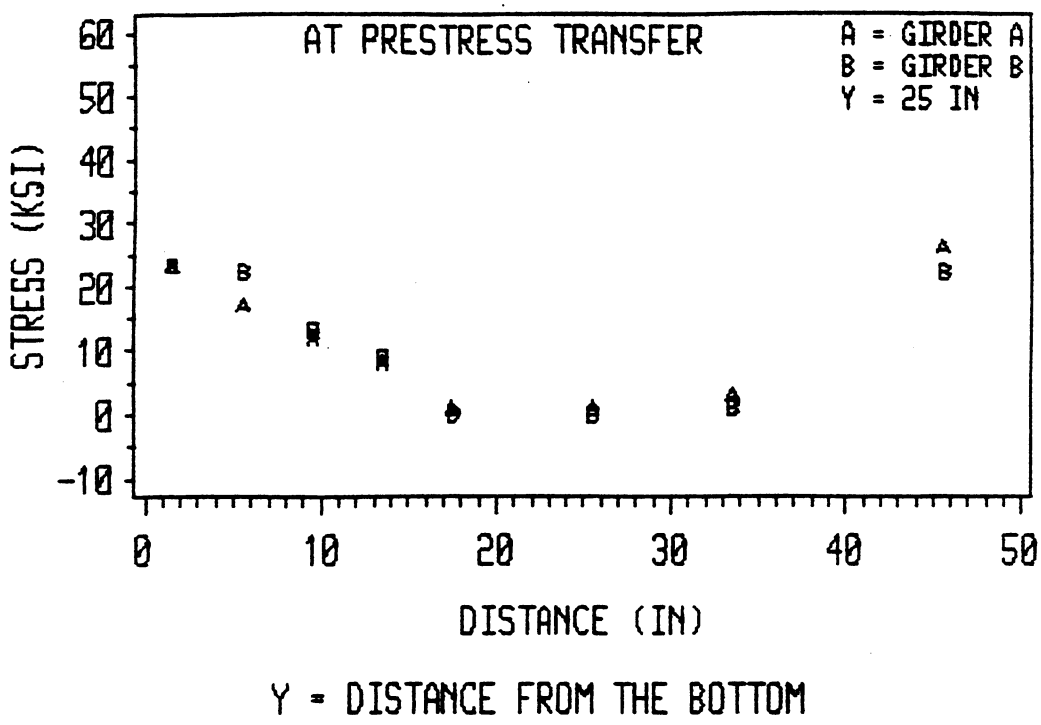

STRESSES IN STIRRUPS VS DISTANCE FROM END

Figure 7.1.b Laboratory Test - Stresses in Stirrups versus Distance from the Continuous End

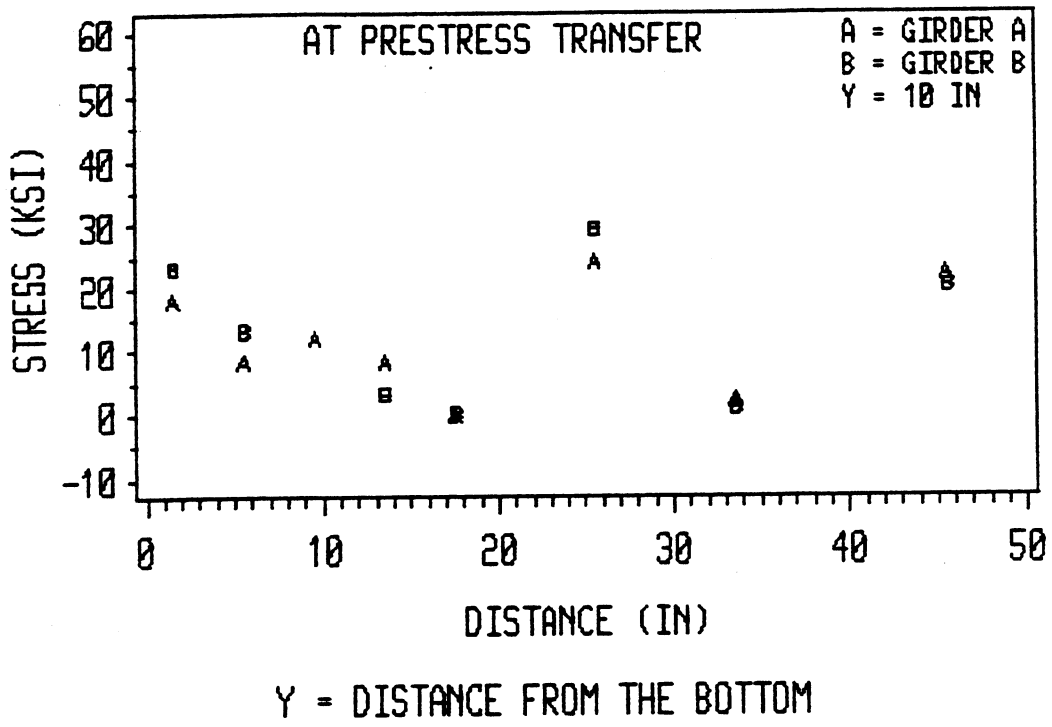

Figure 7.1.c Laboratory Test - Stresses in Stirrups versus Distance from the Continuous End

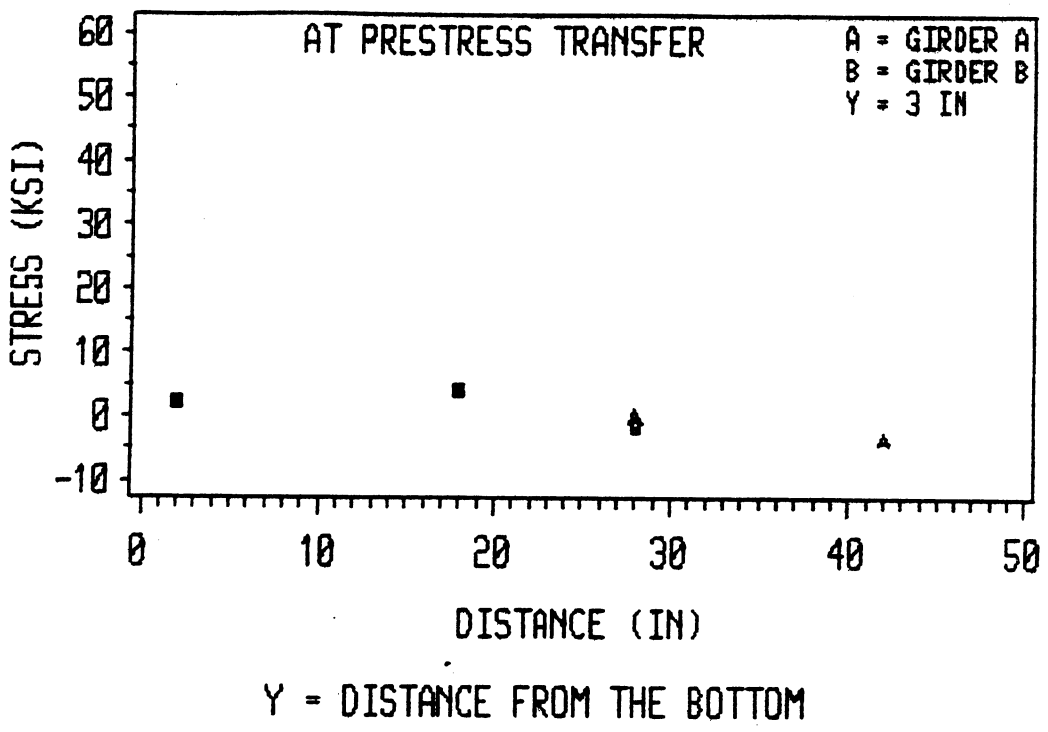

Figure 7.2 Laboratory Test - Stresses in the Bar versus Distance from the Continuous End

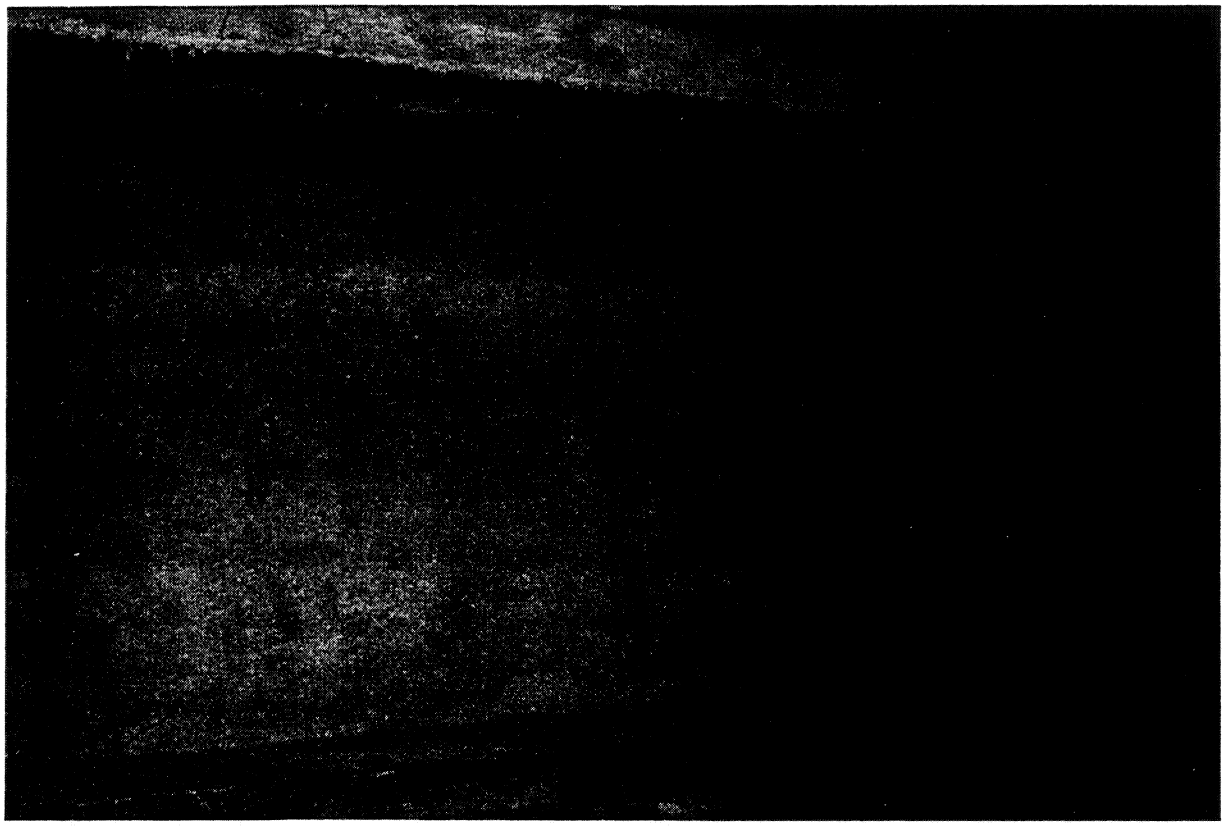

Figure 7.3 Laboratory Test - Cracks in Girder A Adjacent to the Continuous Joint (maximum applied load = 270 kips)

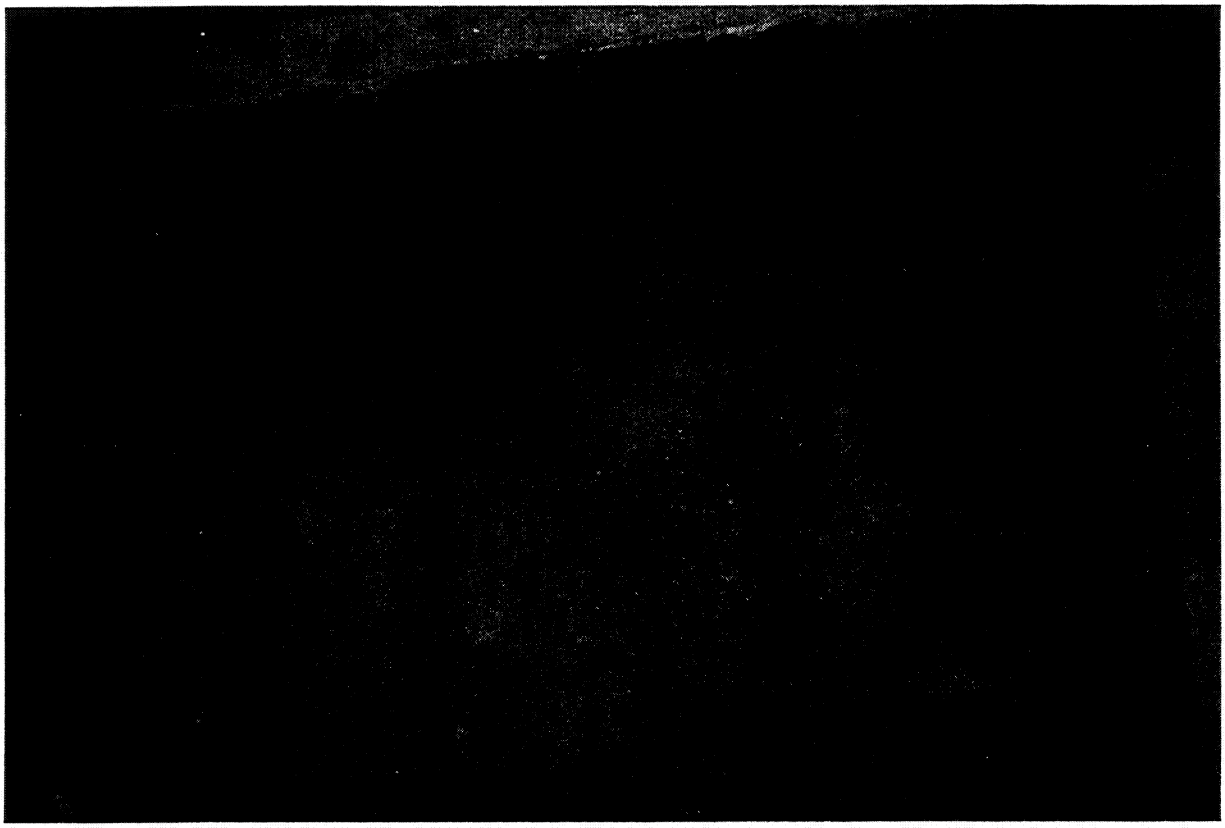

Figure 7.4 Laboratory Test - Cracking of Girder B in Areas Close to the Diaphragm (maximum applied load = 360 kips)

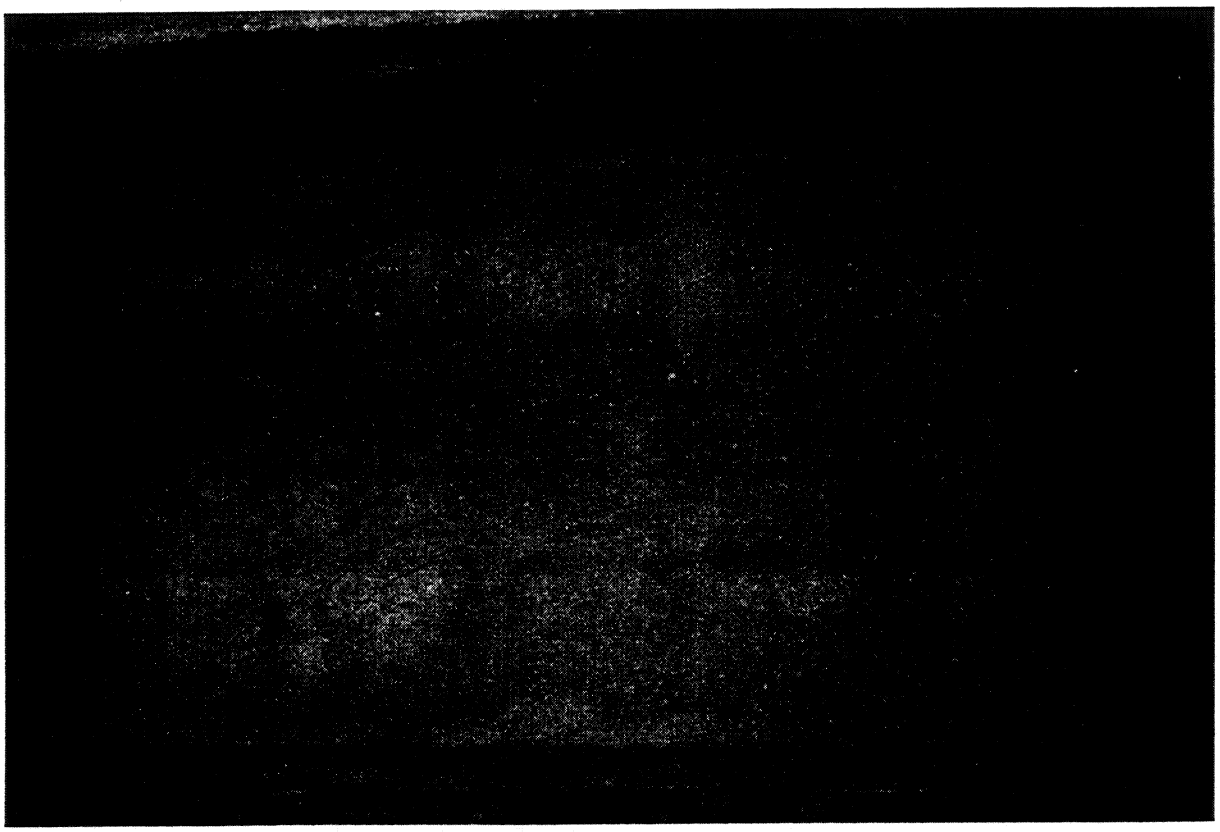

Figure 7.5 Laboratory Test - Cracking of the Web of Girder A (maximum applied load = 360 kips)

Figure 7.6 Laboratory Test - Cracks in Girder B (maximum applied load = 450 kips)

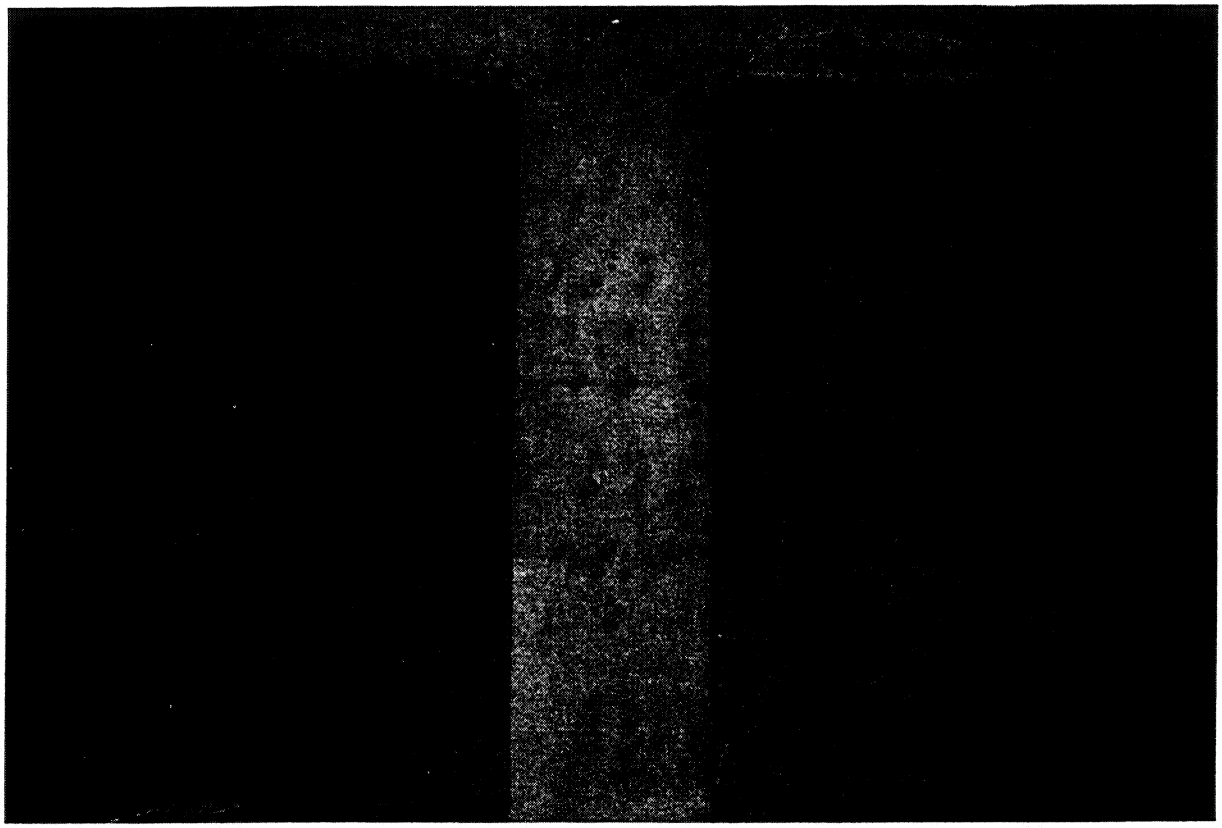

Figure 7.7 Laboratory Test - Cracks in Girders A and B (maximum applied load = 480 kips)

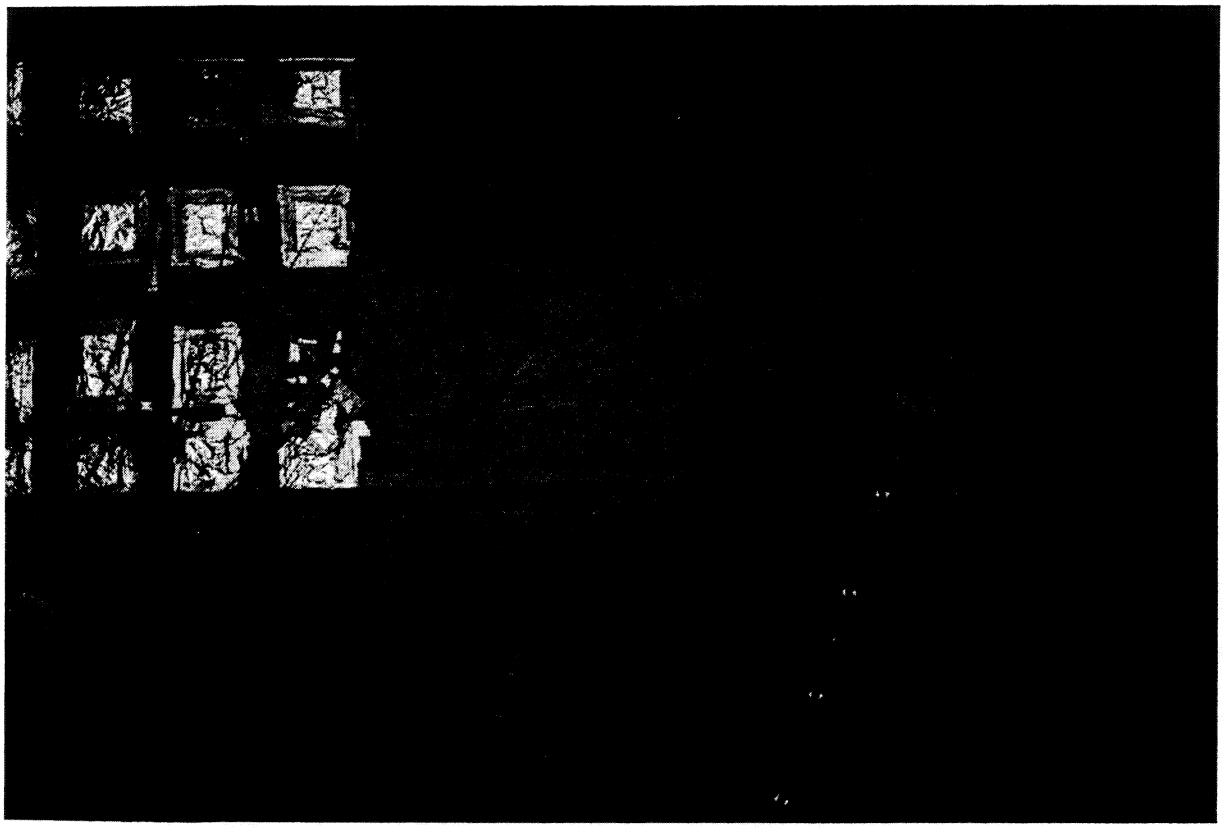

Figure 7.8 Laboratory Test - Cracks in the Web of Girder B

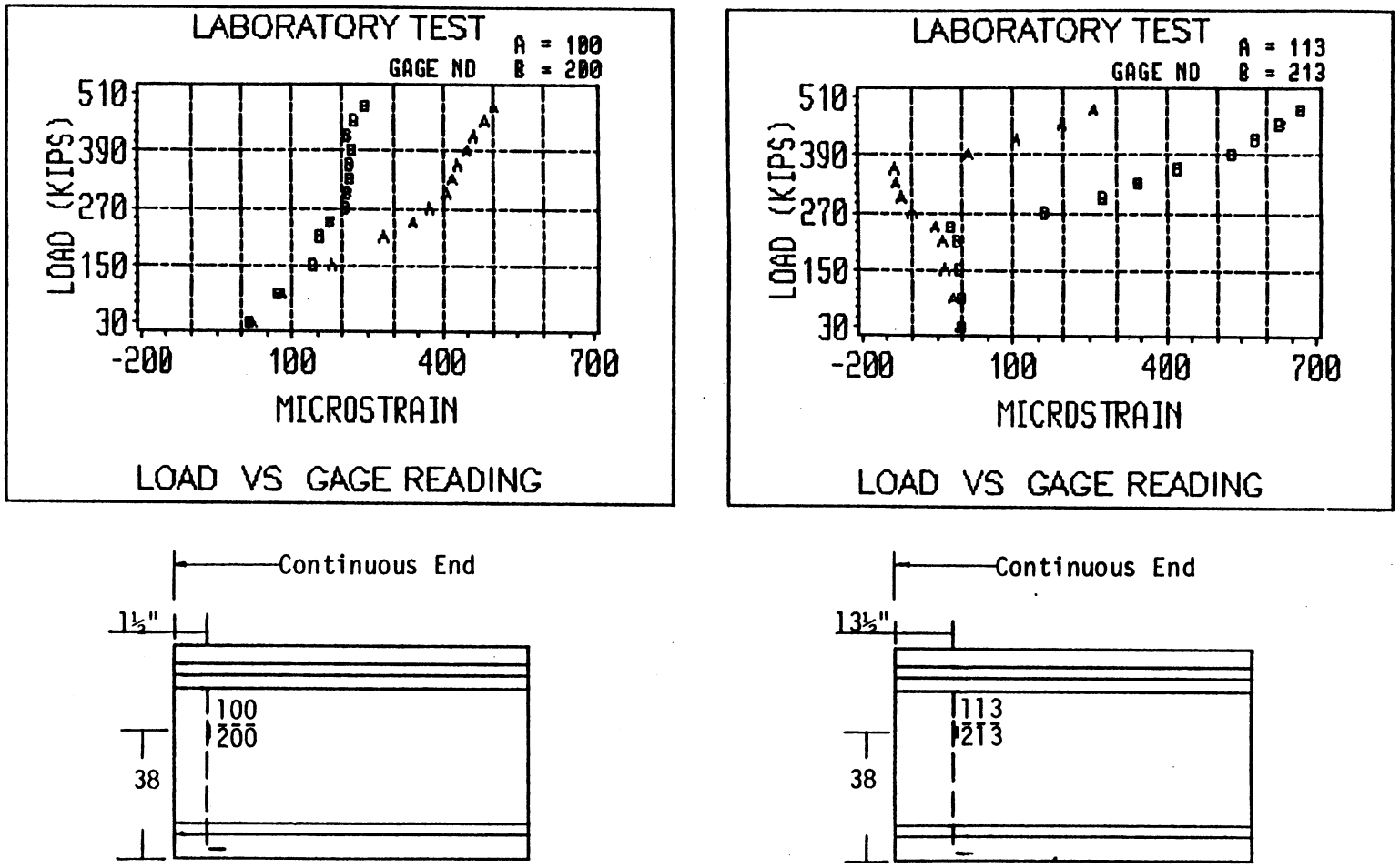

Figure 7.9 Laboratory Test - Strains in Stirrups due to Applied Loads
Gages 100, 200, 113, and 213

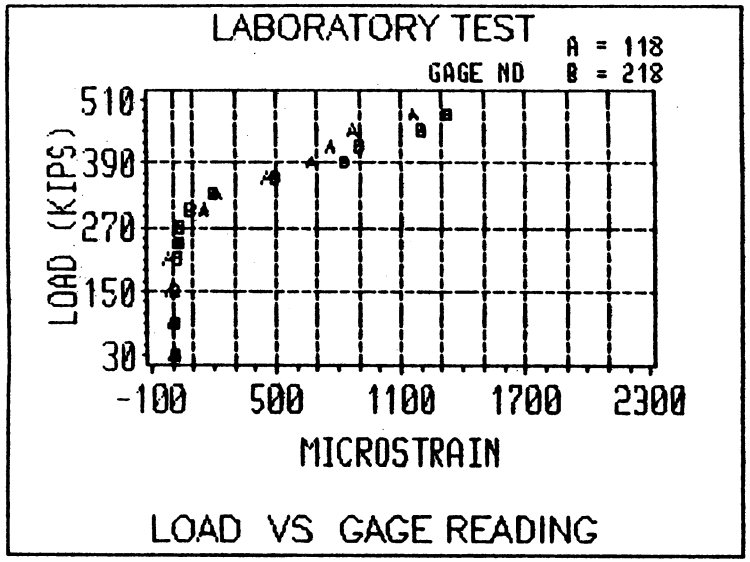

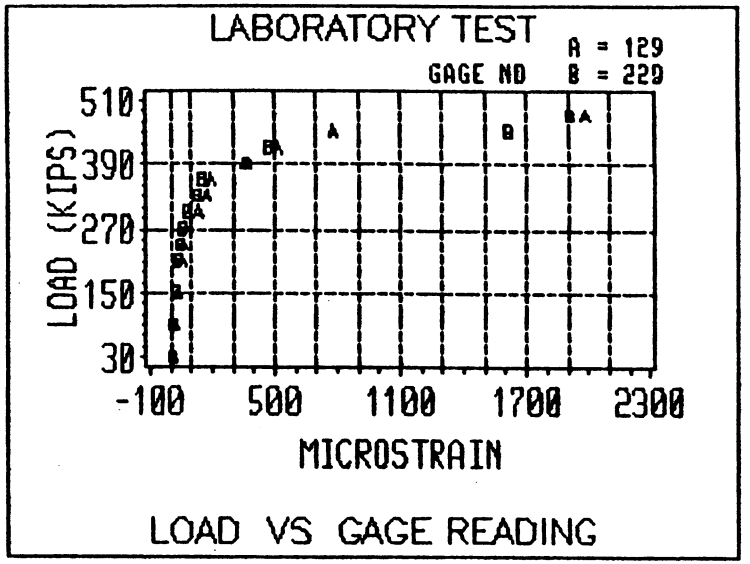

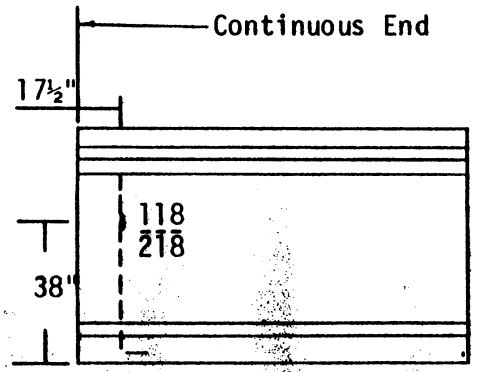

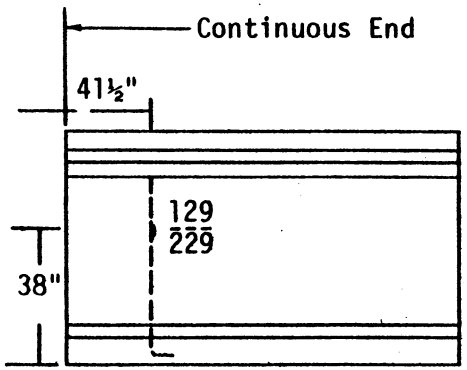

Figure 7.10 Laboratory Test - Strains in Stirrups due to Applied Loads
Gages 118, 218, 129, and 229

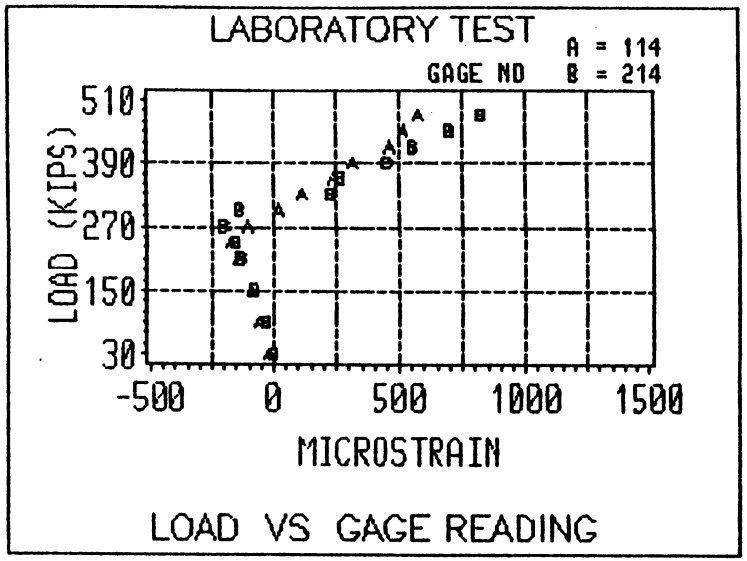

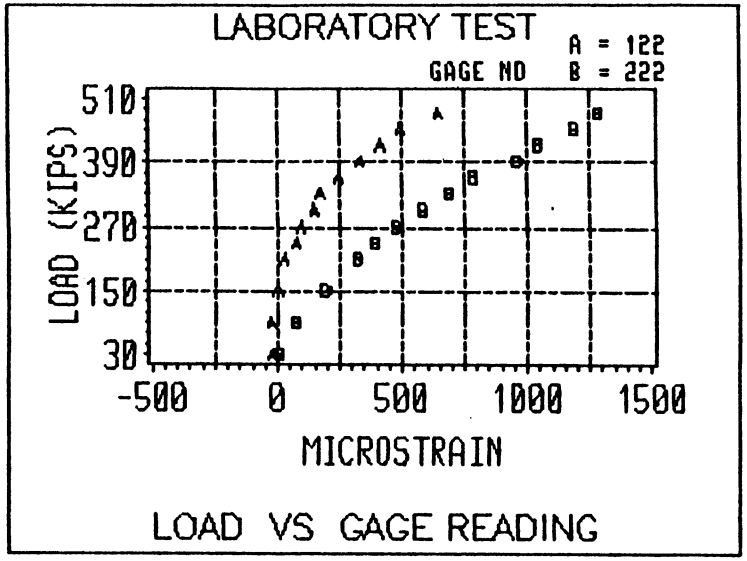

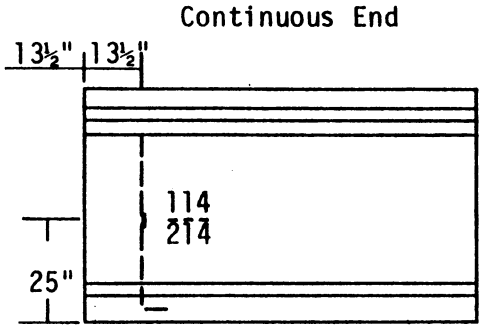

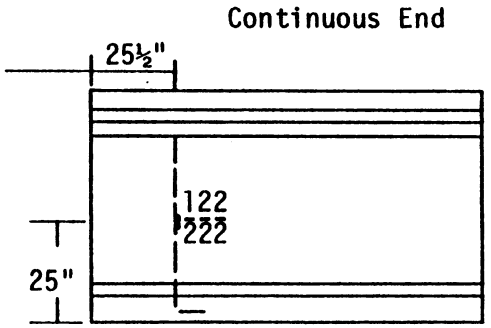

Figure 7.11 Laboratory Test - Strains in Stirrups due to Applied Loads
Gages 114, 214, 122, and 222

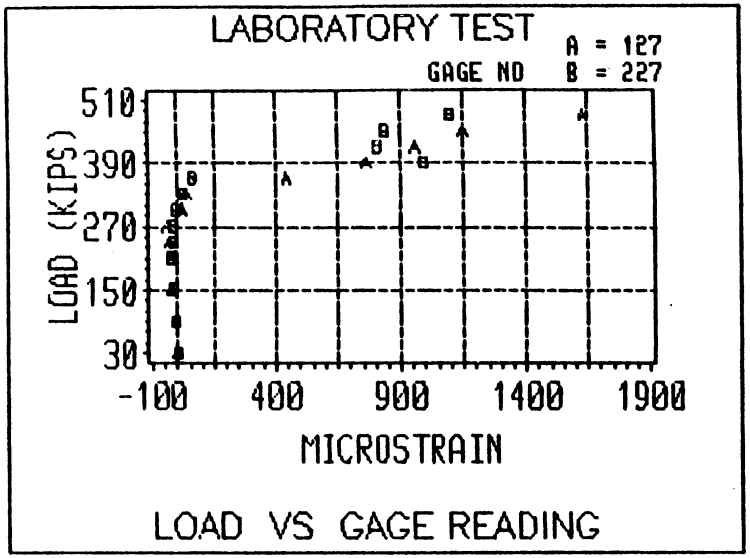

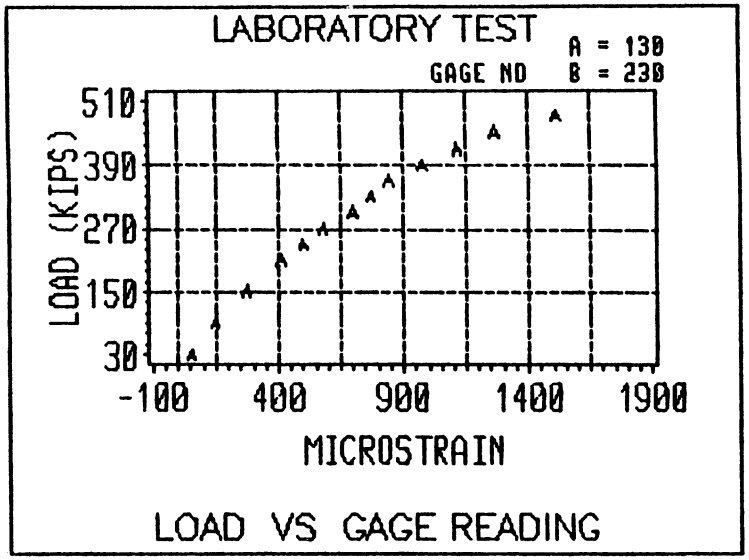

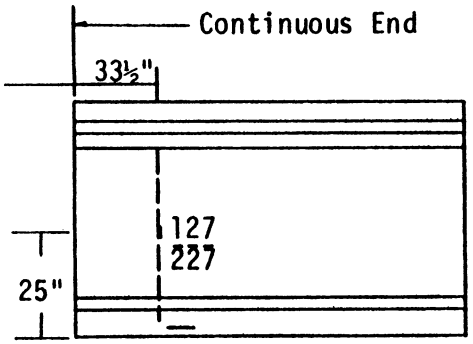

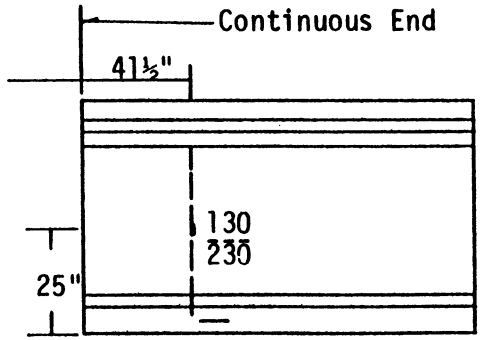

Figure 7.12 Laboratory Test - Strains in Stirrups due to Applied Loads
Gages 127, 227, 130, and 230

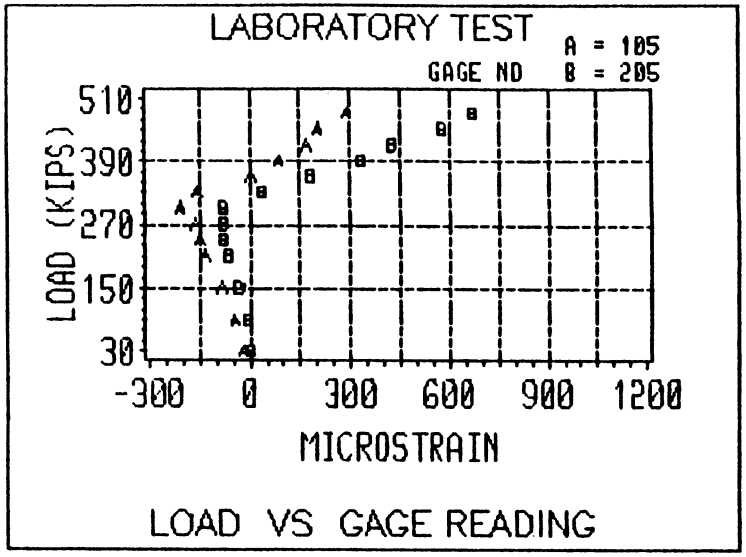

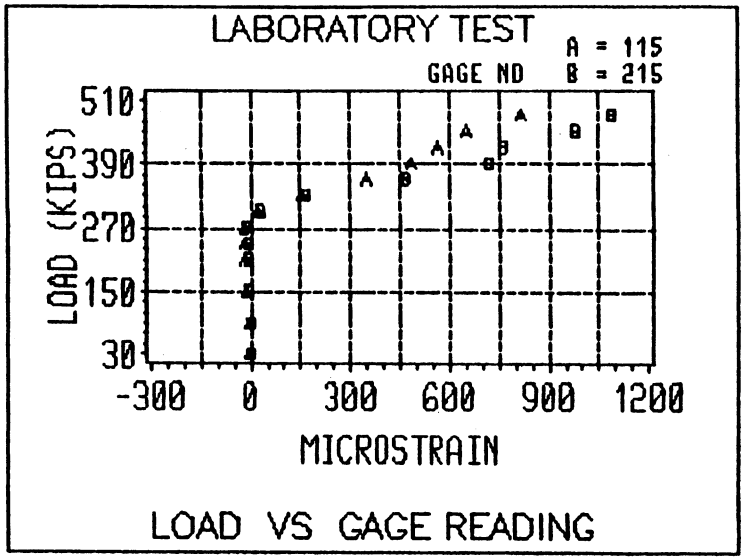

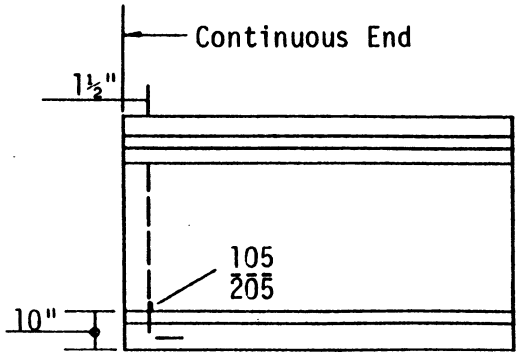

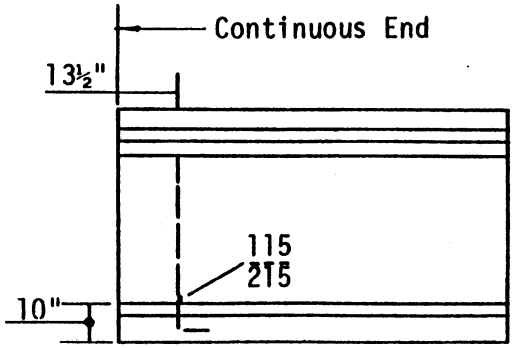

Figure 7.13 Laboratory Test - Strains in Stirrups due to Applied Loads
Gages 105, 205, 115, and 215

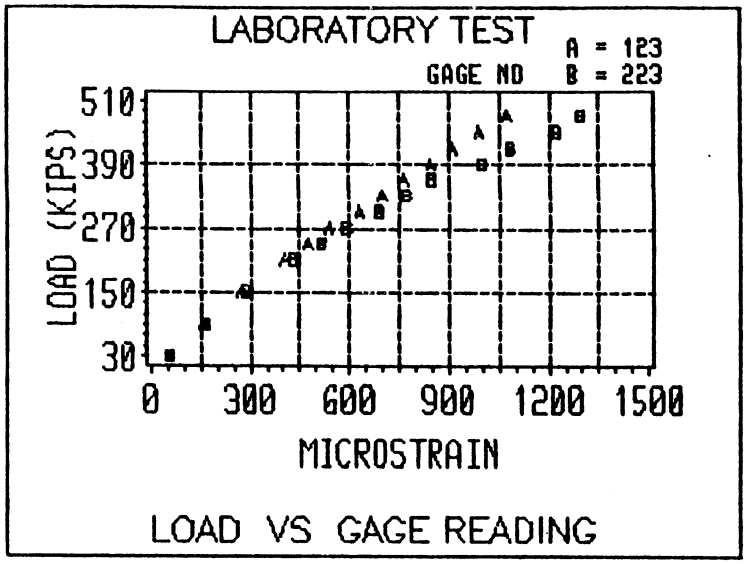

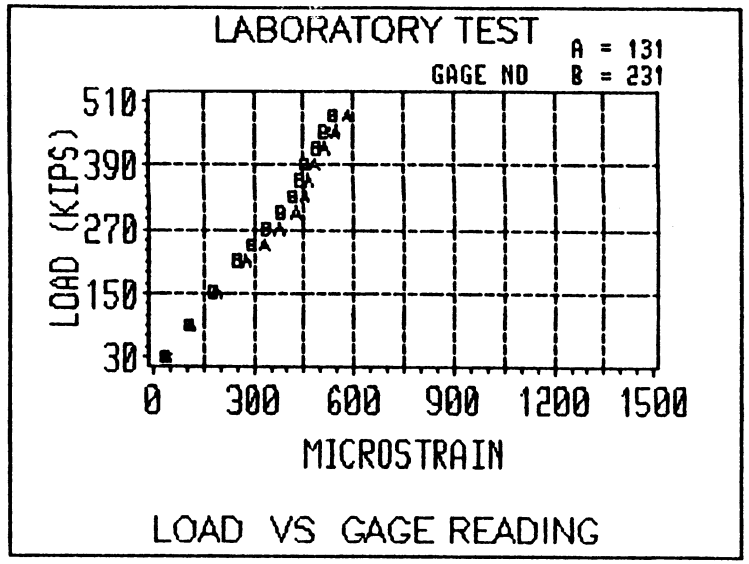

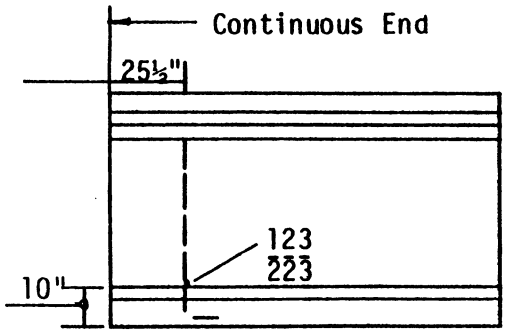

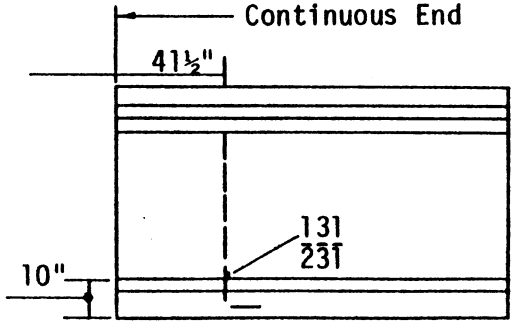

Figure 7.14 Laboratory Test - Strains in Stirrups due to Applied Loads
Gages 123, 223, 131, and 231

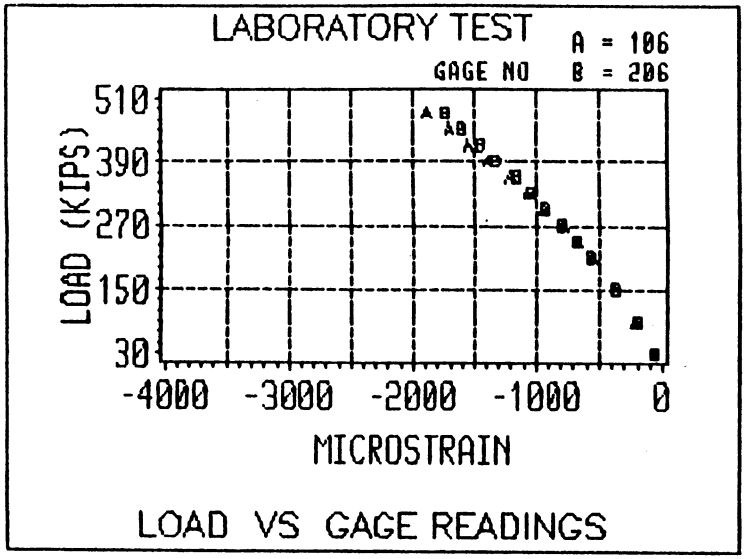

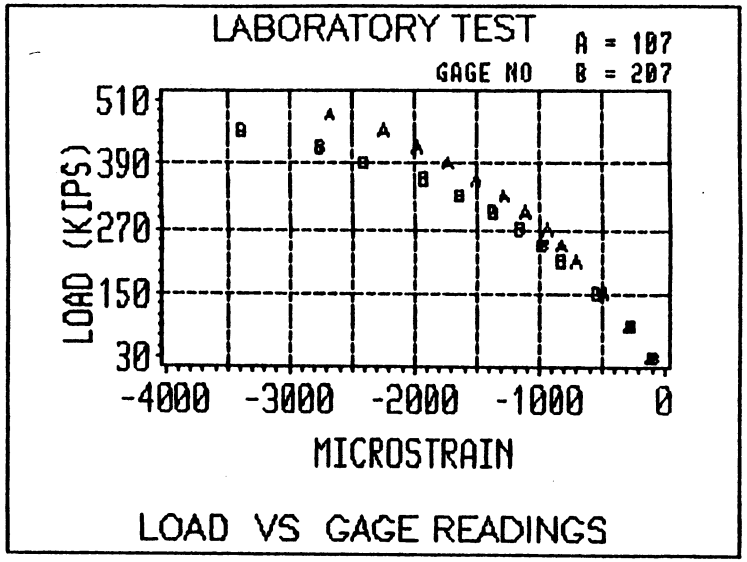

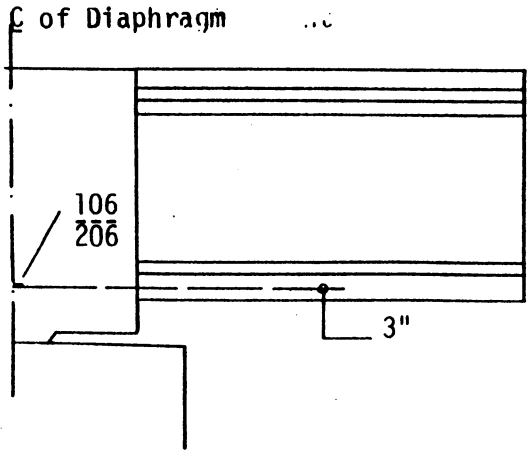

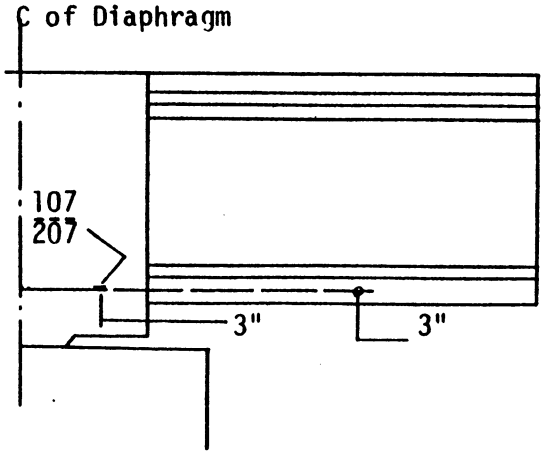

Figure 7.15 Laboratory Test - Strains in the Horizontal Bar at the Center of the Bottom Flange due to Applied Loads
Gages 106, 206, 107, and 207

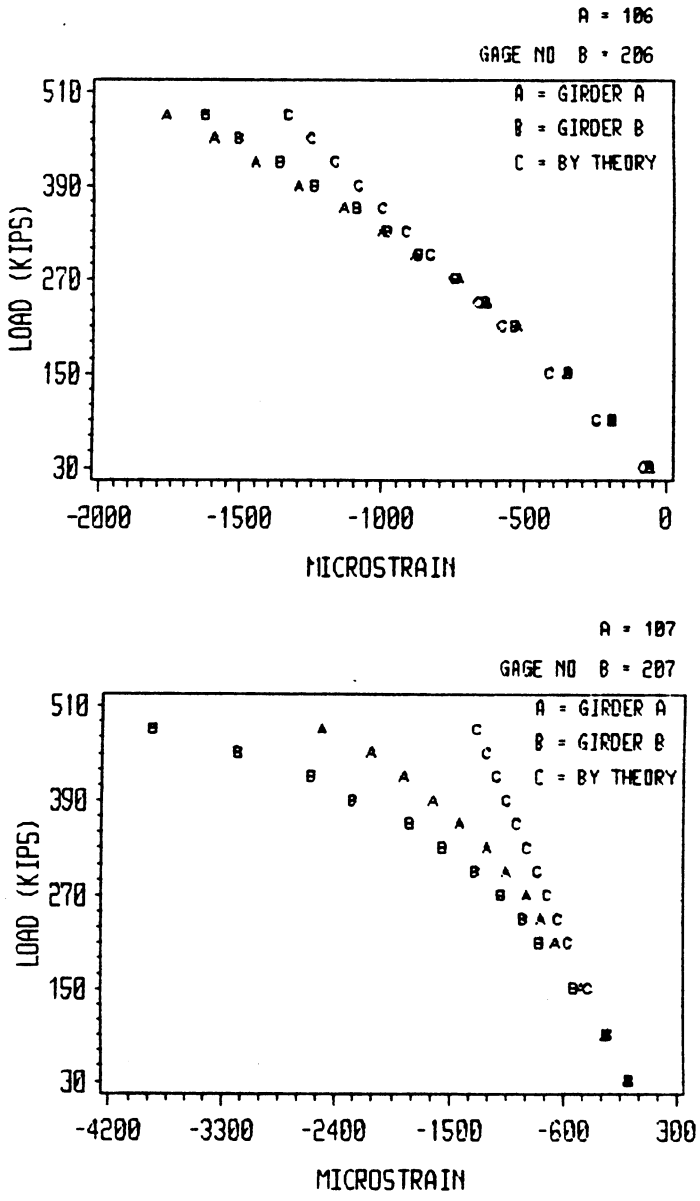

Figure 7.16 Laboratory Test - Comparision of Experimental and Theorotical Results: Gages 106, 206, 107, and 207

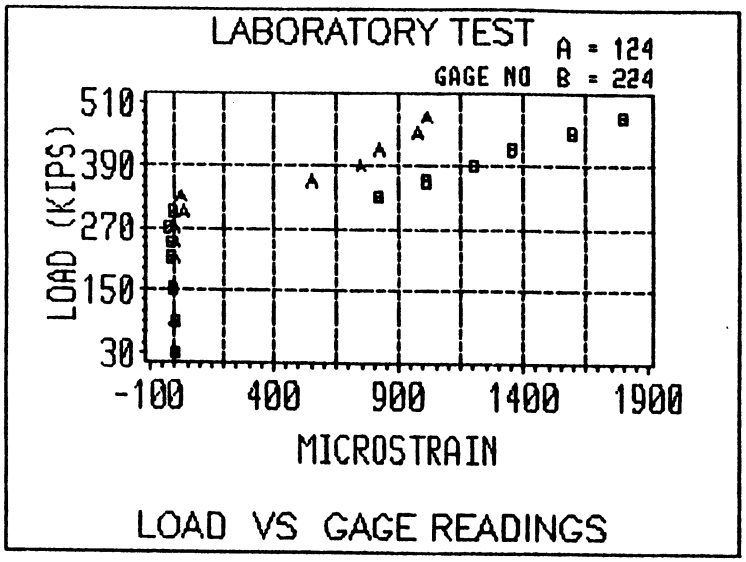

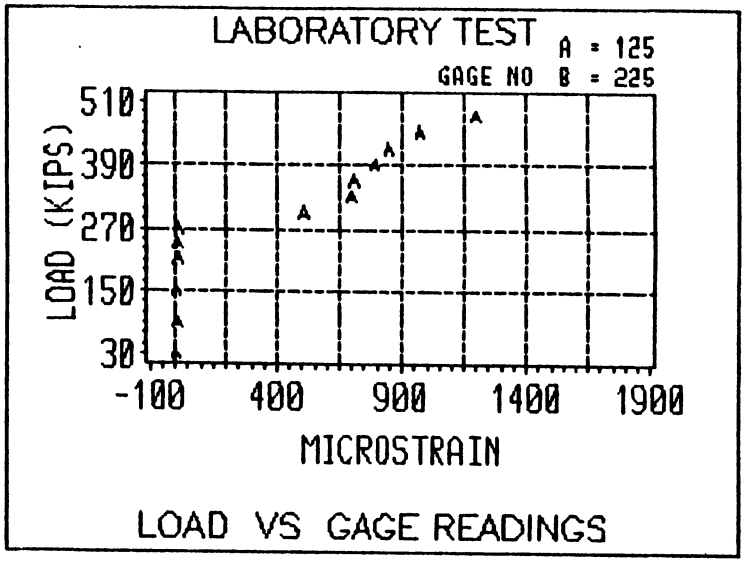

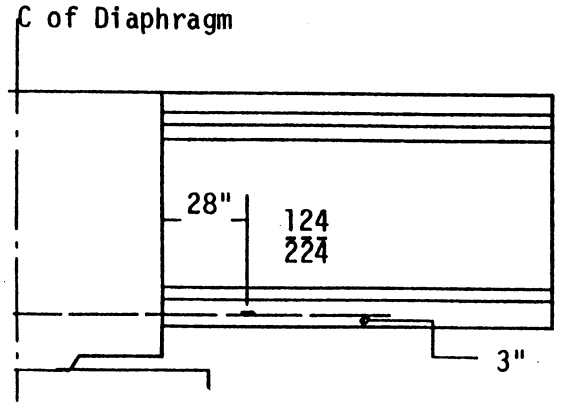

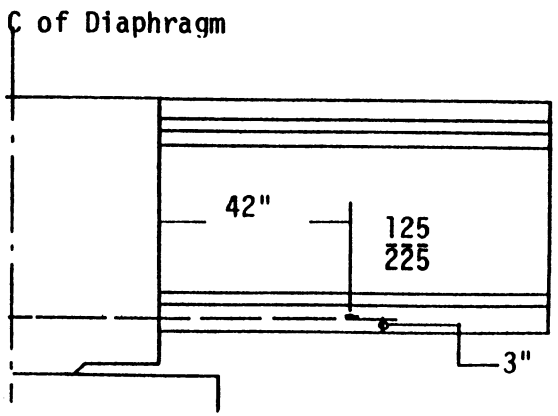

Figure 7.17 Laboratory Test - Strains in the Horizontal Bar at the Center of the Bottom Flange due to Applied Loads
Gages 124, 224, 125, and 225

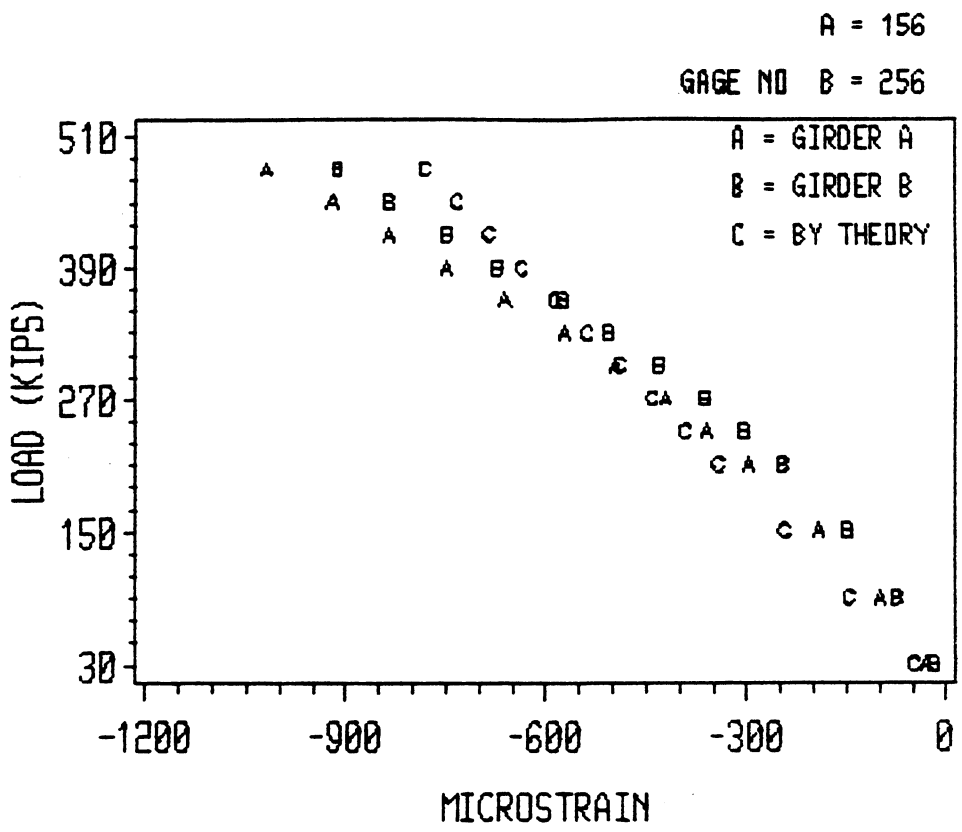

Figure 7.18.a Laboratory Test - Comparision of Experimental and Theorotical Results: Gages 156, and 256

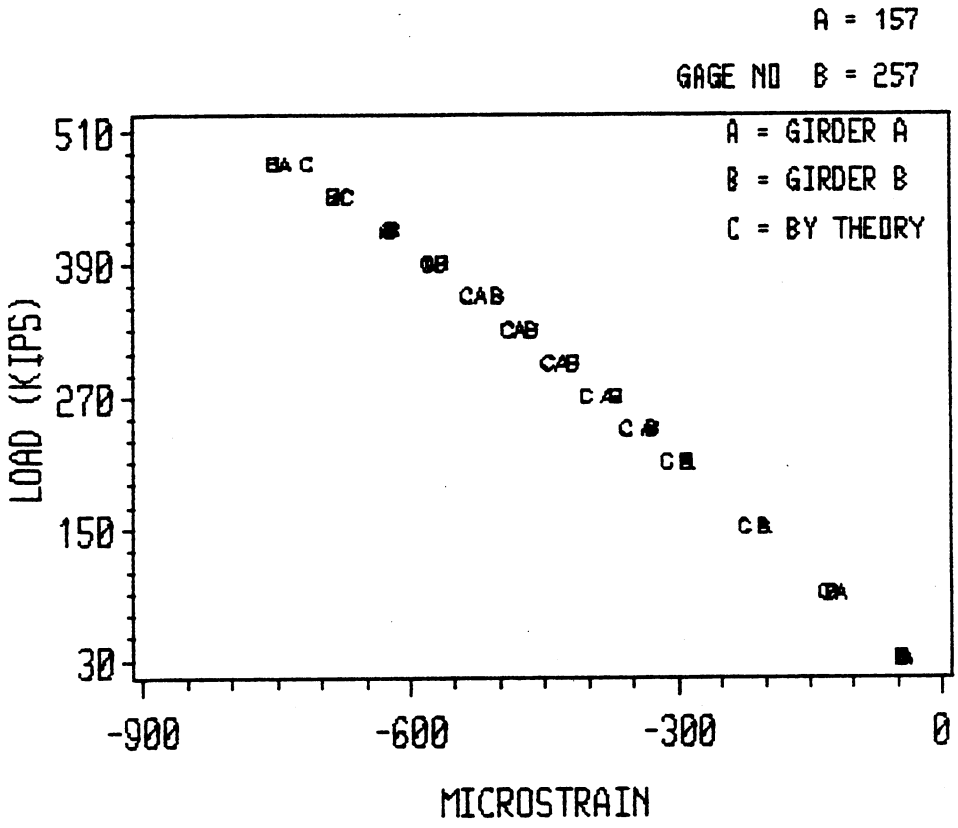

Figure 7.18.b Laboratory Test - Comparision of Experimental and Theorotical Results: Gages 157, and 257

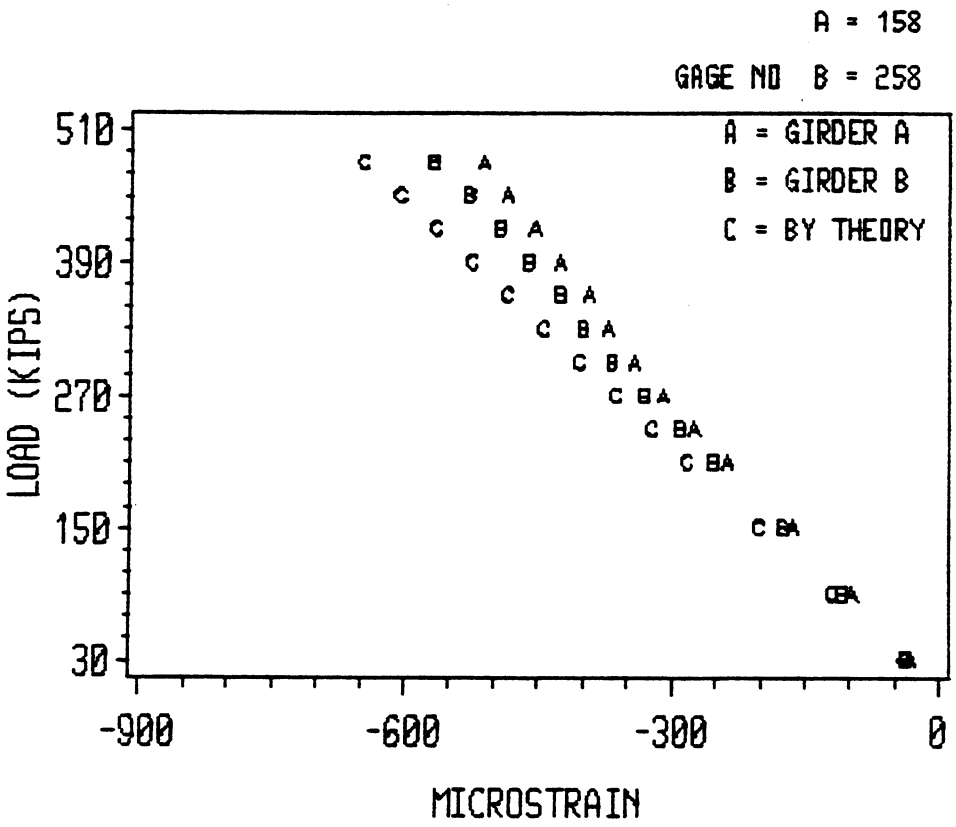

Figure 7.18.c Laboratory Test - Comparision of Experimental and Theorotical Results: Gages 158, and 258

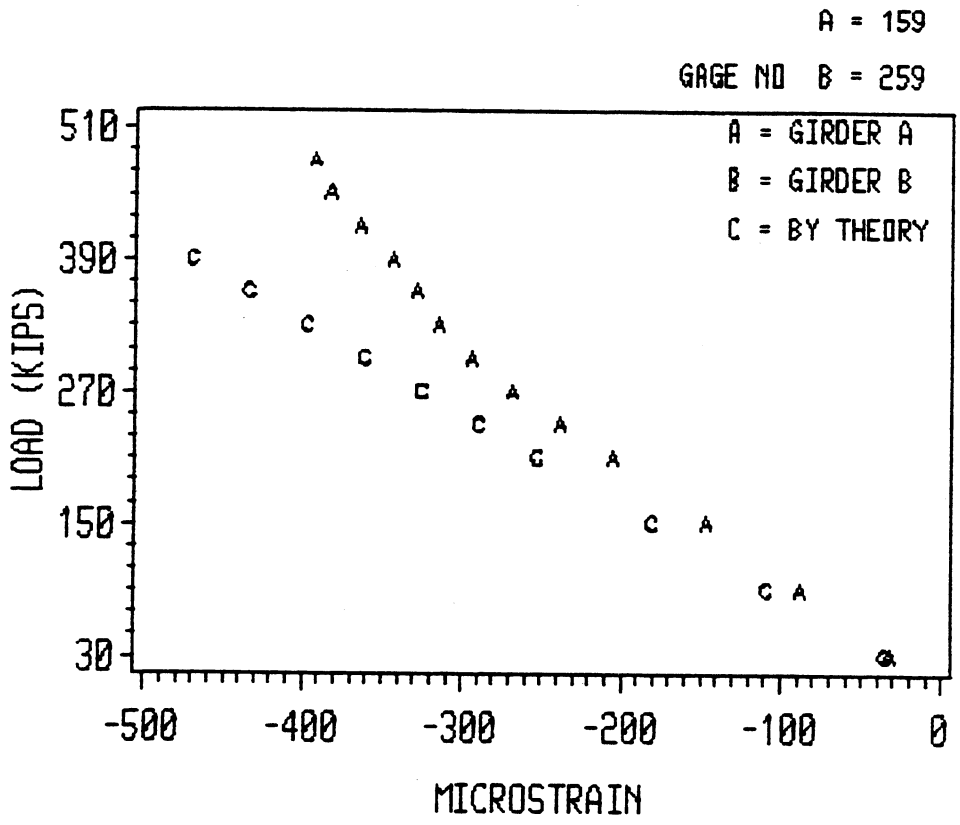

Figure 7.18.d Laboratory Test - Comparision of Experimental and Theorotical Results: Gages 159, and 259

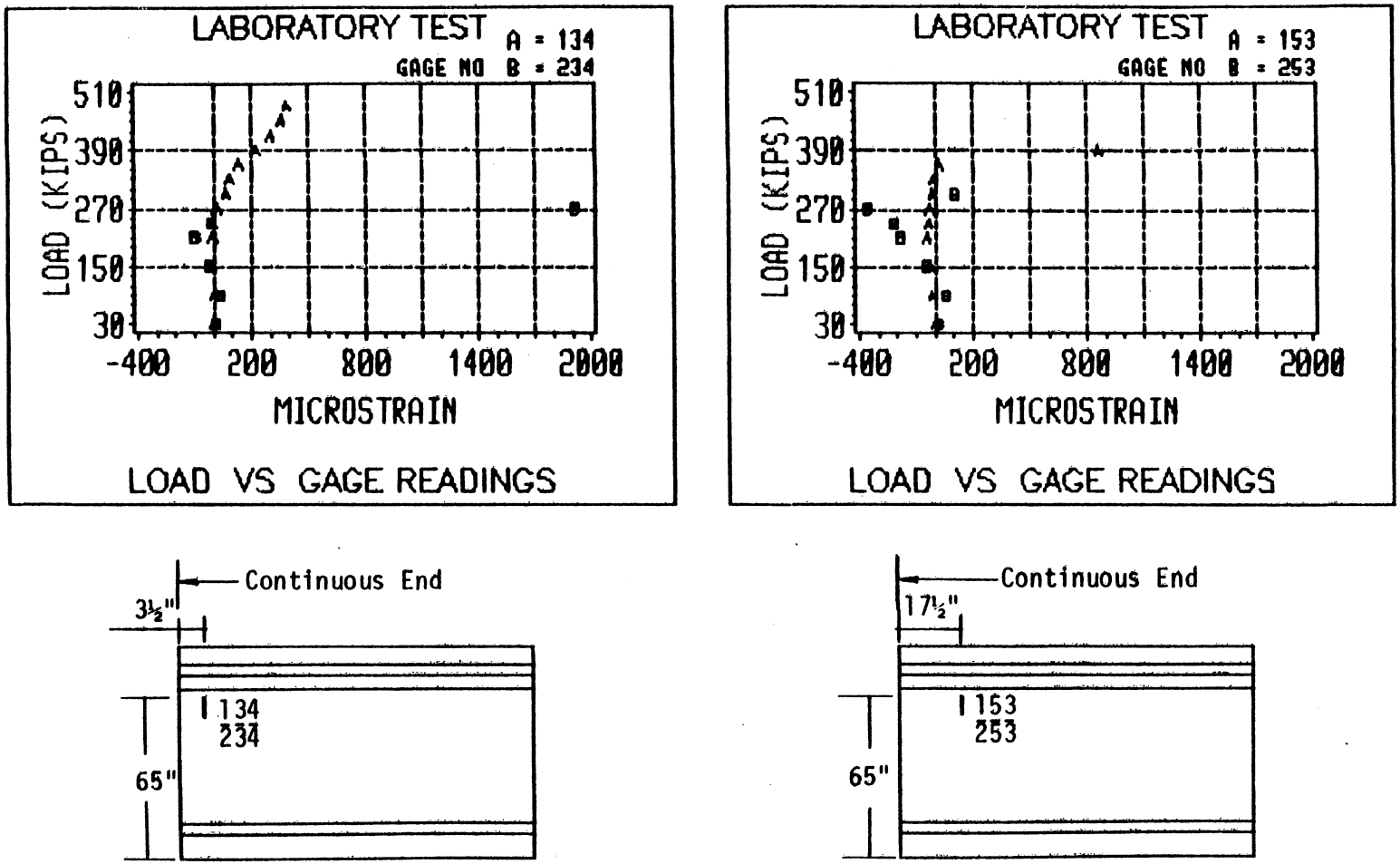

Figure 7.19 Laboratory Test - Strains in the Web Surface of Concrete due to Applied Loads (vertical gages)

Gages 134, 234, 153, and 253

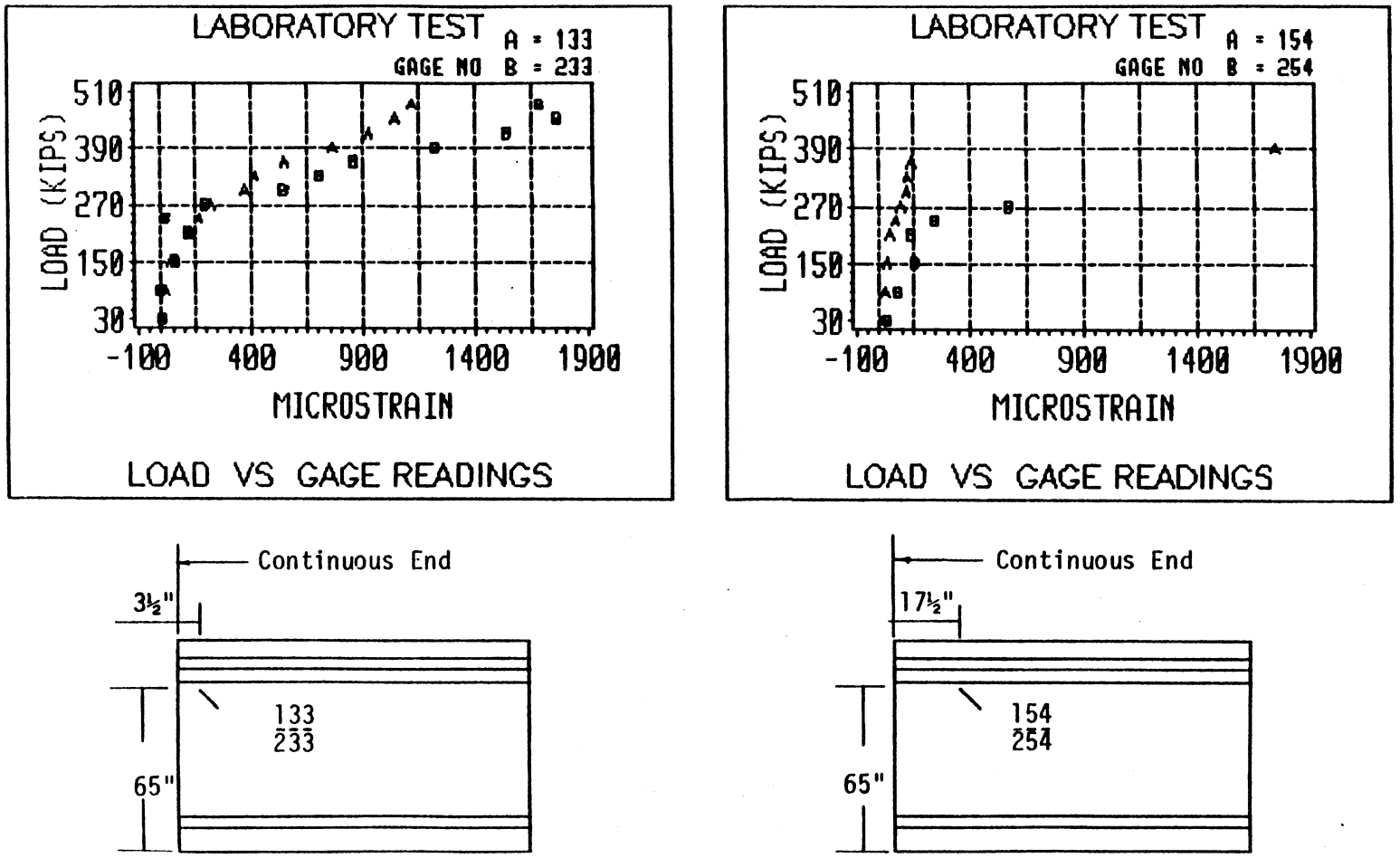

Figure 7.20 Laboratory Test - Strains in the Web Surface of Concrete due to Applied Loads (inclined gages)

Gages 133, 233, 154, and 254

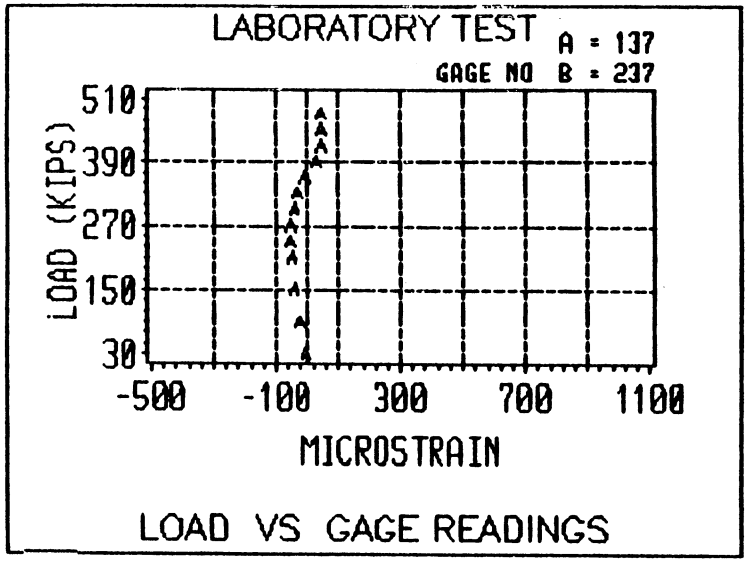

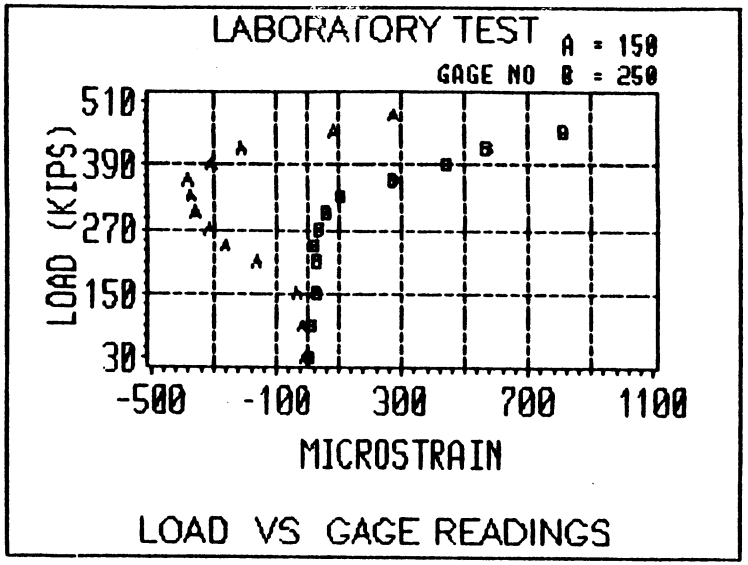

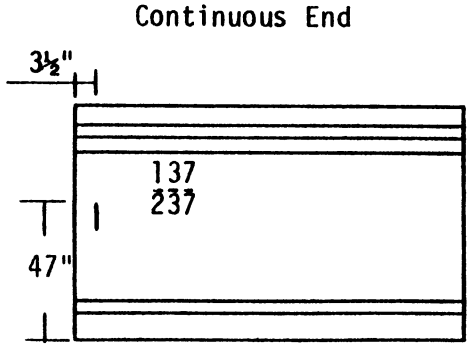

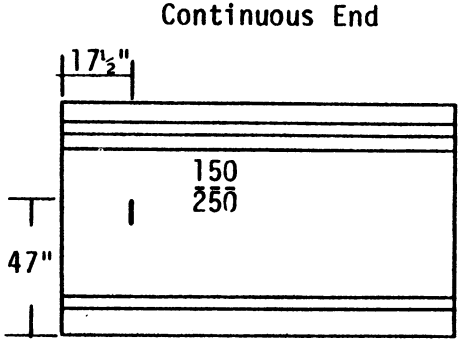

Figure 7.21 Laboratory Test - Strains in the Web Surface of Concrete due to Applied Loads (vertical gages)
Gages 137, 237, 150, and 250

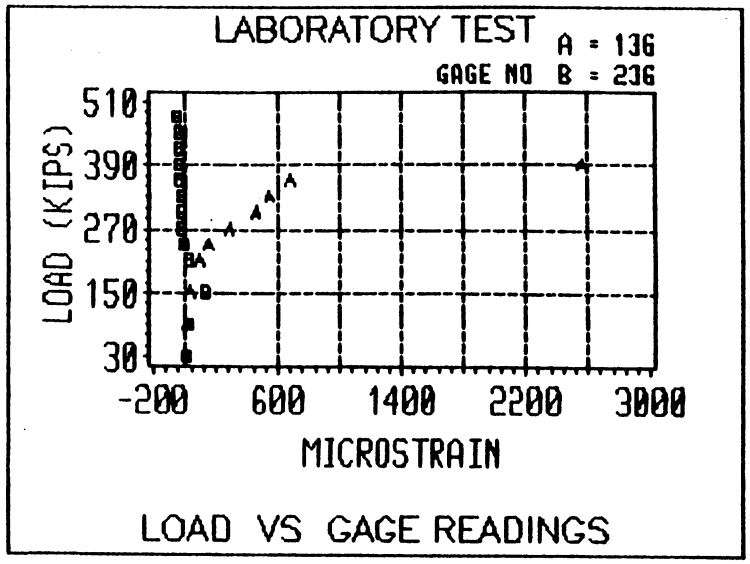

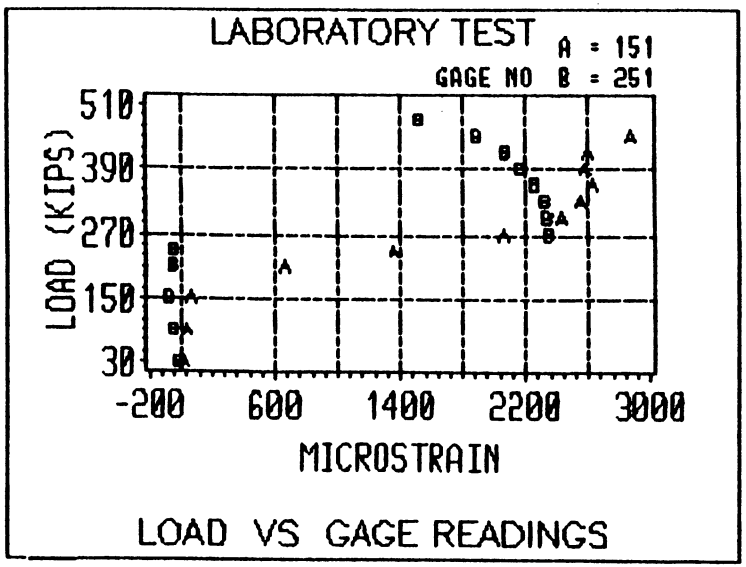

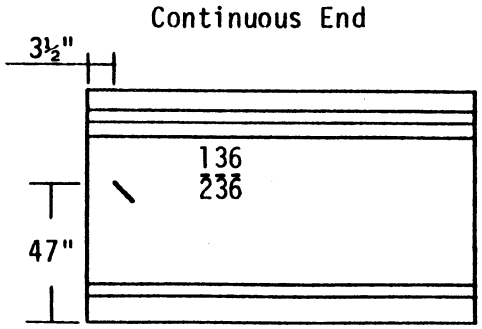

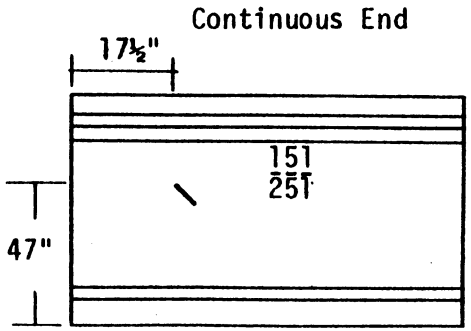

Figure 7.22 Laboratory Test - Strains in the Web Surface of Concrete due to Applied Loads (inclined gages)
Gages 136, 236, 151, and 251

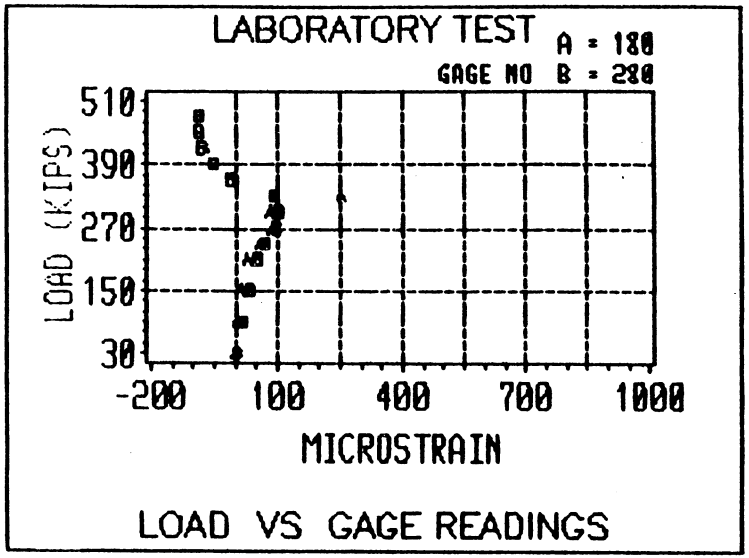

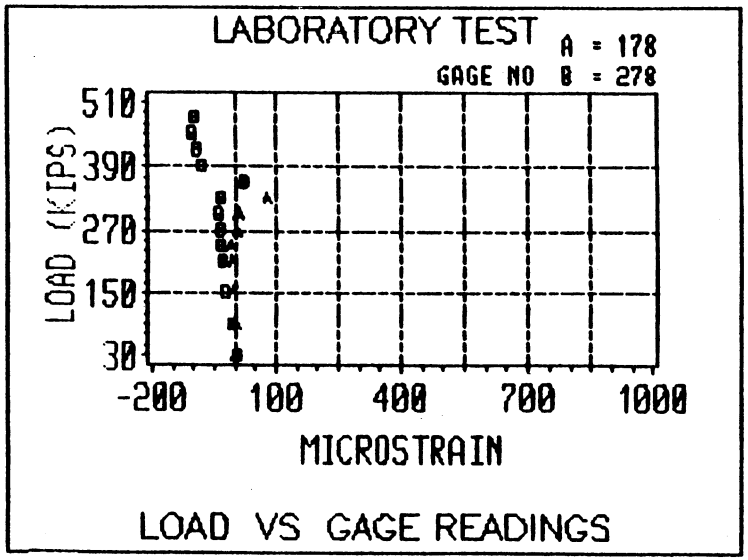

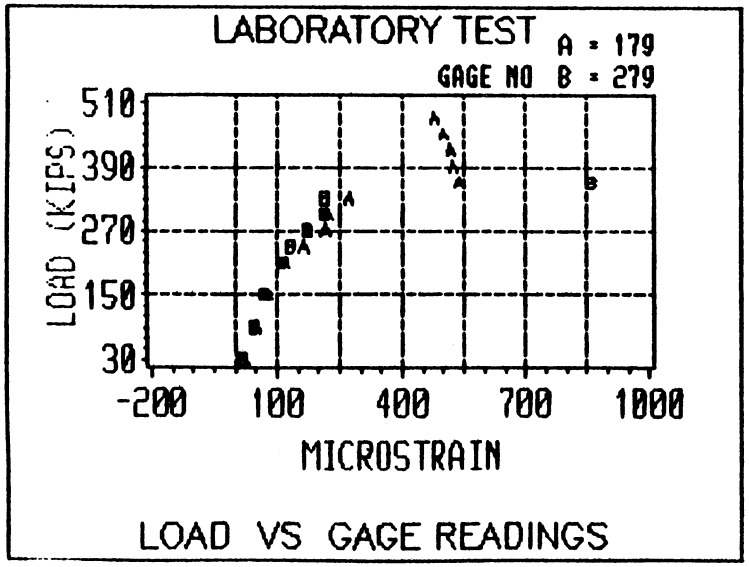

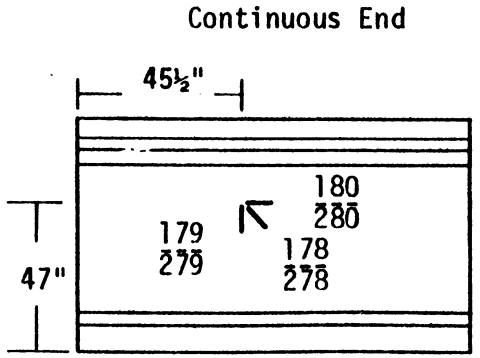

Figure 7.23 Laboratory Test - Strains in the Web Surface of Concrete due to Applied Loads
Rosette at x = 45½ in., y = 47 in.

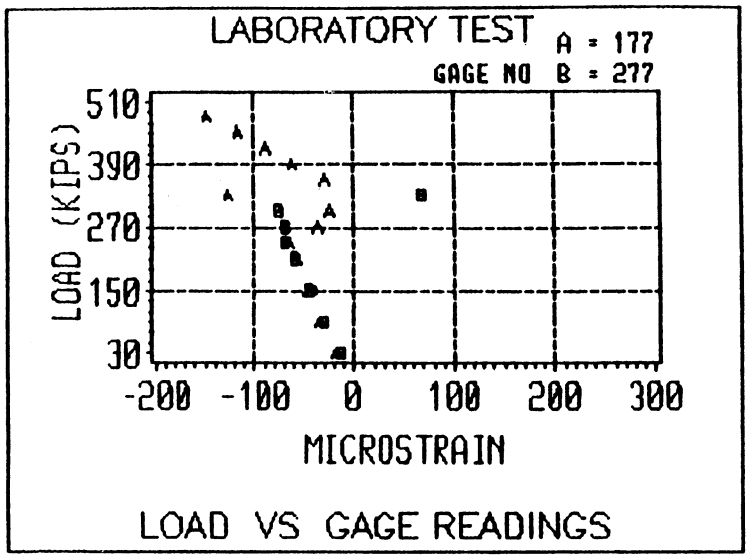

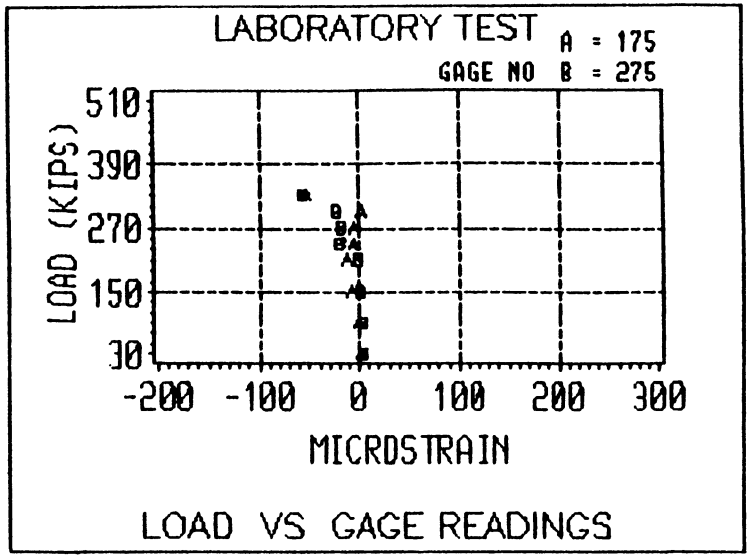

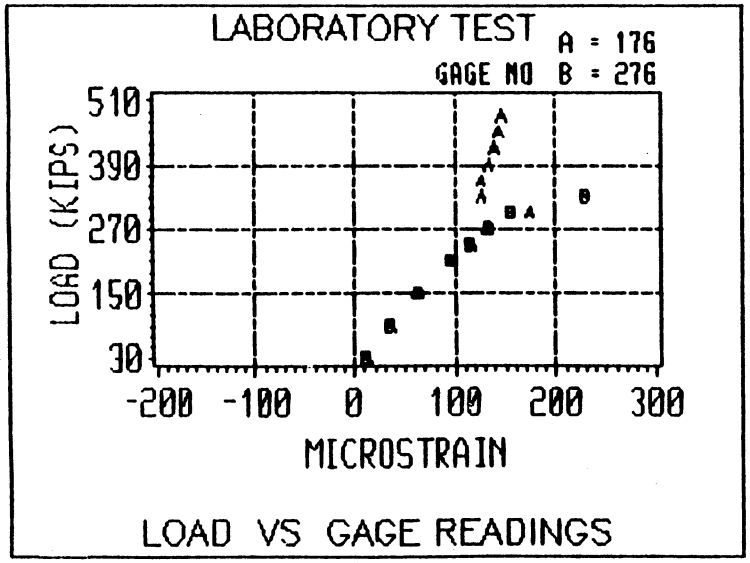

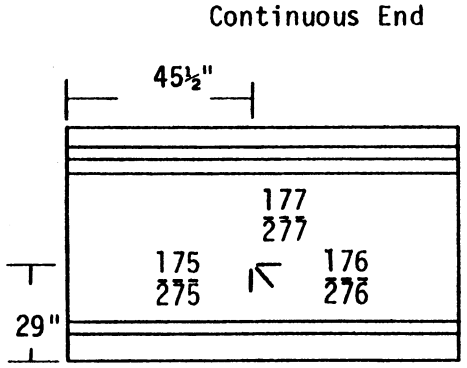

Figure 7.24 Laboratory Test - Strains in the Web Surface of Concrete due to Applied Loads
Rosette at x = 45½ in., y = 29 in.

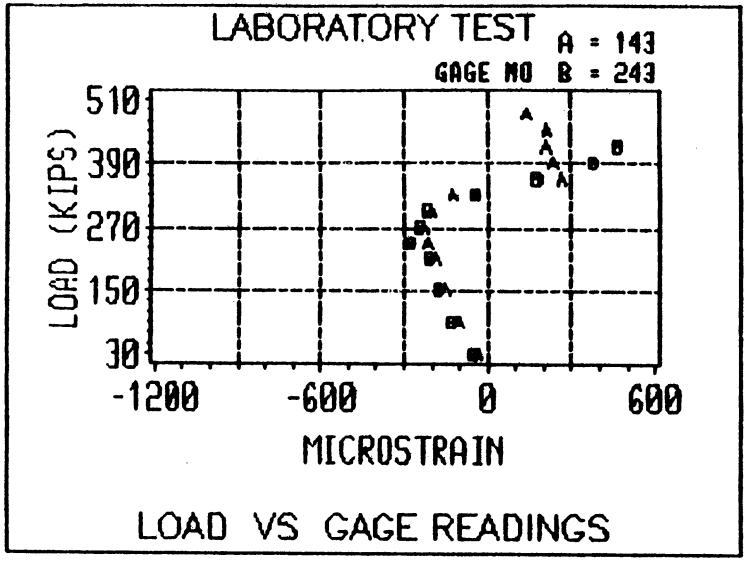

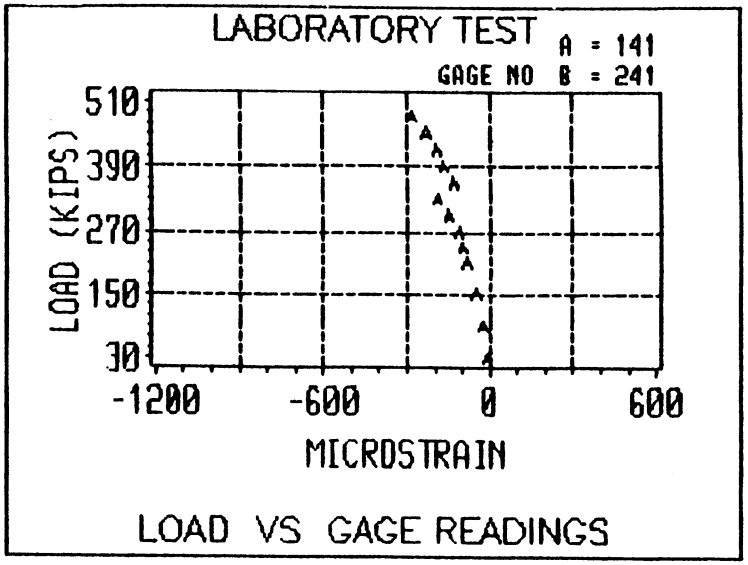

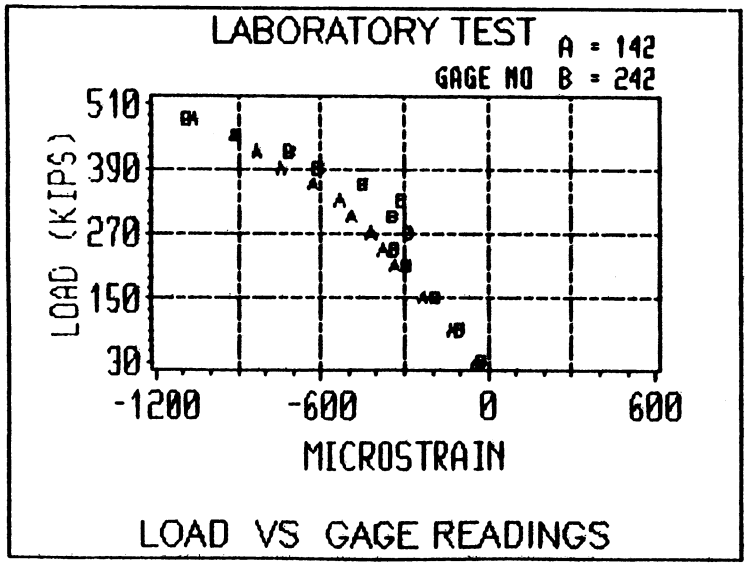

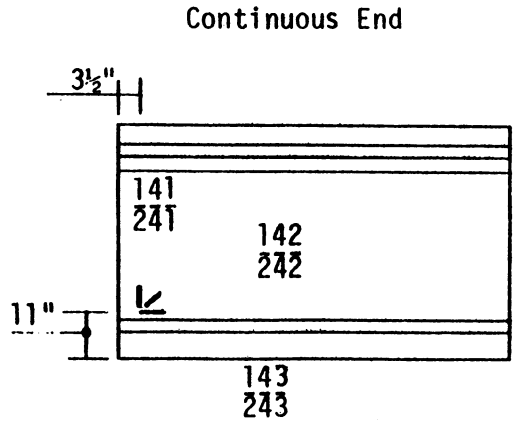

Figure 7.25 Laboratory Test - Strains in the Web Surface of Concrete due to Applied Loads
Rosette at x = 3½ in., y = 11 in.

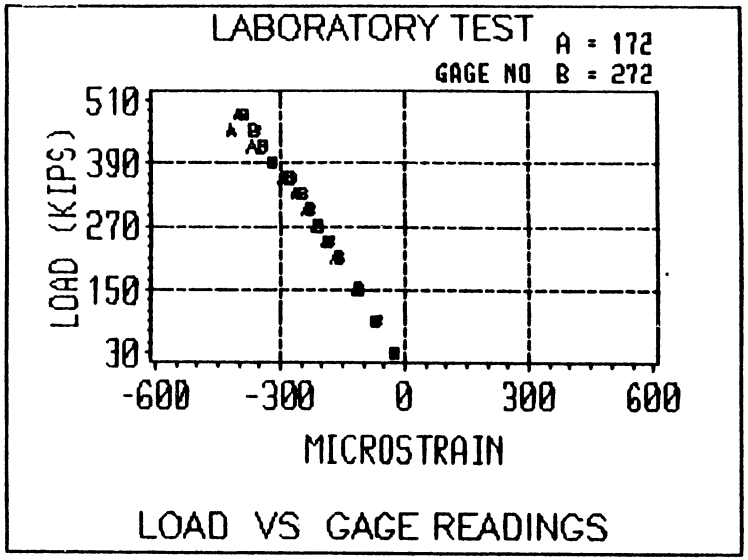

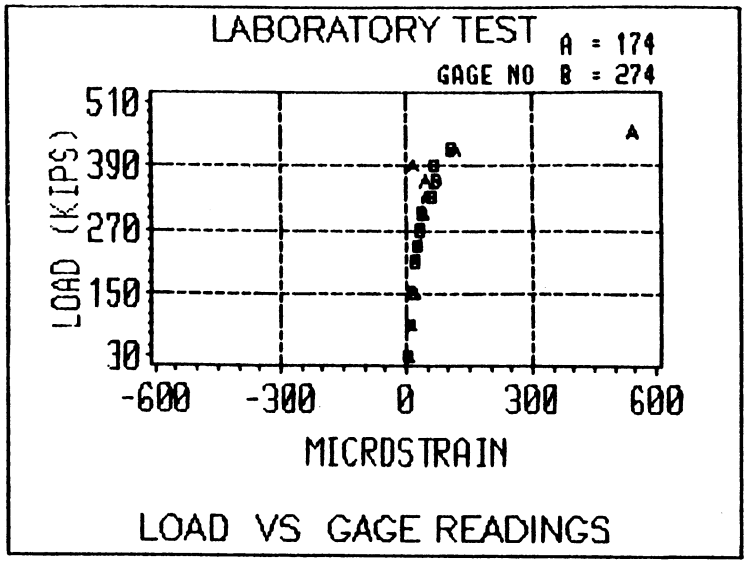

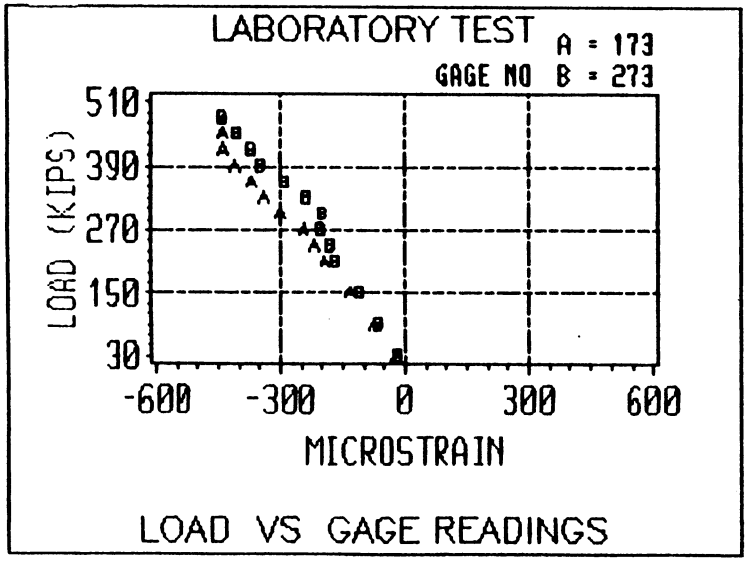

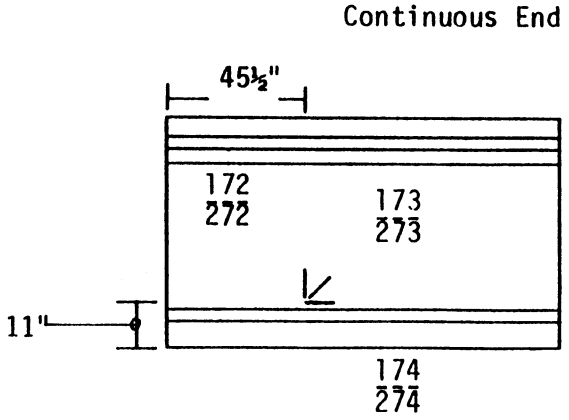

Figure 7.26 Laboratory Test - Strains in the Web Surface of Concrete due to Applied Loads
Rosette at x = 45½ in., y = 11 in.

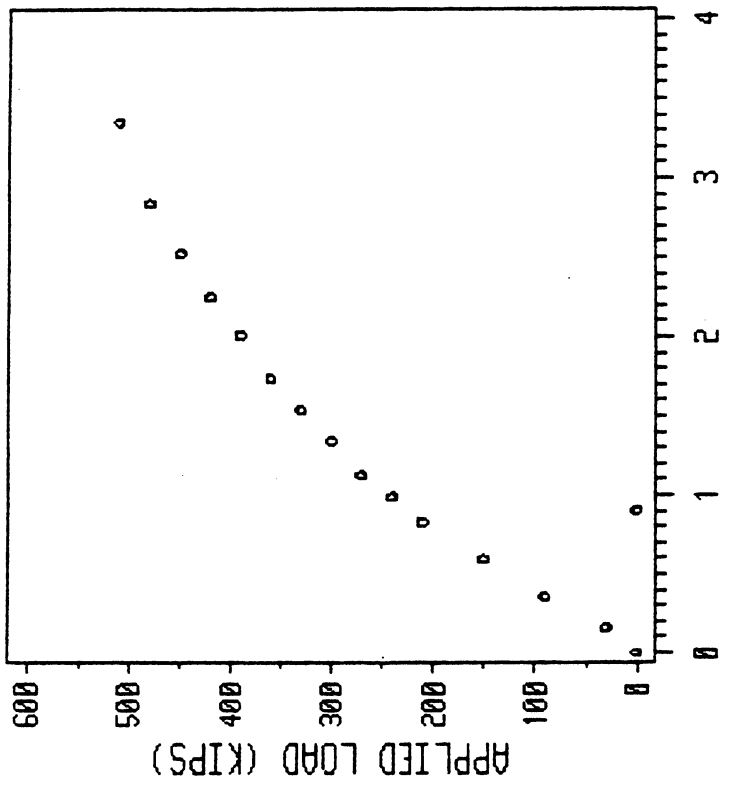

Figure 7.27 Laboratory Test - Load versus Deflection

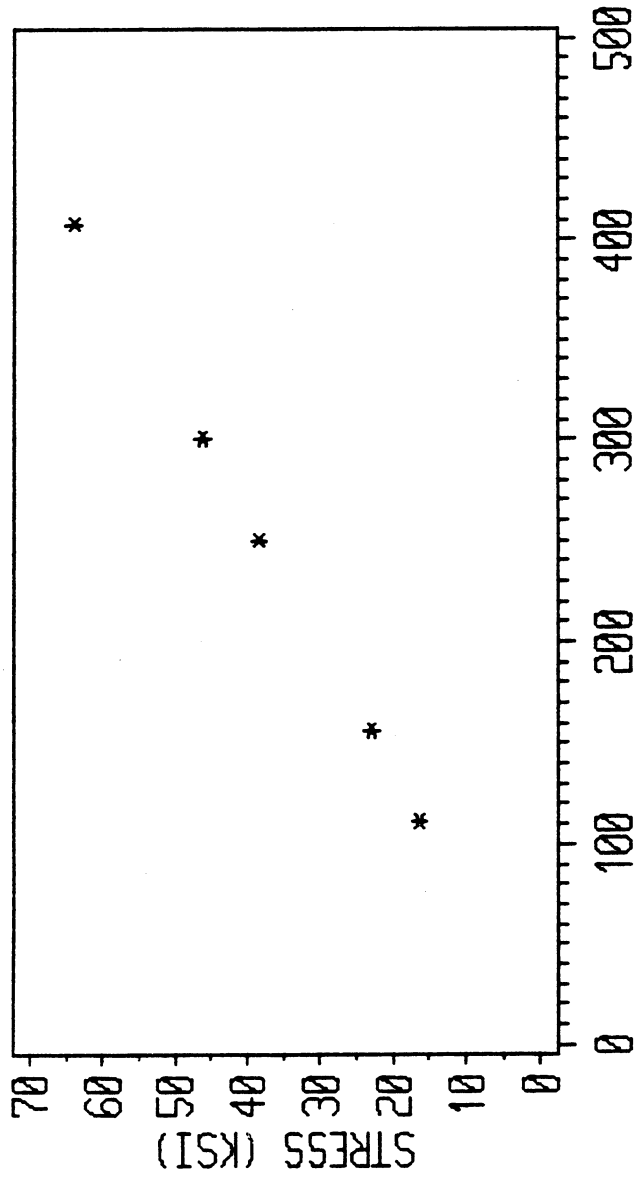

Figure 7.28 Laboratory Test - Stress in Slab Reinforcement versus Maximum Shear

CONCLUSIONS AND RECOMMENDATIONS

Conclusions

The series 14 girders without the end blocks that were tested in the laboratory were designed for a maximum factored shear, V_u, of 274 kips and a moment, Mu, of 3552 ft-kips. The maximum ultimate shear, V_u, for series 14 girders is equal to 325 kips [40]. This is approximately equal to the applied load of 300 kips in the laboratory test plus the maximum unfactored dead load shear of 21 kips. At the applied load of 300 kips, the maximum effective stress in the stirrups was 20 ksi, which was 30 percent of the yield strength. The load corresponded to the beginning of the web cracking. The cracking of the girders did not affect the diaphragm, even though the nominal strength of the concrete in the diaphragm was less than 50 percent of the concrete strength in the girders.

At higher loads the web cracking increased and the stirrups located beyond the transfer length of 25 in. indicated higher stresses than those located within the transfer length. Finally, the first yielding of the stirrups occurred at an applied load of 480 kips, which corresponded to the total shear of 500 kips. As a result, this study concludes that the girders will perform effectively under service loads. Furthermore the girders show an excess capacity of 54 percent beyond the ultimate shear.

The first yielding of the longitudinal steel occurred at a moment of 5407 ft-kips. The maximum ultimate design moment was 3554 ft-kips. Thus the composite section had 52 percent excess moment capacity over the maximum design moment.

Since the strain readings under the truck load were small and affected by environmental noise, a comparison between the field test and the laboratory test was not possible. The traffic on the adjacent existing bridge and the railroad traffic were the main factors that affected the final phase of the field test.

The conclusions stated are summarized below.

1. Continuous series 14 girders without end blocks will perform effectively.
2. The tested girders have an overload capacity of 54 percent in shear and 52 percent in bending for a concrete compressive strength of 9880 psi.
3. At 9880 psi concrete, excess capacity in ultimate shear and bending has been shown. The commonly used 6000 to 7000 psi concrete should provide sufficient ultimate resisting capacity.

Recommendations

For normal support and the sequence of construction described in this report, series 14 girders without end blocks may be used as continuous members. However, it is recommended that they be field tested to evaluate their performance prior to full implementation.

Furthermore, it is recommended one continuous girder without end blocks be used in a planned bridge before acceptance of these recommendations as a state design standards.

REFERENCES

1. AASHTO,"Standard Specifications for Highway Bridges," Thirteenth Ed., 1983.

2. ACI Committee 209, "Designing for Creep and Shrinkage in Concrete Structures," ACI publication SP-76, 1982.

3. ACI Committee 318, "Building Code Requirements for Reinforced Concrete," ACI publication, 1983.

4. ACI Committee 318, "Commentary on Building Code Requirements for Reinforced Concrete," ACI publication, 1983.

5 Arthur, P.D. and Ganguli, S., "Tests on End-Zone Stresses in Pretensioned Concrete I-beams," magazine of Concrete Research, Vol. 17, No. 51, June 1965, pp. 85-96.

6. Avram Constantin et al., "Concrete Strength and Strains," Elsevier Scientific Publication Company, 1981.

7. Bazant, Z.P. and Asghari, Ali A., "Constitutive Law for NonLinear Creep of Concrete," Journal of Engg. Mechanics Div., ASCE, Vol.103, No.EM1, Feb. 1977.

8. Bazant, Z.P. and Wu, Spencer T., "Creep and Shrinkage Law for Concrete at Variable Humidity," Journal of Engg. Mechanics Div., ASCE, Vol.100, No.EM6, Dec. 1974.

9. Bazant, Z.P., and Chern, Jenn-Chuan, "Double Power Logarithmic Law for Concrete Creep," Cement and Concrete Research, Vol.14, No.6, pp. 793-806, 1984.

10. Bazant, Z.P., and Najjar, L.J., "Comparison of Approximate Linear Method for Concrete Creep," Journal of Structure Division, ASCE, Vol. 99, No.ST9, Sept. 1973.

11. Bazant, Z.P., and Wittmann, F.H., "Creep and Shrinkage in Concrete Structures," John Wiley and Sons, 1982.

12. Branson, D.E., Meyers, B.L., and Kripanarayan, K.M., "Time-Dependent Deformation of Non-Composite, and Composite Prestressed Concrete Structures," committee on Mechanical Properties and Concrete.

13. Dilger, W.H., "Methods of Structural Creep Analysis," International Symposium on Fundamental Research on Creep and Shrinkage of Concrete, Swiss Federal Institute of Technology, Lausanne, Switzerland, Sept 1980.

14. El-Shafey, O., Jordaan, I.J., and Loov, R.E., "Deflection of Prestressed Concrete Members," ACI publication SP-76, 1982.

15. Freyermuth, C.L., "Design of Continuous Highway Bridges, with Precast, Prestressed Concrete Girders," PCI Journal, Vol. 14, No. 2, April 1969, pp. 14-39.

16. Gergely, P., Sozen, M.A. and Siess, C.P., "The Effect of Reinforcement on Anchorage Zone Cracks in Prestressed Concrete Members," Structural Research Series No. 271, University of Illinois, Urbana, 1963, p. 170.

17. Guyon, Y., "Contraintes dans les Pieces Prismatiques Soumses a des Forces Appliques sur deurs Bases, en Voisinage de ces Bases," Published by the International Association for Bridges and Structural Engineering, Vol. 11, 1961, pp. 165-226 (English summary).

18. Hass W., "Numerical Analysis of Creep and Shrinkage in Concrete Structures," Wittmann F.H. (ed.) Fundamental Research on Creep and Shrinkage of Concrete, Martinus Nijhoff Publishers, 1982.

19. Hawkins, N.M., "Behaviour and Design of End Blocks for Prestressed Concrete Beams," Institute of Engineers, Australia, Civ. Eng. Trans., Vol. CE8, No. 2, Oct. 1966, pp. 193-202.

20. Itani, R.Y., and Galbreith, R.L., "Design of Prestressed Concrete Girders Without End Blocks," Washington State Department of Transportation Report No. WA-RD 81.1, February 1986.

21. Jáor Tibor, "Creep Observations of Prestressed Concrete Bridges," Wittmann, F.H. (Ed.), Fundamental Research on Creep and Shrinkage of Concrete, Martinus Nijhoff Publishers, 1982.

22. Jevtic D., "Some Results of Testing and Estimation of Deflection and Relaxation of Prestressed Concrete Beams," ACI publication, SP-76, 1982.

23. Khalil M.S., Dilger W.H., and Ghali A., "Design considerations dictated by Creep and Shrinkage in Prestressed Concrete," ACI Publication, SP-76, 1982.

24. Lazic, Jakov D. and Lazic, Vera B., "Generalized Age-Adjusted Effective Modulus Method for Creep and in Composite Beam Structures A Part 1- Theory," Cement and Concrete Research, Vol. 14, No.6. pp 819-832, 1984.

25. Mangel G., "Design of the Ends of Prestressed Concrete Beams," Concrete and Construction Engineering, Vol. 44, No. 5, May 1949, pp. 141-148.

26. Marshall, W.T. and Mattock, A.H., "Control of Horizontal Cracking in the Ends of Pre-tensioned Concrete Girders," PCI Journal, Vol. 7, No. 5, Oct. 1962, pp. 56-74.

27. Mattock Alan H., "Precast Prestressed Bridges 5. Creep and Shrinkage Studies," Journal of PCA Research and Development Laboratories, May 1961.

28. Neville A.M., Dilger W.H., and Brooks J.J., "Creep of Plain and Structural Concrete," Construction Press, Longman Publications, 1983.

29. Nielsen L.F., "On the Applicability of Modified Discharge Equations," Cement and Concrete Research, Vol.7, No.2, pp. 149-160, 1977.

30. Parme, Alfred L. and Paris, George H., "Designing for Continuity in Prestressed Concrete Structures," ACI Journal, Vol. 23, No. 1, Sept. 1951, pp. 45-62.

31. PCA, Research and Development Laboratories, Precast-Prestressed Concrete Bridges, PCA Journal (in 6 parts), May 1960, Sept. 1960, Jan. 1961, May 1961, and Sept. 1961.

32. Rabbat, Basile G. and Russell, Henry G., "Proposed Replacement of AASHTO Girders with New Optimized Sections," Transportation Research Record 950, Second Bridge Engineering Conference, Vol. 2, Sept. 1984.

33. Rand, Juhan, Discussion of a paper by Alfred L. Parme and Paris: "Designing for Continuity in Prestressed Concrete Structures," ACI Journal, Vol. 24, No. 4, Dec. 1952.

34. Roelfstral, P.E., "Computerized Structural Analysis Applied to Large Span Bridges," Wittmann F.H. (ed.), Fundamental Research on Creep and Shrinkage of Concrete, Martinus Nijhoff Publishers, 1982.

35. Rusch, Hubert, Junguirth Dieter, and Hilsdorf Hubert, "Creep and Shrinkage, Their Effects on the Behavior of Concrete Structures," Springer-Verlag, 1983.

36. Russell, H.G., Meyers, B.L., and Daye, M.A., "Observations on Structures," International Symposium on Fundamental Research on Creep and Shrinkage of Concrete, Swiss Federal Institute of Technology, Lausanne, Switzerland, Sept. 1980.

37. Russell, H.G. and Shiu, Nam K., "Creep and Shrinkage Behavior of tall Buildings and Long-Span Bridges," Wittmann, F.H. (Ed.), Fundamental Research on Creep and Shrinkage of Concrete, Martinus Nijhoff Publishers, 1982.

38. Sarles, Dan and Itani, R.Y., "Anchorage Stresses in Prestressed Members, PCI Journal, Dec. 1984.

39. Tadros, Maher K., Ghali, Amin, and Dilger, Walter H., "Time-Dependant Analysis of Composite Frames," Journal of Structural Div. ASCE, Vol. 103, No. ST4, April 1977.

40. Washington State Department of Transportation, "Bridge Design Manual Vol.1 Criteria," July 1982.

41. Washington State Department of Transportation, "Bridge Design Manual Vol.2 Design Aids," September 1982.

42. Wittmann F.H., "Fundamental Research on Creep and Shrinkage of Concrete," Martinus Nijhoff Publishers, 1982.

APPENDIX A

A.1 Gages on Steel

A.1.1 Types of gages used

For the field test QFLA6-11 gages consisting of Cu-Ni foil and polymide base were used. These gages have excellent performance even at high temperature. Therefore, they were thought to be ideal to withstand steam curing of concrete.

In the laboratory test FLA6-11 gages were used. These gages utilized Cu-Ni foil with an extremely thin epoxy base.

The details of the gages are given in reference [2].

A.1.2 Adhesive

M-Bond AE 10 [1]

A.1.3 Protective Coat

M-Coat F [1]

A.1.4 Procedures to mount and protect the gages

The procedures to mount and protect the gages are outlined below. For the details refer [1].

1. Surface Preparation

   Five steps followed in surface preparation are given below.

   1.1 Solvent Degreasing

   Chlorothene Nu was used on an area about twice the gage would occupy. This would remove oils, grease etc., and clean the area.

1.2 Surface Abrading

The surface was abraded to remove the corrogations and to obtain a smooth surface on the reinforcing steel bars. Grit 220 and 320 papers were used with M-Prep Conditioner A [1].

1.3 Gage Layout Lines

A pair of cross reference lines at the point where the strains were to be measured were marked.

1.4 Surface Conditioning

Conditioner A was applied repeatedly to wash away residues due to surface abrading.

1.5 Neutralizing

In order to bring the surface condition back to an optimum alkalinity of 7.0 to 7.5 pH Neutralizer 5 was applied.

2. Installation of Gages

Since adhesive AE 10 was used, procedures outlined in Instruction Bulletin B-137-8 of reference [1] were followed to mount the gages.

3. Protection of Gages

M-Coat F was used to protect the gages. This consisted of Teflon Film, Butyl Rubber Sealant, Neoprene Rubber Sheets, Aluminum Foil Tape. and Air Drying Nitrile Rubber Coating. The elaborate procedures detailed in the Instruction Bulletin B-134 of reference [1] were closely followed.

A.2 Gages on Concrete

A.2.1 Types of Gages

For the field test PL90-11 type and for the laboratory test PL60-11 type gages were used. These were Cu-Ni wire gages utilizing a transparent plastic backing impregnated with a polyester resin. Because of their excellent electric insulation, ease and accuracy of installation these were ideally suited for field testing.

The details of these gages are given in reference [2].

A.2.2 Adhesive

RP-2 [2]

A.2.3 Procedure to Install and Protect Gages

The procedure to install gages is outlined below. The details are given in reference [1].

1. Surface Preparation

   1.1 Filling Up the Pores in Concrete

   Concrete surfaces are usually uneven, rough, and porous. In order to develop a proper surface for gage bonding, a sealing precoat of epoxy was applied. Before applying the precoat, the concrete surface was scrubbed and washed with water.

   1.2 Leveling the Surface

   Excess of the precoat was removed using a rotary grinder with grit 320 papers.

1.3 Gage Layout Lines

The points where the strains were to be measured were marked with a pair of crossed reference lines.

1.4 Neutralizing

In order to bring the surface conditions to an optimum alkalinity of 7.0 to 7.5 pH Neutralizer 5 [1] was applied.

2. Installation of Gages

Strain gages were installed using adhesive RP-2. The necessary pressure required for the proper use of the adhesive was applied using wooden planks.

3. Protection of Gages

Aluminum foil was used to protect the gages from rain, and weather effects.

REFERENCES

1. Micro-Measurements, 'Catalog and Technical Data Binder,' Micro-Measurements Division, Measurements Group, P.O. Box 27777, Raleigh, North Carolina 27611.

2. Tokyo Sokki Kenkyujo Co.,Ltd., 'TML pam E-101 R,' Texas Measurements, Inc., P.O. Box 2618, College Station, Texas 77840.

APPENDIX B

Notation

E_c = modulus of elasticity of concrete, psi

E_s = modulus of elasticity of steel, ksi

f'c = compressive strength of concrete, psi

ϵ_a, ϵ_b, ϵ_c = measured strain in concrete, microstrains

ϵ_s = measured strain in steel, microstrains

ϵ_{p1}, ϵ_{p2} = principal strains in concrete, microstrains

ϵ_x = strain in x-direction, microstrains

ϵ_y = strain in y-direction, microstrains

ϵ_{xy} = shear strain in x-y plane, microstrains

θ_a, θ_b, θ_c = orientation of strain gages with respect to x-axis, degrees

ν = poisson's ratio

σ_{p1}, σ_{p2} = principal stresses in concrete, psi

σ_s = stress in steel, ksi

θ = angle between the principal axis and the x-axis

B.1 Reduction of Strains Measured in Steel

Strain in steel (measured) ϵ_s (microstrains)

Modulus of elasticity of steel(assumed) E_s = 29000 (ksi)

Stress in steel $\sigma_s = E_s e_s = 0.029\ \epsilon_s$ (ksi)

B.2 Reduction of Strains Measured in Concrete

Known quantities

ϵ_a, ϵ_b, ϵ_c = strains measured (microstrains)

θ_a, θ_b, θ_c = orientations of the gages (degrees)

f'c = compressive strength of concrete (psi)

$E_c = 57000 \sqrt{f'c}$ (psi)

ν = poisson's ratio = 0.2 (assumed)

To find

ϵ_{p1}, ϵ_{p2}, θ

σ_1, σ_2

Solution

$$\epsilon_a = \epsilon_x \cos\theta_a + \epsilon_y \sin\theta_a + \epsilon_{xy} \cos\theta_a \sin\theta_a$$

$$\epsilon_b = \epsilon_x \cos\theta_b + \epsilon_y \sin\theta_b + \epsilon_{xy} \cos\theta_b \sin\theta_b$$

$$\epsilon_c = \epsilon_x \cos\theta_c + \epsilon_y \sin\theta_c + \epsilon_{xy} \cos\theta_c \sin\theta_c$$

For $\theta_a = 0°$, $\theta_b = 45°$, $\theta_c = 90°$

$$\epsilon_a = \epsilon_x$$

$$\epsilon_b = 0.5\ (\epsilon_x + \epsilon_y + \epsilon_{xy})$$

$$\epsilon_c = \epsilon_y$$

$$\gamma_{xy} = 2\epsilon_b - \epsilon_a - \epsilon_c$$

For $\theta_a = 0°$, $\theta_b = -45°$, $\theta_c = -90°$

$$\epsilon_a = \epsilon_x$$

$$\epsilon_b = 0.5\ (\epsilon_x + \epsilon_y - \epsilon_{xy})$$

$$\epsilon_c = \epsilon_y$$

$$\gamma_{xy} = \epsilon_a + \epsilon_c - 2\epsilon_b$$

Therefore,

$$\epsilon_{p1} = 0.5\ (\epsilon_a + \epsilon_b) + / (\epsilon_a - \epsilon_c) + (2\epsilon_b - \epsilon_a - \epsilon_c)$$

$$\epsilon_{p2} = 0.5\ (\epsilon_a + \epsilon_b) - / (\epsilon_a - \epsilon_c) + (2\epsilon_b - \epsilon_a - \epsilon_c)$$

$$\tan 2\theta = (2\epsilon_b - \epsilon_a - \epsilon_c)/ (\epsilon_a - \epsilon_c)$$

$$\sigma_{p1} = E_c\ (\epsilon_1 + \nu\ \epsilon_2)/(1 - \nu)$$

$$\sigma_{p2} = E_c\ (\epsilon_2 + \nu\ \epsilon_1)/(1 - \nu)$$

APPENDIX C

Notation

a = depth of equivalent rectangular stress block

A_c = area of composite section, in.^{2}

A_g = area of cross section of a girder, in.^{2}

A_s = area of reinforcement in the slab, in.^{2}

b = width of the slab, in.

b_w = width of the web of a girder, in.

c = depth of the neutral axis, in.

d = effective depth of the section, in.

d_1 = distance between the slab reinforcement and the gages on the bottom flange, in.

d_s = depth of the slab, in.

c_1 = distance between the slab reinforcement and the gage, in.

e = eccentricity of prestressing force, in.

E_{cg} = modulus of elasticity of girder concrete, psi

E_{cs} = modulus of elasticity of slab concrete, psi

E_s = modulus of elasticity of steel, ksi

$f'c$ = specified comprssive strength of concrete, psi

f_{pc} = compressive stress at centroid of composite section, due to both prestress and moments resisted by precast member acting alone, psi

f_{pe} = compressive stress in concrete due to effective prestress forces only at extreme fiber section where tensile stress is caused by externally applied loads, psi

f_s = stress in the slab reinforcement, ksi

f_y = yield strength of the slab reinforcement, ksi

I_c = moment of inertia of the composite section, $in.^4$

I_g = moment of inertia of the girder section, $in.^4$

l = length of the girder, ft.

M_a = moment due to applied load, ft.-kips

M_d = moment due to dead load, ft.-kips

M_n = flexural capacity of the section, ft.-kips

Mt = total moment acting on the section, ft.-kips

M_{umax} = maximum design moment, ft.-kips

P = effective prestressing force after loses

P_a = applied load, kips

P_d = maximum shear at the section due to unfactored dead load, kips

P_t = total load acting on the section, kips

V_{ci} = nominal shear strength provided by concrete when diagonal cracking results from combined shear and moment, kips

V_{cw} = nominal shear strength provided by concrete when diagonal cracking results from excessive principal stress in web

V_d = shear force at section due to unfactored dead load, kips

v_p = vertical component of effective prestress force at section, kips

x = distance of the section from the face of the diaphragm, in.

y_b = distance of the centroidal axis of the composite section from the bottom fiber, in.

y_{bg} = distance of the centroidal axis from the bottom of the girder, in.

y_s = distance of the centroidal axis of the composite section from the top of slab, in.

y_{tg} = distance of the centroidal axis from the top of the girder, in.

y_t = distance of the centroidal axis of the composite section from the top fiber of the girder, in.

σ_a = stress in the top fiber of the girder due to the applied load, psi

σ_b = stress in the bottom fiber due to dead load, psi

σ_r = modulus of rupture or allowable tensile stress, psi

σ_t = stress in the top fiber due to dead load, psi

ϵ_a = strain in the bottom fiber due to applied load

ϵ_b = strain in the bottom fiber due to the dead load

ϵ_e = measured strain

ϵ_t = total strain in the bottom fiber

ϵ_{top} = strain in the top fiber

C.1 Comparision of V_{ci} and V_{cw}

Properties of Girder

1. Type Series 14 without End Blocks
2. f'c = 9880 psi
3. w_g = 156 pcf
4. A_g = 674 in.
5. I_g = 514000 in.
6. y_{bg} = 38 in.
7. y_{tg} = 35 in.
8. E_{cg} = 6391154 psi

Properties of Slab

1. $f'c$ = 4000 psi
2. w_s = 155 pcf
3. b = 42 in.
4. d_s = 7.5 in.
5. E_{cs} = 4027555 psi

Properties of Composite Section

1. A_c = 872.35 in.
2. I_c = 748459 in.
3. y_b = 47 in.
4. y_t = 26 in.
5. y_s = 34 in.
6. w = 1.06 plf
7. l = 20 ft

Properties of Reinforcement in the Slab

1. f_y = 60 ksi
2. A_s = 14.4 in.

Properties of Prestressing Strands

1. Total Number of Strands = 46
2. Number of Harped Strands = 16
3. e = 22 + 0.036 X
4. P = 998 kips (after loss of 25 %) for X > 25 in.
5. V_p = 36 kips for X > 25 in.
6. P = 998 X/25 for X < 25 in.
7. V_p = 36 X/25 for X < 25 in.

7. $V_p = 36\ X/25$ for $X < 25$ in.

Computations

1. $V_{ci} = 0.6\sqrt{f'c}\ b_{wd} + V_d + M_{cr}(V_i/M_{max}) + V_p$

1.1 $0.6\sqrt{f'c}\ b_{wd} = 0.6\sqrt{4000}\ (5)(64.8) = 19.325$ kips

1.2 $V_d = (240 - X)w/12$

1.3 $M_{cr} = (6\sqrt{f'c} + f_{pe} - f_d)\ (I_c/y_s)$

$6\sqrt{f'c} = 6\sqrt{9880} = 596$

$f_{pe} = P/A_c - P(e)(y_s/I_c)$

$= P/872.35 - P(22 + 0.036X)(34/748459)$

$f_d = (240 - X)\ (w/12)\ (y_s/I_c)$

$= (240 - X)\ (w/12)\ (34/748459)$

1.4 $(V_i/M_{max}) = 1/(166 - X)$

Therefore,

$V_{ci} = 19.32 + (240 - X)(1.06/12) + [13129 + 25183^* - 998^*(22 + 0.036X) - (1.06/12)(240 - X)^2/2]/(166 - X) + 36$

2. $V_{cw} = (3.5\sqrt{f'c} + 0.3f_{pc})(b_w)(d) + V_p$

2.1 $3.5\sqrt{f'c}\ (b_{wd}) = 3.5\sqrt{9880}\ (5)(64.8) = 112.75$

2.2 $f_{pc} = P/A_g - P(e)(y_b - y_{bg})/I_g - (240 - X)(w/12)(y_b - y_{bg})/I_c$

$= P/674 - P(22 + 0.036X)(47 - 38)/514000 - (240 - X)(1.06/12)(47 - 38)/748459$

Therefore,

$V_{cw} = 112.75 + 100.44 - 0.07^*X - 5.14^*(240 - X)^2\ (10) + 36$

25.0	169	245
40.0	177	244
60.0	191	243
120.0	278	240

NOTE: Quantities vary with prestressing force which attains its full value within 25 in. from the end of a girder.

C.2 Stresses in Slab Reinforcement

The stresses in the slab reinforcement are calculated at four critical stages based on the strains measured in gage 156. The distance of the point of loading to the strain gage is 13.44 ft. The length of the girder is 19.6 in. The gage was located 3 in. above on the surface of the bottom flange.

i.e. l_d = 19.6 ft.

l_a = 13.44 ft.

d_1 = 74.25 in.

d = 77.25 in.

$c_1 = (e_t d_1)/(e_t + f_s/E_s)$

$c = c_1 + 3$

$a = 0.65\ (c_1 + 3)$

$f_s = (M_t/A_s)/(d - a/2)$

$(d - a/2) = (77.25 - 1.95/2 - 0.65c_1)$

$(d - a/2) = (76.275 - 0.65c_1)$

1. At Rupture of Concrete

$M_d = (19.6)(w/12)/2$

$= (19.6)(1.06/12)/2$

$M_d = 204$ ft.- kips

$\sigma_t = (M_d)(12)(y_s)/I_c = (204)(12)(34)/748459 = 111$ psi

$\sigma_b = (M_d)(12)(y_{sg})/I_c = (204)(12)(44)/748459 = 144$ psi

$\epsilon_t = \sigma_t/E_c = 111/6391154 = 1.73678 \times 10^{-6}$

$\epsilon_b = \sigma_b/E_c = 0.144/6391154 = 2.25 \times 10^{-6}$

$\sigma_r = 7.5\sqrt{f'c} = 7.5\sqrt{9880} = 745$ psi

$\sigma_a = \sigma_r - \sigma_t = 745 - 111 = 634$ psi

$\epsilon_a = \sigma_a/E_c = 634/6391154 = 99 \times 10^{-6}$

$\epsilon_b = \epsilon_a\, y_{sg}/y_s = 128 * 10^{-6}$

$P_a = 91$ kips (applied load from experiment data corresponding to ϵ_a equal to $128 * 10^{-6}$

$P_t = P_a + P_d = 91 + (1.06)(19.6) = 111$ kips

$M_a = (91)(13'10") = 1210$ ft.-kips

$M_t = M_a + M_d = 1210 + 204 = 1414$ ft.-kips

$\epsilon_t = (M_t/I_c)(y_s/E_c) = (1414/748459)(34/6391154)$

$\epsilon_t = 122 \times 10^{-6}$

$c_1 = 263/(3.538 + f_s)$

$a = 1.95 + 171/(3.538 + f_s)$

$f_s = M_t/[A_s\ (76.275 - 85.5/(3.538 + f_s)$

solving for f_s

$f_s = 16.4$ ksi

For $f_s = 16.4$ ksi

$a = 1.95 + 171/(3.538 + 16.4) = 10.5$ psi

This means the stress block extends into the web. Therefore, the resultant of compressive forces is at 3.45 in from the bottom of the girder.

Therefore,

$f_s = Mt/[As\ (76.275 - 3.45)]$

$f_s = 16$ ksi95

$P_t = 111$ kips

2. At First Visible Crack i.e. @ $P_a = 210$ kips

$P_t = P_a + P_d = 210 + (1.06)(19.6)$

$M_a = (210)(13.44) = 2822$ ft.-kips

$M_t = M_a + M_d = 2822 + 204 = 3026$ ft.-kips

$f_s = (M_t/A_s)/(76.275 - 196/(8.12 + f_s))$

solving for f_s

$f_s = 35$ ksi

$P_t = 231$ kips

3. $A_t\ M_t = 2019$ ft.-kips

$M_a = 2019 - 204 = 1815$ ft.-kips

$P_a = Ma/13.44 = 135$ kips

$P_t = P_a + P_d = 135 + 21 = 156$ kips

$\epsilon_e = 150 \times 10^{-6}$ (from the experimental data)

$\epsilon_t = \epsilon_e + \epsilon_b = (150 + 23) \times 10^{-6} = 173 \times 10^{-6}$

$a = 1.95 + 242/(5.017 + f_y)$

$f_s = (M_t/A_s)/[76.275 - 121/(5.017 + f_s)]$

substituting appropriate values and solving for f_s

$f_s = 23$ ksi

$P_t = 156$ kips

3. At M_{umax} i.e. @ $M_t = (M_{umax}/0.9)$

$M_t = 3949$ ft.-kips

$M_a = M_t - M_d = 3949 - 204 = 3745$ ft.-kips

$P_a = M_a/13.44 = 279$ kip

$P_t = 279 + (1.06)(19.6) = 300$ kips

$\epsilon_e = 400 \times 10^{-6}$ (from experimental results)

$\epsilon_t = \epsilon_e + \epsilon_b = (400 + 23) \times 10^{-6} = 423 \times 10^{-6}$

$a = 1.95 + 296/(f_y + 12.267)$

$f_s = (M_t/A_s)/(76.275 - 296/(f_s + 12.267)$

sustituting appropriate values and calculating $\backslash f_s$

$f_s = 46.3$ ksi

$P_t = 300$ kips

4. At Total Load of 250 kips

$P_t = 250$ kips

$P_a = P_t - (1.06)(19.6) = 250 - 21$ kips

$\epsilon_e = 325 \times 10^{-6}$

$\epsilon_t = \epsilon_e + \epsilon_b = (325 + 23) \times 10^{-6} = 348 \times 10^{-6}$

$f_s = (M_t/A_s)/[76.275 - 244/(10.092 + f_s)]$

substituting for appropriate values and calculating f_s

$f_s = 38.4$ ksi

$P_t = 250$ kips

5. At Flexural Capacity of the Section

$M_t = M_n = 5407$ ft.-kips

$M_a = M_t - M_d = 5407 - 204 = 5203$ ft.-kips

$P_a = M_a/13.44 = 5203/13.44 = 387$ kips

$P_t = P_a + P_d = 387 + 21 = 408$ kips

$\epsilon_t = 698 \times 10^{-6}$

$f_s = (M_t/A_s)[76.275 - 488/(20.24 + f_s)]$

sustituting appropriate values and calculating f_s

f_s = 64 ksi

P_t = 408 kips